PERFORMANCE OF LIVE-MUSCLE TISSUE AS AN *IN-VITRO* MECHANICAL ACTUATOR

by
Cem Tutcu

Submitted to Graduate School of Natural and Applied Science
in Partial Fulfillment of the Requirements
for the Degree of Master of Science in
Mechanical Engineering

Yeditepe University
2014

PERFORMANCE OF LIVE-MUSCLE TISSUE AS
AN *IN-VITRO* MECHANICAL ACTUATOR

APPROVED BY:

Prof. Mehmet A. Akgün ..... 
(Thesis Supervisor)

Assist. Prof. Fethi Okyar ..... 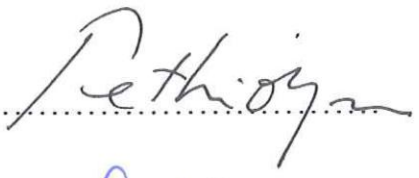

Assist. Prof. Gökhan Ertaş ..... 

DATE OF APPROVAL: ..../..../2014

ACKNOWLEDGEMENTS

I had the privilege to work with a scientist, noted for his knowledge, with a teacher noted for his devotion. My thesis supervisor Prof. Dr. Akgün, not only provided necessary tools to accomplish this challenging task but also enriched my knowledge with a personal interest. I appreciate his effort for teaching, and assure Dr. Akgün to exploit my skills in scientific development at high degree of enthusiasm as him, through my future professional endeavors.

I present my gratitude to Asst. Dr. Cıblak for his contributions in my professional life, who offers a perspective to his students, that outstrips the conventional way of thinking in engineering. During my studentship I enjoyed the innovative discussion platform held by him.

I am delighted to work with Anıl Özdemirli, a great engineer and a great friend. By courtesy of signal generator and amplifier circuits he designed, goals of the thesis are achieved. I acknowledge him with all my respect, regarding his commitment to science and progress.

For her companionship and help in experiments, I am thankful to Görkem Cemali. I appreciate her friendship due to her thoughtful attitude. I kindly acknowledge M.D Yalçın Günal, Sinem Ethemoglu and Melis Mistay for their help in experiments as well as Emirhan Sayhan for his effort in the manufacturing of experimental setup.

For her support at every challenge that I cope with, I present my special thanks to Sinem Yurdaözer.I appreciate our friendship with Asil Arif Aksekili and Efe Ünal which escalated more as we achieved professional goals as a team.

ABSTRACT

PERFORMANCE OF LIVE-MUSCLE TISSUE AS AN *IN-VITRO* MECHANICAL ACTUATOR

Developing creative solutions in mechanical actuation is an essential need for the rapidly progressing technological applications. Studies in the field are becoming more challenging due to increasing demands of lighter and smaller actuators with higher efficiency. This thesis introduces a new approach for the problem by considering live muscle tissue as an actuator for macro mechanical systems, thus investigates the in-vitro performance of muscles in a mechanical perspective. Muscle tissue is a kind of smart material and a perfect mechanical actuator with its compact architecture that integrates force and position sensors, power generating units and energy reserves within a single organ. Unlike most conventional mechanical or electromechanical actuators muscle tissue is able to adapt to changes in power needs, has adjustable mechanical impedance and uses a renewable energy source. Most of the research on the subject focuses on developing bio-actuators for micro pumps while few of them investigate macro scale bio-actuators. Former studies point to the significance of developing a robust control strategy in order to have an effective actuator. For this study performance parameters are chosen as controllability, service life and feasibility. A muscle testing apparatus is designed and manufactured for muscle characterization and control purposes. Mechanical response and fatigue behaviour of *gastrocnemius* muscle of *Rana esculenta* frog is characterized and various models are prepared accordingly. Models are used to test and improve control algorithms. As a result the effect of stimulation parameters on muscle mechanical output is determined similar to the studies presented in the literature. Control trials are carried out with a certain accuracy and muscle specimens remained functioning up to 36 hours. These outcomes reveal a general perspective of advantages and challenges in using muscle tissue as a bio-actuator and show that the muscle is a possible actuator in mechanical systems. The interdisciplinary approach yields a promising solution to certain mechanical actuation problems and opens up remarkable new possibilities in bio-mechatronics especially for medical field such as developing bio-mechatronic prostheses and robots.

ÖZET

IN-VITRO EYLEYİCİ OLARAK CANLI KAS PERFORMANSI

Günümüzdeki teknolojik gelişmelerin öncelikli ihtiyaçlarından biri mekanik hareketlendirme sağlayacak gelişmiş eyleyicilerin geliştirilmesidir. Konu üzerindeki araştırmalar, yüksek verimli, az yer kaplayan ve hafif eyleyicilere duyulan talep doğrultusunda gün geçtikçe daha zorlu hale gelmektedir. Bu tez, canlı kas dokusunu mekanik bir sistemde eyleyici olarak kullanmayı değerlendirerek, probleme farklı bir yaklaşım sunmaktadır. Verimli bir eyleyici olan kas dokusu, içerisinde bulundurduğu pozisyon ve kuvvet sensörleri, güç üreten birimleri ve enerji rezervleri ile bir akıllı malzeme olarak değerlendirilebilir. Alışılagelmiş eyleyicilerden farklı olarak kas dokusu entegre edildiği sistemin güç taleplerindeki değişikliklere uyum sağlayabilir ve yenilenebilir eneji kaynağı kullanmaktadır. Konu üzerindeki bir çok araştırma biyo-eyleyicilerin mikro-pompalar üzerinde yapılmış olup, makro uygulamalarla ilgilenmiş az sayıda çalışma bulunmaktadır. İlk çalışmalar etkin bir biyo-eyleyici uygulamasının en önemli kısmın güvenilir kontrol stratejileri geliştirmek olduğunu vurgulamıştır. Bu çalışma için kasın performans kriterleri kontrol edilebilirlik, servis ömrü ve uygulanabilirliği olarak belirlenmiştir. Amaca yönelik kas karekterizasyonu ve kontrolü için kullanılmak üzere bir kas test aparatı tasarlanmış ve üretilmiştir. *Rana esculenta* kurbağasının *gastrocnemius* kası karakterize edilmiş ve modellenmiştir. Modeller daha sonra kontrol algoritmalarının geliştirilmesi ve testi için kullanılmıştır. Sonuç olarak uyarı sinyali parametrelerinin kas mekanik cevabı üzerindeki etkisi literatürdeki veri ile tutarlı olarak ölçülmüştür. Kontrol çalışmaları ardışık kısa süreli kasılmalar için başarılı olmuş ve kas dokuları 35.5 saat fonksyonel kalmıştır. Bu neticeler kas dokusunun eyleyici olarak kullanıldığı sistemlerin geliştirilmesindeki avantajları ve zorlukları gösteren genel bir perspektif çizmiştir. Mevcut disiplinler arası yaklaşım birtakım mekanik hareketlendirme problemlerine umut verici çözümler sunmakta ve özellikle medikal alanda, biyo-mekatronik protezlerin ve biyo-mekatronik robotların geliştirilmesinde yeni imkanlar ortaya koymaktadır.

TABLE OF CONTENTS

LIST OF FIGURES

LIST OF TABLES

LIST OF SYMBOLS/ABBREVIATIONS

A_i	Activation rate
ACSA	Anatomical cross-sectional area
CE	Contractile element
d	Delay
f	Frequency
F_{Active}	Active force
F_e	Force at end of stimulation
F_L	Force measured by the load cell
F_i	Fatigue rate
F_{max}	Force when all fibers activated
F_p	Peak force
FES	Functional electric stimulus
$N_i^{fib\ A}$	Number of active fibers
$N_i^{fib\ F}$	Number of fatigued fibers
$N_i^{fib\ R}$	Number of fibers in rest
$N^{fib\ 0}$	Total number of fibers
PCSA	Physiologic cross-sectional area
PE	Parallel elastic element
pw	Pulse-width
R_i	Recovery rate

SOL	*Soleus* muscle
SE	Serial elastic element
V_{adj}	Adjustable voltage
V_L	Voltage output of load cell.
T	Period
T_i	Inter-stimulus duration
T_s	Stimulation duration
TA	*Tibialis anterior*
τ	Fatigue time constant

1. INTRODUCTION

Developing advanced techniques in mechanical actuation has a vital role in achieving technological goals in science and engineering. Although conventional mechanical actuators meet the requirements of majority of engineering applications, some recent applications require more efficient and light-weight actuators with an application-feasible energy source. Limitations of conventional actuation methods, namely, "electro-mechanical, hydraulic, pneumatic etc." seriously hinder technological advancements in many different fields, thus emphasizing the need for innovative actuators. As an example in wearable robotics current actuation methods have an adverse effect on widespread and successful introduction of advanced products in society due to their low performances/features such as low torque to power density, low efficiency, backlash and noise, and low accuracy [1]. For aerospace applications a light-weight, simple and reliable actuator is in strong demand to replace bulky hydraulic actuation systems in aircraft. In some medical applications such as micro medical robotics, developing micro-scale actuators which are powered without external power source is a requisite to manufacturing micro robots for explorations within biological domains or drug delivery [2]. To cope with the aforementioned problems revealed by conventional actuators, various advanced methods have been presented in the literature previously such as piezo-electric, shape memory alloys (SMA), polymer, magnetostrictive and electro-static actuators which have certain strengths and weaknesses regarding the application [3]. Although these artificial actuators present effective solutions a bio-actuator has some advantages and outperforms them especially in biomedical applications. Although research on bio-actuators have recently accelerated and demonstrate promising results, it is still an open field for research and requires much more accumulation of knowledge to be able to solve complex problems. Nevertheless bio-actuators will enable us to develop and design adaptive and robust bio-mechatronic robots and prosthesis in the future [4]. Bio-hybrid actuators will be a key component of machines which safely and smoothly interact with the surrounding environment and people [5].

The aim of this thesis work is to investigate performance and feasibility of muscle cell based macro scale bio-actuator and to acquire essential knowledge in bio-mechatronic system design. This work is performed with the scope of using bio-actuator in robotic applications which is functioning *in-vitro*. Regarding the aims of the thesis, goals are divided into two essential categories as performance and feasibility assessment and acquiring experiences in bio-mechatronic systems design. Performance and feasibility assessment is accomplished in three subcategories by discussing mechanical output limits, controllability, and life cycle. Experiences in bio-mechatronic systems design is acquired by applying and developing methods in muscle stimulation, muscle mechanical output measurement, tissue to mechanical and electronic systems integration and maintaining muscles in *in-vitro* conditions.

One of the missions of this thesis is to show that, building a machine which is actuated by live muscle tissue is possible. Despite the advantages of such system explained in following sections, it has many challenges and engineering problems to be solved. First of all muscle is a live tissue which needs certain ambient conditions to be maintained such as temperature, PH, ion concentration, presence of nutrition, and preferably, presence of antibiotics; briefly, conditions similar to *in-vivo*. The neuro-muscular system has a fascinating physiology for muscle stimulation and control. Currently we are not able to mimic the system completely because of the technological limitations, that results in a worse muscle control performance for bio-actuator applications. Regarding these limitations it is obvious that developing a commercially accepted bio-mechanic robots and prosthesis is a goal for the future. However this thesis presents a preliminary work for developing such machines and a motivation for the subject. To achieve project goals thesis work is conducted in several essential steps as follows.

1. Gaining fundamental knowledge on muscle behavior under *in vitro* stimulation.
2. Selecting source of muscle tissue for experiments and gaining experience on specimen removal techniques.
3. Designing and manufacturing an experimental setup for muscle testing. Designing tissue-to-electronics and tissue-to-mechanism interfaces.
4. Characterizing muscle tissue via open loop stimulation protocols.
5. Developing mathematical system models.
6. Closed loop contraction force control of muscle.

7. Assessment of performance criteria.

In Section 2, fundamental knowledge on skeletal muscle physiology and muscle mechanics are given. Section 3 gives previous achievements in bio-mechatronics, muscle stimulation, modeling and *in-vitro* muscle testing. Section 4 includes experimental methods, thesis goals, materials, and information about experimental setup. Theoretical work and mathematical models are presented in Section 5. Results of the experiments and models are given in Section 6. As a conclusion performance, advantages and disadvantages of bio-actuator are discussed in detail for various applications in Section 7. Appendix A gives the medical terms and jargon. Appendix B gives brief information about electronic hardware and sensors. In Appendix D some of the MATLAB codes are given which were used in this thesis.

1.1. Bio-Actuators

A bio-actuator is defined as the biological element generating mechanical movement in an artificial electro-mechanical / mechanical system. The research is conducted under the interdisciplinary field named as bio-mechatronics which integrates mechanical elements, electronics and parts of biological organisms encompassing robotics and neuroscience. Most of the bio-actuators presented in the literature are muscle cell based structures integrated in MEMS (Micro Electro Mechanical Systems). Micro scale bio-mechatronic system architecture includes muscle cells cultured on micro mechanisms while macro scale systems are actuated via muscle tissue or whole muscle organ removed from an animal. Here, in this thesis “bio-mechatronic device” term is used to define the mechatronic system actuated by live biological elements.

1.1.1. Advantages and Disadvantages of Bio-Actuators

Muscle tissue is a perfect mechanical actuator which presents outstanding advantages in certain applications and may allow the rise of new generation machines, with life like movements. Despite the wide range possibilities of artificial actuators muscle tissue presents better performance especially concerning inertia, back-drivability, stiffness control

and power consumption [5]. Muscle tissue undergoing hypertrophic and hyperplastic growth is able to conform to changes in power needs [4, 5]. It can modify itself as a function of imposed stresses and strains and is able to repair itself [5]. The fuel it consumes is glucose which is a renewable energy source that has environmentally compatible waste products [4] thus, does not require an external power source for *in-vivo* applications [2].

In the Table 1.1 a comparison of muscle and artificial actuators is given [3]. Muscle has the highest efficiency, strain, life cycles and lowest density as shown in the table. However the stiffness, contraction stress, peak power, energy density is lower than the artificial actuators. Muscle tissue can only function if proper ambient conditions are maintained that keep cells alive thus they are not suitable for extreme environmental conditions. Also developing muscle actuated bio-mechatronic systems require greater challenges in science and engineering [4]. Here a general overview of advantages and disadvantages of muscle cell based bio-actuators is given.

Tabel 1.1 Comparison of muscle with artificial actuators [3]

Class	SubClass	Example	Density kg/m^3	Stress MN/m^2	Stiffness GN/m^2 Δ	Strain %	Strain rate s^{-1}	Power W/kg	Energy kj/m^3	Life Cycles	Eff %
Muscle	Skeletal	Human	1.037	0.35	0.06 5	>40	5	>100	0.8	$>10^9$	>35
	Cardiac	H.heart	1.037	0.1	0.05 5	>40	4	>100	0.8	$>10^9$	>35
Piezo-electric	Ceramic	NEPEC-10	7.5	35	40 11	0.09	>10	>1000	>10	$>10^8$	>30
	Polymer	PVFD	1.78	3	3 >1.2	0.1	>1	>100	>1	$>10^6$	<1
SMA	NiTi	Fiber	6.45	>200	78 3	>5	3	>1000	>10	$>10^5$	>3
Polymer	Gel	PVA-PAA	~1.3	0.3	<0.1 10	>40	0.1	>5	0.4	$>10^5$	30
	Conductin	Polyanilin	~1.5	180	5 1.7	>2	>1	>1000	>1	$>10^5$	>30
Magneto Strictive	Rare-earth	Terfenol-D	9.25	70	35 1.4	0.2	1	>1000	>10	$>10^5$	<30
Electro-Static	Polyimide	SVCMA	1.061	0.04	<0.01 ?	>10	>1	>10	1	?	>20

2. SKELETAL MUSCLE PHYSIOLOGY

2.1. Gross Anatomy

Muscle is a soft tissue which functions to produce force and motion. In the body muscle is responsible for maintaining and changing posture, locomotion and movement of internal organs. Muscles are divided into three types namely skeletal (striated), cardiac and smooth muscles. Although all muscle types are similar in a micro-anatomical point of view, only skeletal muscle will be reviewed in this section since skeletal muscle is chosen as an actuator in this thesis for which the reason will be explained in the following chapters.

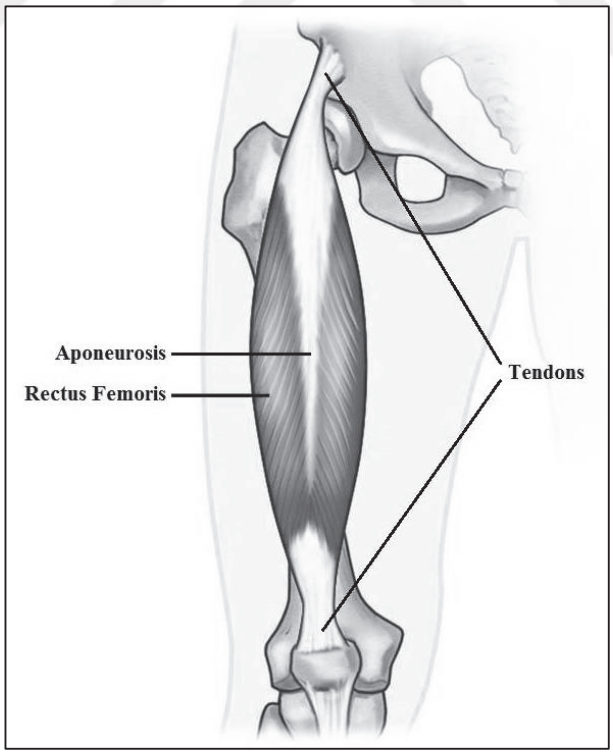

Figure 2.1 Rectus femoris and connective tissue **[7]**

Muscle is made of fibers and each fiber is named as muscle cell. Fibers are located in fascicle which is a connective tissue gathering all fibers into a bundle as a muscle organ. Skeletal muscle fibers are connected skeletal system through *aponeurosis* and *tendons*. The concept is shown in Figure 2.1. *Aponeurosis* is a connective tissue that connects muscle fibers to skeletal system or other tissues. In musculoskeletal system *aponeurosis* is connected to joints via *tendos*. Muscles crossing only one joint are named as *mono-articular* muscles while muscles passing through more than one joint are named as *multi-articular*. Muscle fiber and connective tissue architecture has differences among various muscles and species. These architectures may be divided into two basic categories regarding the fiber structural arrangement, namely fusiform and pinnate. Fusiform muscles are wider cylindrical in the middle and tapered through the *distal* and *proximal* ends which the fibers are arranged parallel to the muscle longitudinal axis. Unlike fusiform muscle with parallel fibers, pinnate muscles are oriented with an angle (pennation angle) to the longitudinal axis of muscle and connected to *aponeurosis.* An example of pinnate muscle is *Rectus Femoris.* The pennation angle can be seen in Figure 2.2.

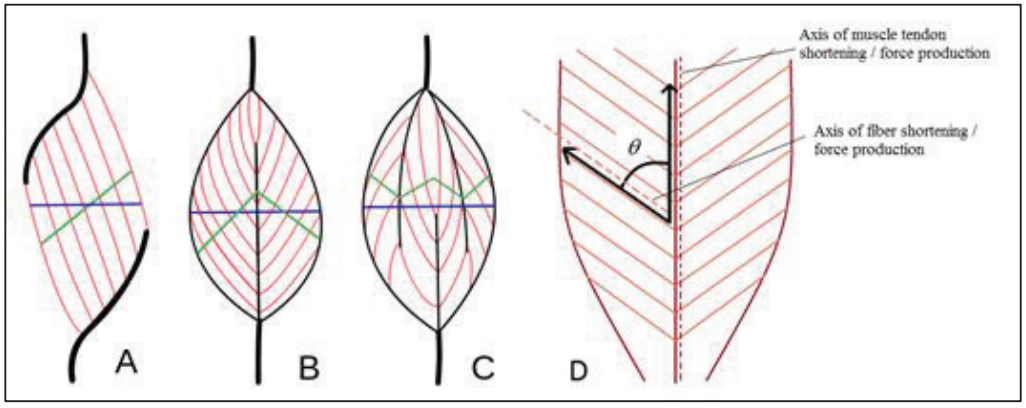

Figure 2.2 Pinnate muscle, (a) Unipennate, (b) Bipennate, (c) Multipennate, (d) pennation angle PCSA green lines, ACSA blue lines **[7]**

Pinnate muscles have different patterns as shown in Figure 2.2. If all fibers are parallel to each other (not parallel to longitudinal axis) the muscle is called as unipennate (a). If muscle is divided into halves by a central *aponeurosis* it is called as bipennate (b). For the

muscles divided into more than one part it is called as multipennate muscle (c). Physiologic cross-sectional area (PCSA) is defined as the area of the cross section of a muscle perpendicular to its fibers. PCSA has a significant role to calculate muscle contraction properties. Anatomical cross-sectional area is the cross-sectional area (ACSA) of a muscle cut by transverse plane of muscle organ. In Figure 2.2 green lines indicate PCSA and blue lines indicate ACSA. PCSA is basically calculated by Equation. 1.1 for parallel (fusiform) muscles and by Equation 1.2 for pinnate muscles.

$$PCSA = \frac{m}{dl} \tag{1.1}$$

$$PCSA = \frac{m}{dl}\cos\theta \tag{1.2}$$

Where, **m** is muscle fiber mass, **d** is muscle fiber density, **l** is the muscle fiber length and **θ** is the pennation angle. Pennation angle increases with shortening muscle [6].

2.2. Muscle Morphology

Skeletal muscle is a combination of smaller power generating units integrated into a larger scale. Whole muscle is surrounded by *epimysium* which is a connective tissue. *Epimysium* consists of collagen fibers, connective tissue cells and fat that are distributed irregularly. *Fascicle* is a smaller muscle bundle and surrounded by *perimysium* similar to *epimysium*. In *fascicle* muscle fibers are located. A muscle fiber is considered as a muscle cell. *Facia* isolate muscle fibers electrically from the ones located in other fascicles but does not isolate mechanically. In Figure 2.3 morphology of muscle is shown.

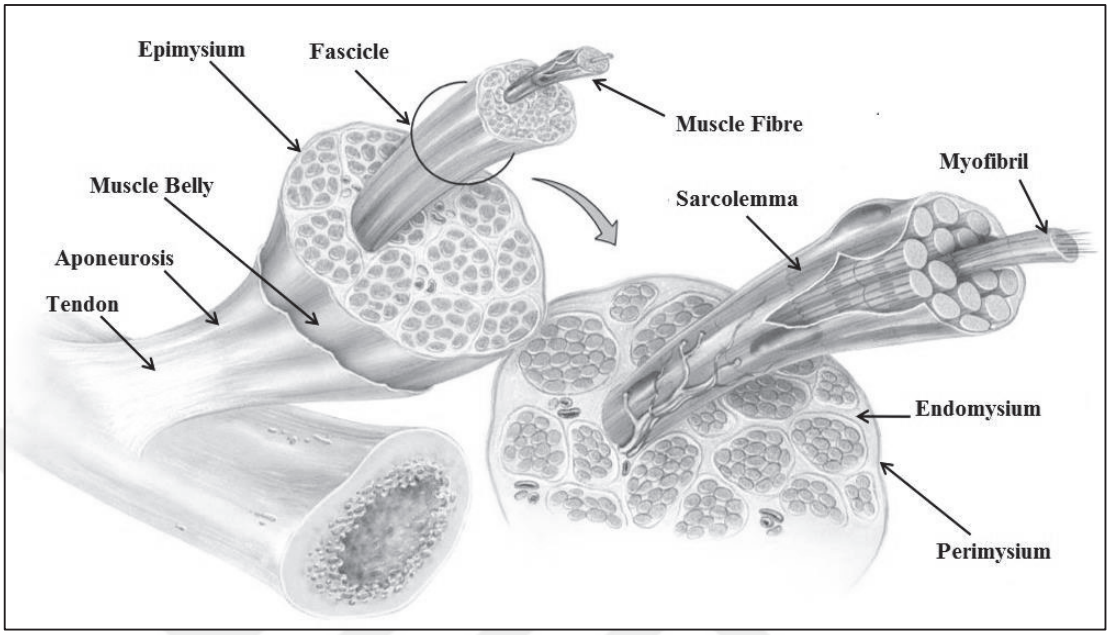

Figure 2.3 Muscle morphology **[7]**

2.2.1. Morphology in Micro Level

Myofibril is a composition of serially located *sarcomeres*. *Sarcomere* is the basic contractile unit in muscle and placed between two z-discs. Figure 2.4 shows a detailed view for a *sarcomere*. In *sarcomere* two proteins namely *actin* (thin filament) and *myosin* (thick filament) are located in parallel. These proteins are the key elements for generating the contraction which the contraction process will be explained in detail following this section. *Sarcomere* is divided into zones as shown in (b). A band covers the overlapping zones and H zone where no *actin* filaments present. I band is the place where *myosin* filaments is not present. M line divides *sarcomere* into two halves. *Titin* protein mechanically connects *myosine* protein to the Z disc.

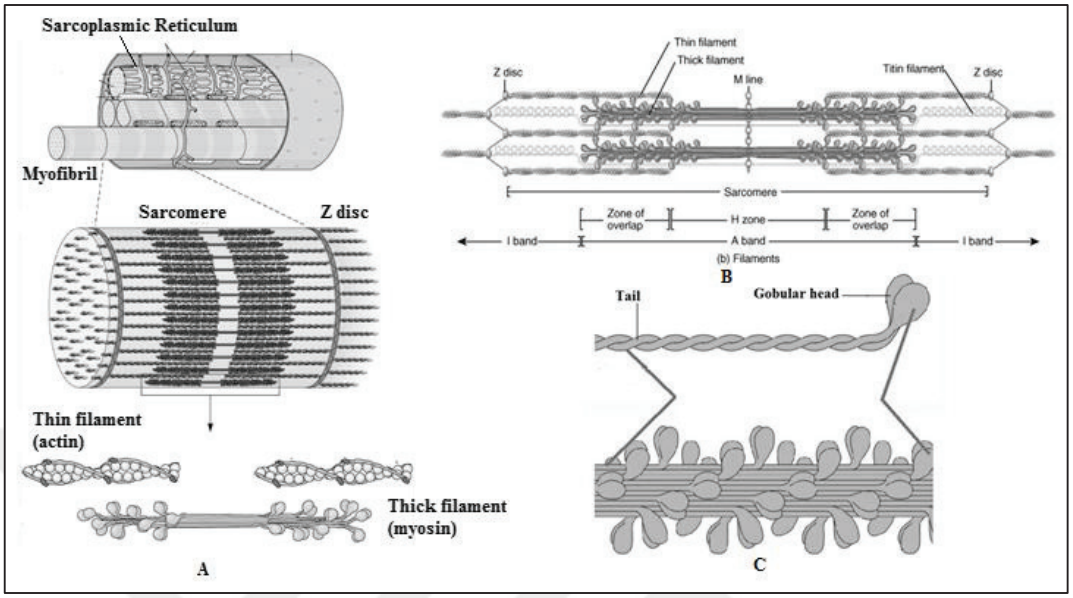

Figure 2.4 (a) Detailed view of sarcomere, (b) Filaments, (c) Thick Filament **[8]**

Sarcoplasmic Reticulum may be separated into two parts namely longitudinal and transverse tubules and surrounds myofibrils as shown in Figure 2.5. Longitudinal tube forms two *lateral sacs* (outer vesicles) near Z-discs. These lateral sacs and transverse tubule are named as *triad.* Transverse tubules are indentations of cell membrane and *sarcolemma* which are going deeply into muscle fiber.

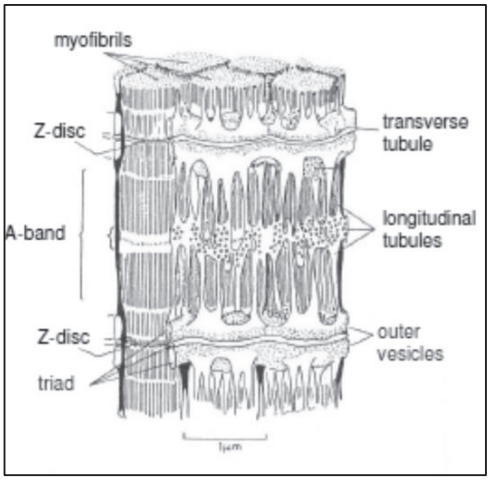

Figure 2.5 Tubular system **[8]**

2.2.2. Connection between Nervous System and Skeletal Muscle

Skeletal muscles are capable of contracting voluntary. The activation process requires an activation signal from nervous system. Muscle that is integrated with nervous system is called as neuromuscular system. Figure 2.6 shows a schematic for muscle nerve connection. A single motor neuron connects many muscle fibers of same type. Exact number depends on the size and function of the muscle. The connection point is named as motor end plate as shown in (c) [9].

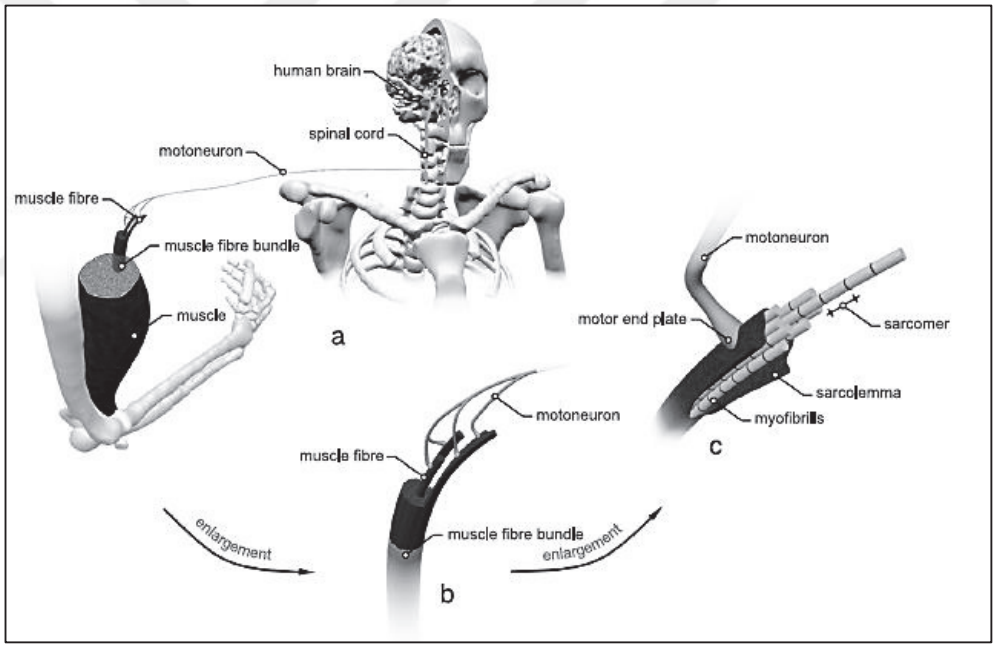

Figure 2.6 Connection of nervous system to muscle **[9]**

2.3. Muscle Mechanics

2.3.1. Mechanisms of Muscle Contraction

Process of muscle contraction starts with several electrochemical reactions on cell membrane triggered by the signal from nervous system which depolarizes muscle fiber. If the certain threshold is exceeded action potential occurs and spreads over *sarcolemma* in wave-like manner. The action potential passes through longitudinal tubules of each *sarcoplasmic reticulum* which are connected each other via *triads* and through transverse channels as well. Sacs are the storages of Ca^{2+} and have voltage-controlled Ca^{2+} channels. As action potential passes through *sarcoplasmic reticulum* calcium permeability increases and Ca^{2+} is released into *sarcoplasm.*

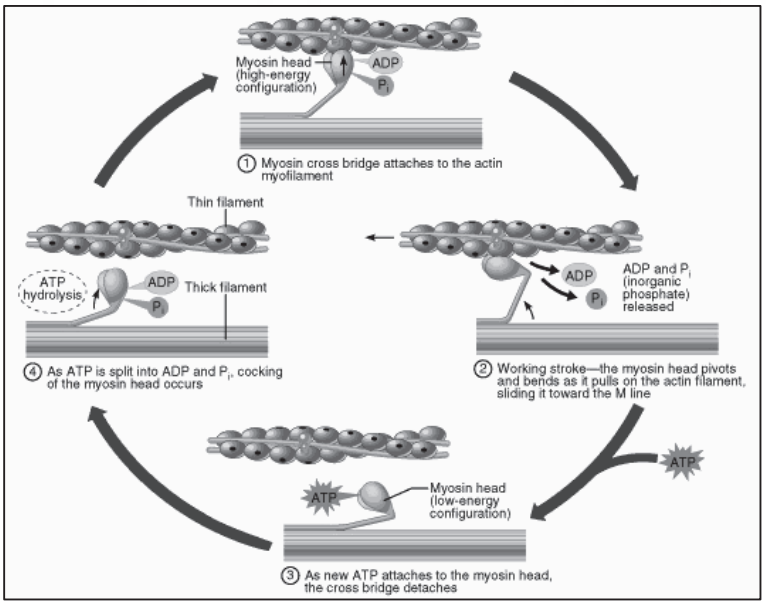

Figure 2.7 Sliding filament theory **[7]**

The power cycle is shown in Figure 2.7 with steps. *Myosin* head attaches to the *actin* myofilament and forms cross bridges (1). *Filaments* slides wrt. each other due to the pull-force applied by cross head by releasing ADP and phosphate (2). New ATP molecule

attaches to *myosin* head and cross bridge detaches (3). At this state *actin* binding sites are blocked by *troponin* molecule and cross head (*globular* head) is not connected to actin filament (3). Calcium ion binds to *troponin* which changes its orientation exposing the binding site for *globular* head. Hydrolysis of ATP splits to ADP and phosphate and cocking of *myosin* head occur (4). Then, the new power cycle begins. As a result *actin* filaments move in the medial direction towards the M line which reduces the H zone. The resultant tensile force of *sarcomere* depends on the length of H zone. If *actin* filaments are apart from the M line (large H zone) or overlapping each other (small H zone) the contraction force is less than the optimum length where the H zone length is in the middle of these two extremities. This muscle contraction theory is called as sliding filament theory [10, 11].

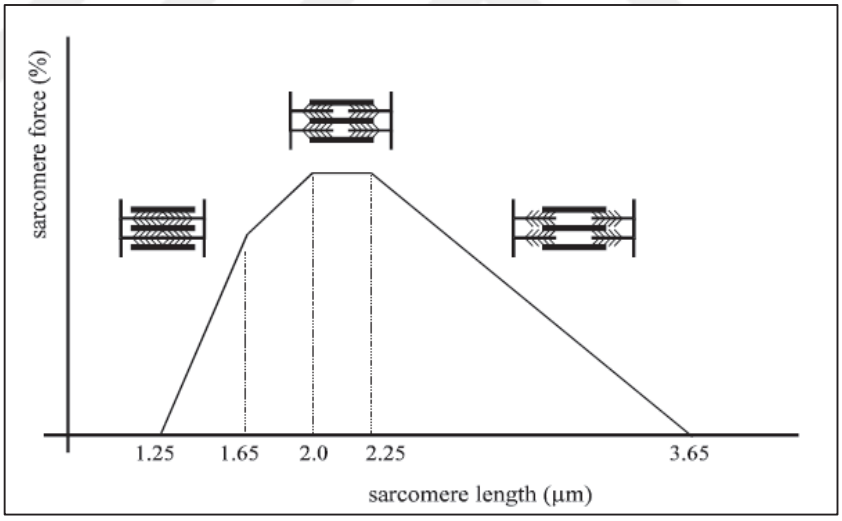

Figure 2.8 Sarcomere length, force characteristics **[12]**

In Figure 2.8 contraction force for different *sarcomere* lengths is shown. For small *sarcomere* lengths *actin* filaments overlap each other and the number of binding sites is decreased that results less contraction force. Similarly for larger *sarcomere* lengths the number of binding sites is decreased since they are moving apart from the cross-heads which also decreases the contraction force. Briefly a calcium signal is necessary for contraction and the calcium signal is triggered by electric potential between intercellular and extracellular space called action-potential. In literature most studies in muscle

mechanics defines the muscle length where the muscle has the highest contraction force as optimum muscle length.

2.3.2. Macro Scale Muscle Contraction

In Figure 2.9.a phases of action potential are given. As stated previously action potential is the initial signal which triggers the contraction process; thus, calcium signal and contraction force increases. While the electric potential decaying to its resting state voltage sensitive *sarcoplasmic reticulum* collects calcium ions and reduces the Ca^{+2} concentration in intercellular space. Eventually the contraction force decreases within the absence of Ca^{+2}. Figure 2.9.b shows time varying electric potential, calcium signal and the twitch force caused by single action potential. The contraction type shown below is induced by single action potential which is called as twitch.

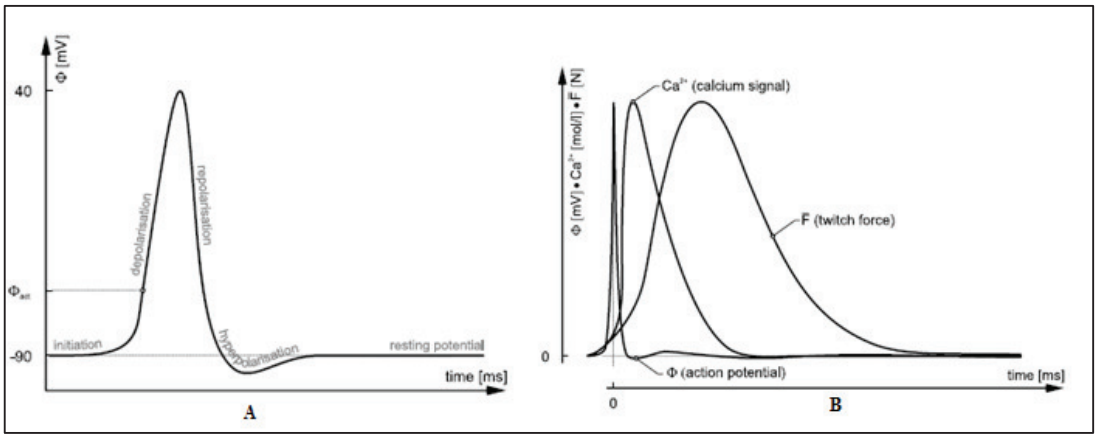

Figure 2.9 (a) Phases of action-potential, (b) Calcium signal and twitch **[9]**

If the frequency of action-potential increases the intracellular Ca^{+2} concentration is increased by the next action potential before the Ca^{+2} is not completely settle to its resting state. Thus Ca^{+2} concentration increases as a summation and the force increases as well. Briefly if the second twitch starts before the first one is over they sum up and resultant force is greater than a single twitch. If train of stimulus is given, twitches are superimposed

at stimulation frequency and the total force reaches to a steady magnitude. This type of contraction is called as unfused tetanus for which ripples caused by twitches is observed (shown in Figure 2.10). If the frequency increases the magnitude of ripples decrease and disappear eventually. The type of contraction where no ripples are present is called as tetanic fusion (tetanus). At tetanus, maximum force is reached which cannot be increased anymore with increasing the stimulation frequency. In Figure 2.10 twitch, unfused tetanus and tetanus are shown. These contraction behaviours of muscle as an organ are same as the fiber.

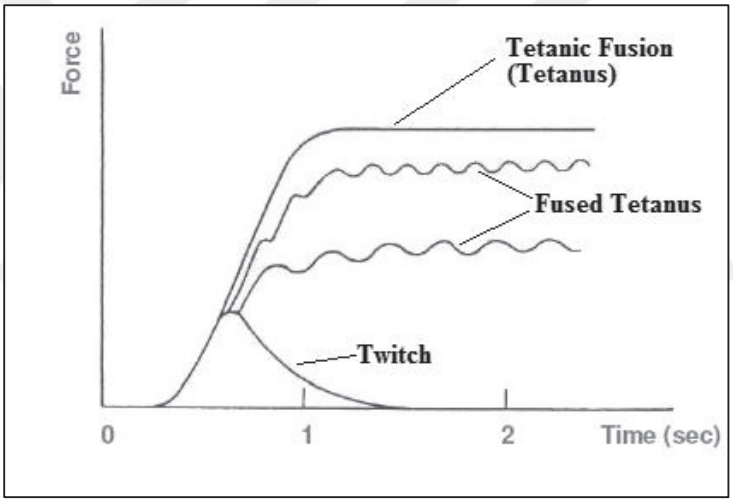

Figure 2.10 Contraction Types **[7]**

In the live organism skeletal muscles go under contraction with different mechanical boundary conditions. Skeletal muscles are both responsible for movement and maintaining posture.

Contraction types are divided into two namely; isometric and isotonic.

Isometric: Contraction force varies but muscle length remains constant (posturing)
Isotonic: Muscle length varies but contraction force remains constant (lifting a weight)

2.3.3. Muscle Fatigue

Muscle fatigue is considered as temporary reduction in force generation capability of muscle. One of the reasons for muscle fatigue is the scarcity of energy sources inside the muscle after contracting at high workloads such as tetanic activations [13]. The other reason is the accumulating metabolites in muscle which interact with Ca^{+2} ions or hinders the ability of Ca^{+2} to stimulate muscle. Muscle fatigue occurs in the fiber level. A muscle fiber may be fatigued, active or recovering. Muscle fatigue is not only dependent to workload but also dependent on muscle fiber type. Muscle fibers are divided into two main categories as red muscle fibers and white muscle fibers. The color to red muscle fiber is given by higher content of *myoglobin* which is capable of binding, storing and releasing oxygen. It promotes rapid diffusion of oxygen for high demands. Thus they have aerobic based metabolism. Red muscle fibers are further divided into two subcategories namely fast twitch fibers and slow twitch fibers. Slow twitch fibers are fatigue resistant, have less twitch peak and longer twitch times. Fast twitch fibers can contract more quickly but moderate in endurance type performances. White muscle fibers have anaerobic based metabolism. They can contract very rapidly and produce large forces but they fatigue easily. Table 1.2 shows the differences between fiber types Type I, Type IIA and Type IIX (red slow, red fast, white muscle fibers respectively)

Table 2.1 Comparison between fiber types **[7]**

Properties	**Type I fibers**	**Type IIA fibers**	**Type IIX fibers**
Motor Unit Type	**Slow Oxidative (SO)**	**Fast Oxidative/Glycolitic (FOG)**	**Fast Glycolitic (FG)**
Twitch Speed	Slow	Fast	Fast
Twitch Force	Small	Medium	Large
Resistance to fatigue	High	High	Low
Glycogen Content	Low	High	High
Capillary Supply	Rich	Rich	Poor
Myoglobin	High	High	Low
Red Color	Dark	Dark	Pale
Mitochondrial density	High	High	Low
Capillary density	High	Intermediate	Low
Oxidative Enzyme Capacity	High	Intermediate-high	Low
z-Line Width	Intermediate	Wide	Narrow
Alkaline ATPase Activity	Low	High	High
Acidic ATPase Activity	High	Medium-high	Low

3. LITERATURE SURVEY

Development of a bio-mechatronic device requires a similar design procedure with any conventional dynamic system. Acquiring knowledge about the available actuator is the first prerequisite to design such systems. Thus, in this section previous studies are presented in an order according to the development/design process. First, studies on bio-mechatronic devices are presented. Secondly previous studies for muscle stimulation and characterization are given. Then some mechanical and electro mechanical muscle models are presented. As a final part of this chapter, studies on muscle control and *in-vitro* experiments are presented. In following chapters information about previous researches and methods will be given regarding the subject as required.

3.1. Biomechatronic Devices

Current research on bio-actuation aims to develop robust and feasible bio-mechatronic systems; yet there is no such commercial product available currently. However researchers have noticed the advantages of machines actuated by biologic elements such as muscle cell/tissue, and presented several proof of concepts to give a perspective for future studies. Research on muscle-cell based bio-actuators and integrated devices are mainly conducted in two different scopes due to their order of scales. A micro scale muscle-cell based bio-mechatronic device is the hybrid system driven by cultured muscle cells. In studies where macro scale bio-mechatronic systems are presented, muscle cells are cultured to fabricate muscle tissue or whole muscle organ is isolated from animal. Currently micro scale applications have a larger place in the literature.

One of the examples for micro scale bio-mechatronic devices is the bio-micro pump, driven by previously frozen *cardiomyocytes* [14]. In the study cultured thin *cardiomyocite* sheet contracts and actuates mechanism made of PDMS in a microchip and sets fluid in motion. This bio-micro-pump has a significant advantage compared to previously developed microfluidic devices since bio-micro-pump does not require any external energy

source for *in-vivo* applications such as electricity. These systems may be used as implants for example an insulin pump releasing insulin due to glucose concentration in body or as physiological models for circulatory system as well as for medical diagnoses [14]. The development of mammalian skeletal muscle strip actuated, hydrogel robot (bio-bot) is reported in [15]. Bio-bot has an asymmetric geometry and has a strip of muscle cells on one side. Muscle tissue is stimulated via bi-polar electric signal which induces the action potential and contracts the muscle, strip causing a crawling motion of bio-bot. In studies [2, 5] overview for muscle actuated micro-bio-systems are given.

A macro scale bio-mechatronic device is presented by [4]. The study presents a proof of concept on developing macro scale bio-mechatronic devices. In the study a swimmer designed which has a tail driven by a pair of *semitendinosus* muscles isolated from frog (*Rana pipiens*). The concept is shown in Figure 3.1. Muscles (M) are connected to tail (T) at connection points (s) and the tail is connected to main chassis (D) with pinned joint at point (a).

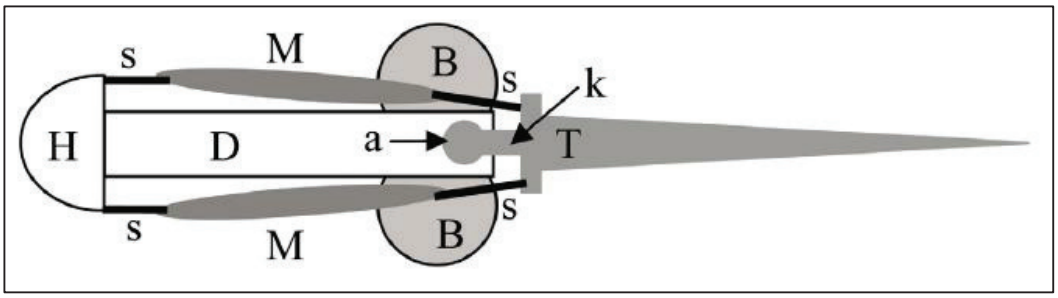

Figure 3.1 Bio-mechatronic swimmer [4]

Muscles are stimulated via alternating bipolar square wave electric pulse train. To control the speed or for steering duration of pulse train is adjusted from remote controller via infrared sensor on the bio-mechatronic device. For stimulation, wire type electrodes are looped around *distal* and *proximal* ends of muscles. Swimmer is controlled by open loop stimulations. The swimmer is capable of making basic maneuvers such as strait line swimming and turning, with adjustable speed. The robot remained active for 42 hours with

maximum speed of 1/3 of its body length per second. The study lists some failure modes for muscles functioning *in-vitro* as given below.

- Core necrosis due to lack of oxygenation/capillary perfusion and large diffusion distances
- Sepsis
- Exogenous toxicity
- Electrochemical damage resulting from excessive electrical stimulation
- Accumulated contraction-induced injury
- Sarcomeres heterogeneity leading to loss of thick and thin filament overlap in regions of muscle fibers exacerbated by prolonged periods at or above the optimal length.
- Direct mechanical damage to the muscle from external sources, such as the robot frame, attachment hardware, or electrodes.

3.2. Muscle Stimulation and Mechanical Response of Electrically Stimulated Muscles

Muscle stimulation has been investigated for many years and many achievements have been acquired up to now. Most of these are conducted for physiological studies, diagnosis and physiotherapy [16]. Muscle can be activated by two ways either by chemical activation [17, 18] or electrical activation [4, 19, 20, 21, 22].

One example for chemical stimulator is *acetylcoline.* It behaves as an excitatory neurotransmitter at neuromuscular junctions in skeletal muscle [7]. Muscle is contracted in the presence of *acetylcoline* [17] however it must be removed from ambient if the contraction has to be terminated. This thesis focuses on muscle stimulation with electric signal, the reason for which is explained in following chapters.

Electrical stimulation has mostly been made by polar or bi-polar rectangular wave signal. Although rectangular waveform for stimulation signal is the most common for electrical stimulation, there are some studies with sinusoidal waveform. As an example in [23], it is shown that sinusoidal waveform stimulation prevents muscle atrophy of deeper layers

while rectangular waveform is effective only on preventing muscle atrophy of superficial layers for an electric stimulation therapy. In the following section effect of rectangular wave stimulation signal parameters on isometric contraction force is given.

3.2.1. Frequency Effect on Isometric Contraction Force

As stated in previous chapter an impulse (one action potential) generates a twitch contraction of muscle and as the frequency of action potential increases muscle generates fused tetanus or tetanus. Muscle as a whole organ actuated by artificial electric signal has the same behavior of a single fiber. In [22] isometric contraction force of *soleus* (SOL) muscle of mice is measured *in-vitro*. Contraction force is plotted due to stimulation frequency, where stimulation amplitude and pulse-width are fixed (shown in Figure 3.2). For frequency of 5 Hz no tetanic contractions are induced. As the frequency increases, peak contraction force increases and the ripple amplitude decreases. Similar results on frequency effect are given by [21]. In the literature a limit for frequency is introduced named as "fusion frequency". Fusion frequency is defined as the frequency which yields a ripple amplitude of less than or equal to 10 per cent of peak force [24]. Tetanic fusion or fused tetanus is generated by summation of identical twitches. This type of force enhancement is named as temporal summation.

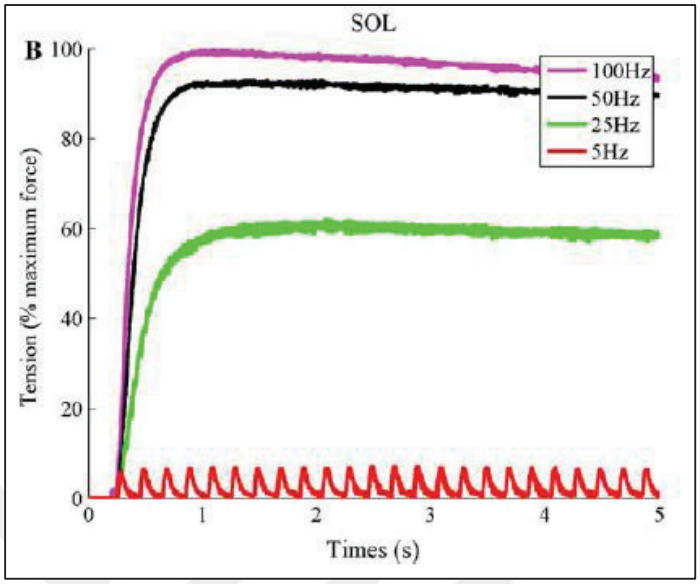

Figure 3.2 Effect of stimulation frequency on muscle ısometric contraction force **[22]**

3.2.2. Amplitude and Pulse Width Effect on Isometric Contraction Force

For an artificially stimulated muscle, number of activated fibers is dependent on the signal amplitude and pulse width. A stimulation signal having a larger amplitude or pulse width increases the transmembrane potential above the threshold for more inactive fibers, thus increases the number of fibers recruited. Briefly amplitude and pulse-width increases force by recruiting more fibers for contraction. In [21] isometric contraction force of *tibialis anterior* (TA) muscle of Wistar rat is measured *in-vivo* for various amplitudes and frequencies. Figure 3.3 gives the response of isometric contraction force due to signal amplitude and pulse width. Pulse-width recruitment curve is non-linear due to the uneven distribution, orientations, and innervation rates of motor axons in muscle [24].

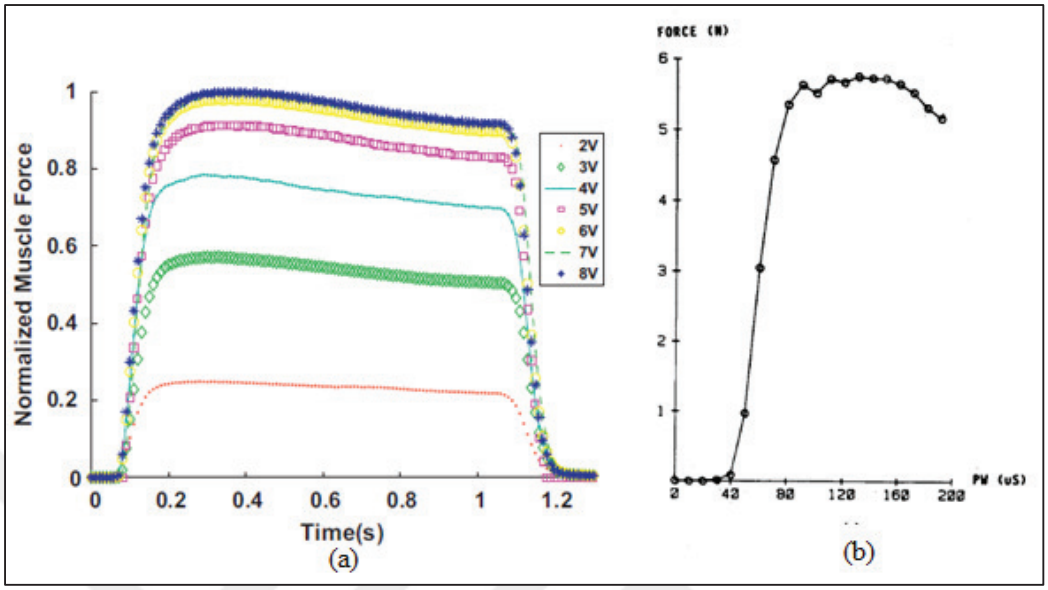

Figure 3.3 (a) Response of tetanic contraction to various signal amplitudes with fixed frequency (90 Hz) and pulsewidth **[21]**, (b) Effect of signal pulse widths on peak contraction values for constant amplıtude (9mA) and period (116 ms) **[20]**

The peak contraction force increases as the pulse-width increases up to a limit. This limit is the state where all the fibers are recruited. For signal amplitude the concept is the same and this threshold is named as full recruitment voltage ("full recruitment current" for current controlled stimulators). For example in the study by [19] stimulation signal applied at the full recruitment voltage.

3.3. Muscle Models

Many musle models have been developed previously. These models may be divided into three cathegories namely Hodgkin-like models [22] , Hill-type models [25, 26] and models based on continuum mechanics [27, 28]. Hodgkin-Huxley-like models describe the behaviour of muscle contraction on cellular level due to electro-physiological and biochemical principles, Hill-type models describe the mechanical behaviour of muscle using lumped-parameter models [29]. Continium based models mostly focuses on mechanics of muscle contraction and ignores the activities governing muscle contraction in cellular level such as cell membrane excitation and activation [28, 29] .

3.3.1. Hill Muscle Model

In [25] an equation (Equation 3.1) relating muscle contraction force and velocity is presented. It is an emprical based model.

$$(v + b)(P + a) = b(P_0 + a) \tag{3.1}$$

$$b = a\frac{v_0}{P_0} \tag{3.2}$$

Where; **a** is the coefficient of shortening heat, **v** is velocity of contraction, $\mathbf{P_0}$ is the maximum isometric contraction force generated in the muscle, $\mathbf{v_0}$ is the maximum velocity of contraction and **P** is contraction force [7]. To develop this model, Hill made quick release experiments on frog *sartorius* muscle. In the experiment muscle organ (whole muscle as bundle) is connected to test setup and both ends are fixed (isometric test). Then, muscle is stimulated and max. isometric force is measured. One end of muscle is released suddenly to a force **P** smaller than $\mathbf{P_0}$ and contraction velocity **v** is measured [8]. In Figure 3.4 schematic of experimental setup is given. The initial rate of shortening is calculated with the slope of the line shown below (Figure 3.4.a). The curve representing the velocity of shortening due to load **P** is given in Figure 3.5. Hill proposed a model which supports the equation. In this model the muscle is combination of three elements namely parallel elastic element (PE), serial elastic element (SE) and contractile element (CE). CE is identified as the active force generating element with the number of cross-bridges between actin and myosin elements. SE stands for the elasticity of actin, myosin proteins and cross bridges between them. PE stands for intermuscular connective tissues, cell membranes, collagenous sheets. Since CE is not capable of sudden length change SE is responsible from the sudden shortening $\mathbf{\Delta x_1}$ shown in Fig 2.4 and further length change is fully attributed to CE [8].

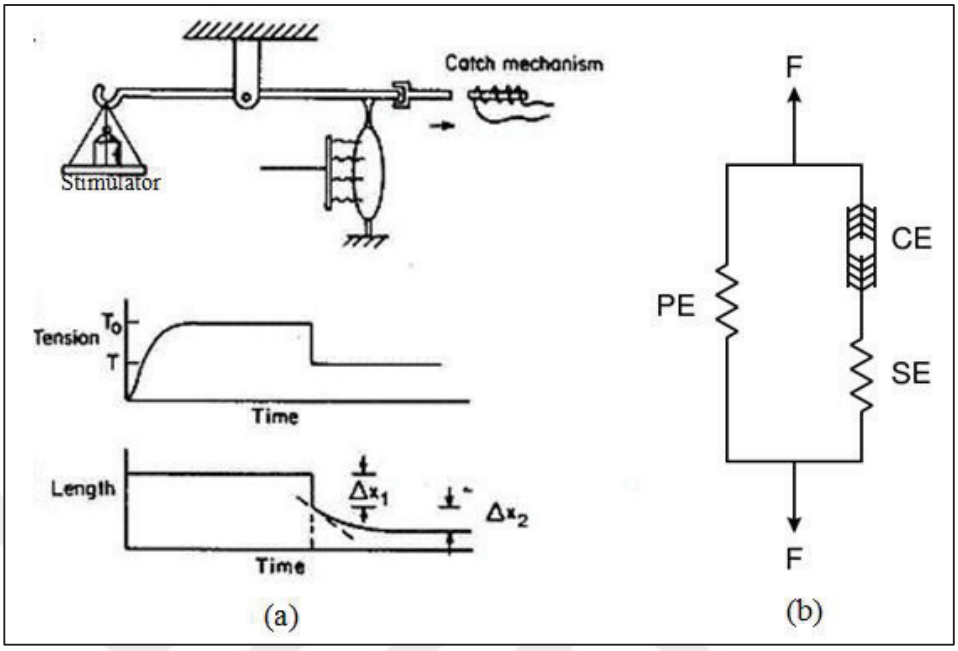

Figure 3.4 (a) Quick release experiment and measurements **[8]**, (b) Hill's muscle model **[7]**

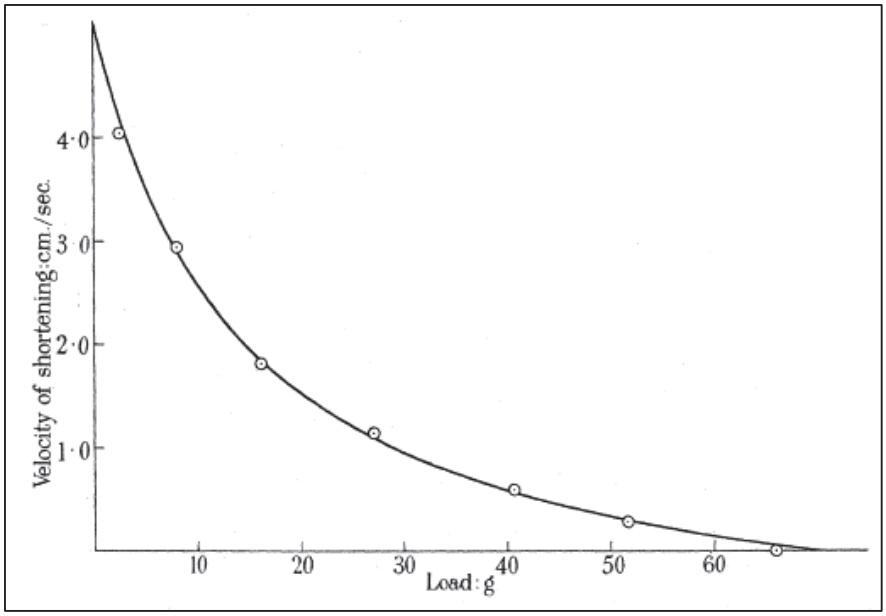

Figure 3.5 Velocity of shortening vs. Load **[8]**

3.3.2. Huxley or Cross-Bridge Model

A model proposed in [30] based on cross-bridges dynamics. When the muscle is stimulated, globular heads in the vicinity of an attachment site on actin filament is expected to attach that site. A tensile force is developed with the contraction of myosin elastic tails which were in the extended state as they were attached to sites. Thus, the displacement of the sarcomere is dependent on the number of cross-bridges involved. The model relates cross-bridges dynamics (number of attached cross-bridges, attachment and detachment rates) to contraction force and velocity. For details refer to [30].

3.3.3. Constitutive Models

First constitutive muscle models were considering a 1D formulation to describe the interaction between muscle, tendons and joints within the muscoskeletal system. However an appropriate model requires a 3D representation allowing a physical prediction of transversal and volumetric material response [31]. Some mechanical models describing contractile properties [27, 32, 33] and models describing electromechanical coupling in the skeletal muscle [9, 29, 34] are proposed.

Developing a bio-mechatronic device requires a coupled electromechanical model for muscle which relates the stimulation parameters to force enhancement and displacement. To exploit such model 3D architecture of fibers has to be obtained for finite element analysis (FEA). One of the methods for obtaining 3D structure of muscle is to measure the coordinates of points on single fiber using digitizers. With this method path and length of the muscle fiber may be obtained, however it requires much effort to digitize all fibers in a muscle organ. More accurate and easier method is to use magnetic resonance imaging (MRI) data to construct the geometry digitally [35].

3.4. Muscle Control

Many studies on muscle control presented previously which most of them have the particular interest of restoration functional movement of paralyzed and paretic people [36, 37, 38]. Although control strategies developed regarding biomedical applications for paralyzed people, they are also applicable for bio-mechatronic devices. However controller design for *in-vitro* bio-mechatronic devices has some additional challenges such as variations in system characteristics due to reasons referred in [4] (such as rapid muscle fatigue, sepsis etc.). There are very few studies in the literature which have a scope for *in-vitro* muscle control [19, 39].

Muscle control strategies are basically divided into three categories regarding the force generation method; named as control with recruitment modulation method [20, 24, 36, 37, 38, 40], temporal summation method [41] and controlling with both temporal summation and recruitment modulation [42, 43]. As mentioned previously recruitment modulation is the force generation method via adjusting the number of fibers involved in the contraction which the controlling variable may either be pulse-width or pulse amplitude. Temporal summation is the force generation by summing twitches with the same number of muscle fibers involved in the contraction. The controlling variable is the stimulus frequency (stimulation signal frequency) for temporal summation method.

In [42] isometric force of cat *soleus* (SOL) muscle is controlled *in-vivo* by both temporal summation and recruitment modulation methods. The isometric contraction force is controlled by both varying pulse-width and frequency simultaneously using a PI (Proportional and Derivative controller) controller. The aim of this strategy is to minimize muscle fatigue. Fatigue is minimized by stimulating the muscle with longest possible stimulus interval (stimulation period) which allows an adequately fused contraction and with minimum number of activated fibers that generates contraction force at desired level. Similarly in the study by [41] a PID (Proportional, Integral and Derivative controller) controller is presented to control cat *soleus* muscle for both isometric and isotonic contractions. This study introduces an open-loop non-linear compensator with PID controller. The controlling performance is compared for PID combined with non-linear compensator and PID only. PID combined with non-linear compensator improved

performance only if the model is accurate. If the modeling error is high non-linear compensator decreased the performance.

The study [24] presents and adaptive controller for the control of isometric force response of *Tibialis Anterior* (TA) muscle of cat *in-vivo*. A direct, minimum prediction error, one-step-ahead controller was implemented and pulse width is adjusted. An adaptive controller is found to be effective for electrically stimulated muscle due to its accuracy and stability.

In the study [44] contraction force of hand is controlled to regulate grasping. A fixed-parameter, discrete-time, first order, feedback control system is implemented. Both isometric and isotonic contraction are controlled which is aiming to achieve a constant stiffness of grasp (relationship between grasp force and grasp opening). Experiments conducted on quadriplegic patients and a robust control achieved.

In studies [20, 43] isometric contraction force of cat muscle is controlled. Studies consider a closed loop controller. In [20] pulse width is the controlling parameter while in [43] both pulse width and stimulus period are the controlling parameters. It is shown that controlling with both pulse width and stimulus period simultaneously improves the controller performance and results in a better control of transient responses than with pulse-width modulation alone.

3.5. *In-Vitro* Muscle Testing

In the literature most of the studies presented on muscle testing for physiological studies are conducted *in-vivo*. However many examples on *in-vitro* testing is present in the literature. Here an overview of studies and experimental setups used in these studies are presented. As mentioned previously, *in-vitro* muscle testing requires strictly controlled ambient conditions to keep muscle tissue alive and functioning.

One of the first *in*-vitro muscle experiments is conducted in [25] on frog *sartorius* muscle. In study [4] *semitendinosus* muscle of frog (*Rana pipiens)* is isolated with tendons. Specimen is connected to swimmer mechanism via surgical silk suture and placed into amphibian's ringer solution. Stainless steel electrode wire is wrapped around the specimen.

In another study [45] *Iliofibularis* muscle of *Rana proposa brevipoda* frog is isolated for a physiology study. Specimens are fixed to force transducer and servomotor, from both ends via fixing to metal hooks by cotton thread. The study aims to show the differences in muscle contraction for direct and indirect stimulation thus, specimens are stimulated from both nerve and directly on muscle bundle. Experiments conducted in circulated Ringer solution. In Figure 3.6 a schematic of experimental setup is given.

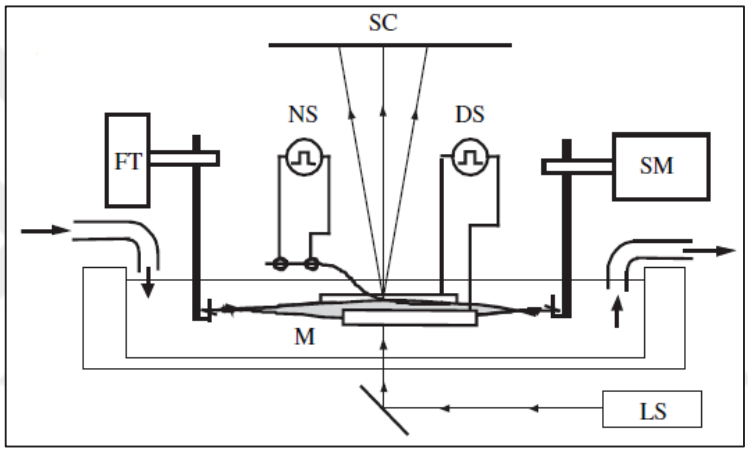

Figure 3.6 Experimental Setup **[45]**

In [19] an apparatus for *in-vitro* muscle testing is designed and manufactured. Apparatus is a test platform for many studies such as muscle mechanics, energetics, functional electrical stimulation (FES) and fatigue. Isolated muscle is connected to apparatus from both ends to servo motor and force transducer. Apparatus is able to generate various boundary conditions to muscle by controlling the servo motor movement, which moves one end of the muscle linearly. In the experimental setup muscle is also controlled thus, it has two control loops running simultaneously. Apparatus is suitable for isolated muscles in the length range of 15-25 mm such as muscles extracted from *Rana pipien* frogs namely; *semitendinosus, semimembranosus, platarus longus,* etc. Apparatus has a pool which circulates solution (ringer, krebs) and an insertion point for oxygen bubbling in the solution. In Figure 3.7 a photo of apparatus is given and in Figure 3.8 control loops are shown. This muscle testing apparatus is used in [39].

A similar apparatus is developed in [46]; however in this setup muscle force is not controlled. In the study *plantarus longus* muscle of *X.leavis* frog is isolated and tested to link the muscle output and hydrodynamics in a robotic perspective.

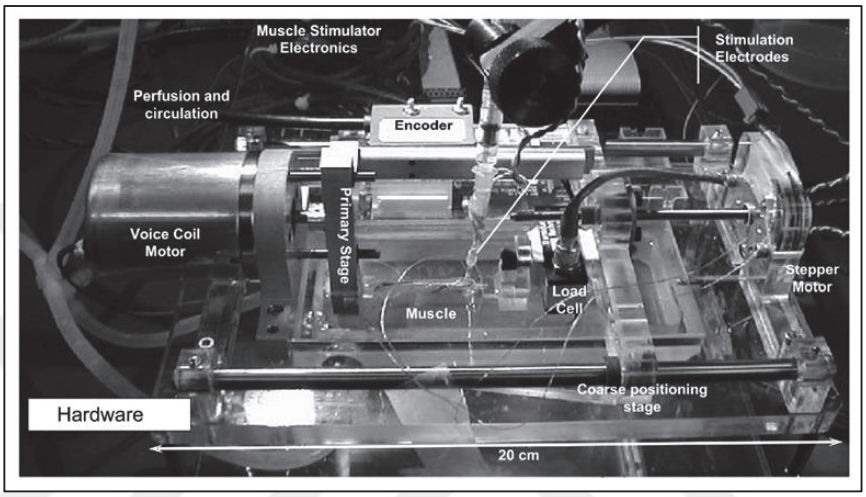

Figure 3.7 Muscle Testing Apparatus **[19]**

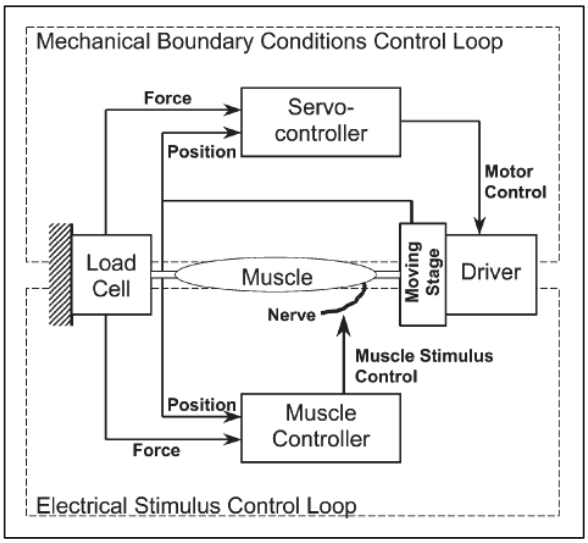

Figure 3.8 Control loops **[19]**

In the study by [47] *gastrocnemious* muscle of *Rana chensinensis* frog is isolated for model validation purposes. The specimen is hanged vertically where one end is connected to force transducer and the other is connected to dead weight. Muscles are submerged into ringer

solution as they are isolated and kept moistened during the experiment. Muscle is stimulated from *sciatic* nerve. In Figure 3.9 schematic and photo of the experimental setup is given.

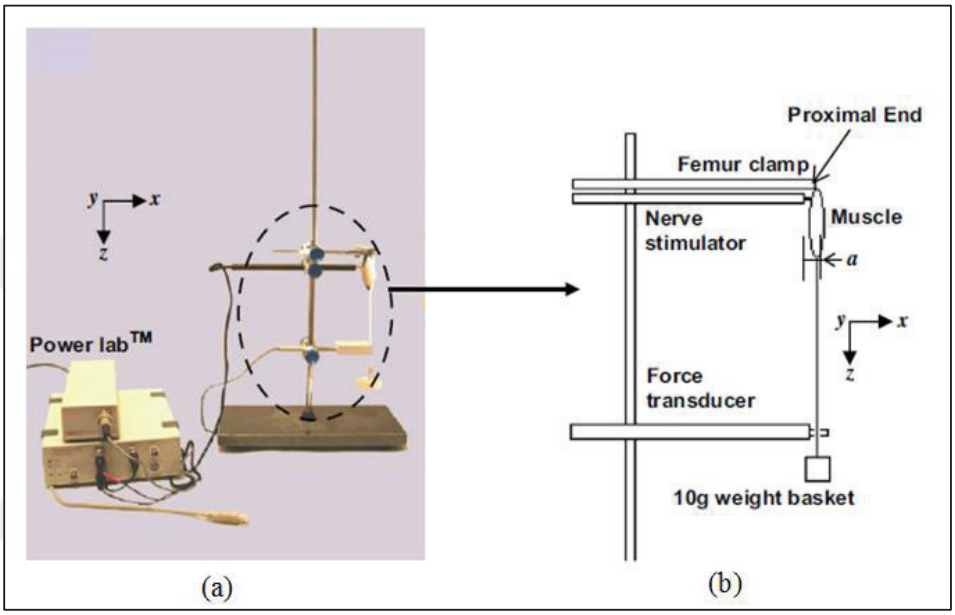

Figure 3.9 (a) Experimental setup photo, (b) schematic **[47]**

3.6. Discussion

There are few studies in the literature which have the scope of developing a macro scale bio-mechatronic device while plenty of studies have considered micro scale bio-mechatronic devices. It is obvious that macro scale bio-mechatronic device development needs further research. Further development of the technology presented by [4] will constitute an innovation. Here some future research paths are pointed which is not implemented in the bio-mechatronic swimmer developed by [4].

- The bio-mechatronic device is driven by an open loop stimulator. A feedback controlled muscle actuator will lead the development of robust bio-mechatronic device that can execute more complex tasks.

- *In-vitro* conditions and muscle-to-mechanical electronic interfaces have to be improved for robustness and longevity.

Mechanical characteristics of electrically stimulated muscles and characterization methods have been investigated deeply and fulfill the requisites of muscle based bio-mechatronic device development [20, 21, 22, 48].

In previous studies various muscle models were investigated among which continuum based models, namely, FEM-models were the most accurate ones for bio-mechatronic device design. FEM-models encompass fiber architecture of muscles and provide accurate details. Recent studies present considerably accurate models for mechanical behavior of muscles [27, 32, 33] and for electromechanical behavior as well [9, 29, 34].

In the literature robust muscle control strategies have been developed. Most of these strategies had the focus of restoring the muscle activity for paralyzed patients and improve FES strategies for physiotherapy applications and implemented on *in-vivo* experiments [20, 24, 41, 42, 43, 44]. However few of them aim to control muscles *in-vitro* with the scope of developing bio-mechatronic devices [19, 39]. Thus, studies for *in-vitro* muscle control have to be conducted and control strategies encompassing *in-vitro* effects.

Although many methods for *in-vitro* muscle testing methods have been developed [19, 45, 47], innovative methods has to be researched to achieve less hostile *in-vitro* conditions and more feasible infrastructure to supply these conditions for bio-mechatronic device applications.

4. METHODS

A research path is designed to achieve the goals of the study. Although this thesis work has a fundamental aim to investigate performance and feasibility of muscle for robotic applications, it also may be considered as the first step of a research path to design a macro scale bio-mechatronic robot. Thus, in addition to methods that were used in this thesis work alternative methods are presented as well, according to the literature. Main steps of experimental and theoretical work are listed below. In this section methods are given in the following order.

1. Selecting source of muscle model.
2. Designing and manufacturing an experimental setup for muscle testing.
3. Characterizing muscle mechanical response of muscle tissue due to stimulation parameters.
4. Developing system models.
5. Experiments for controlling muscle contraction force.
6. Experiments to investigate the feasibility of a muscle based bio-mechatronic device.

4.1. Selecting the Source of Muscle Model

Many different muscle models have been used in the previous studies. These models may be categorized into two basic types as; artificially fabricated tissues and tissues isolated from animals. In the literature micro-scale bio-mechatronic devices are driven by muscle tissue are fabricated as thin films [14] or cultured directly on the micro structure (micropillars) [5, 49]. Although there are some studies to fabricate fully functional muscle tissue [50, 51] which also may be applied to macro scale systems, they have some technological challenges and are not feasible to be used in a bio-mechatronic device for the moment. In Figure 4.1 an engineered muscle tissue is given from a project aiming to develop macro scale bio-mechatronic device [52]. In the project muscle tissue is fabricated with muscle-tendon interferences and muscle-nerve interferences however 50% adult skeletal muscle contractility in the engineered muscle is not reached.

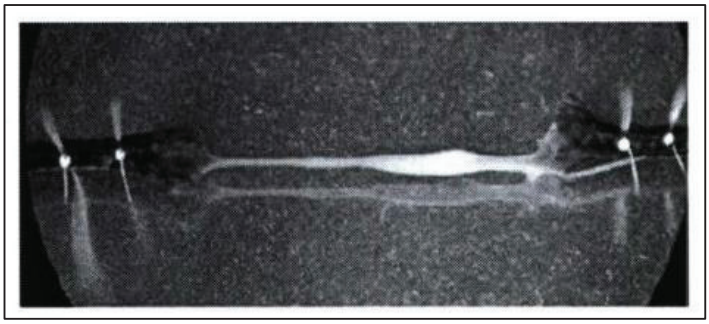

Fig 4.1 Functional Self Organizing Cardiac Muscle **[52]**

Although ethical point of view using engineering muscles are better choice rather than harvesting specimens from animals, due to challenges of fabricating muscle tissue would hinder the achievements of the thesis work thus in this thesis muscle tissue is isolated from animals. Previously in many studies muscle models harvested from animals such as frog [4, 25, 45, 47, 46], rat or mouse [21, 53] and cat [24, 42].

In this thesis frog is chosen for the muscle model source; may be explained with two main reasons. Frog has a lower place in the phylogenetic scale than mammals and frog muscle tissue is more durable in *in-vitro* conditions. They have longer service life and require less strict control of *in-vitro* conditions such as ambient temperature (mammalian tissue requires a body temperature of 27°C while frog tissue is able to function even at 4°C). Another advantage of harvesting specimens from frog is the easier surgical procedures due to frog's simpler musco-skeletal system. Furthermore facilities to maintain frogs require less features and effort than the ones for rats and mice. However few experiments were conducted on Wistar rat TA muscle for feasibility assessment compared to frog muscles. Muscle specimens harvested from frog in most of the experiments.

Skeletal muscle is chosen as the model since it is not functioning with short relaxations and contractions as cardiac muscles. Skeletal muscle is controllable and has mechanical hard points such as tendons and bones which makes them easier to integrate in a mechanical system. Among many specimen targets in frog body, *gastrocnemius* muscle is chosen as the model since it is one of the biggest muscles in lower extremities and requires less surgical effort. It has connections to *Tibia* and *Femur* on one end and to *Achilles* tendon on other end which are hard points for muscle to mechanical system interfaces and *sciatic*

nerve can be used to stimulate muscle with electric signal. In Figure 4.2.a location of *gastrocnemius* muscle is shown.

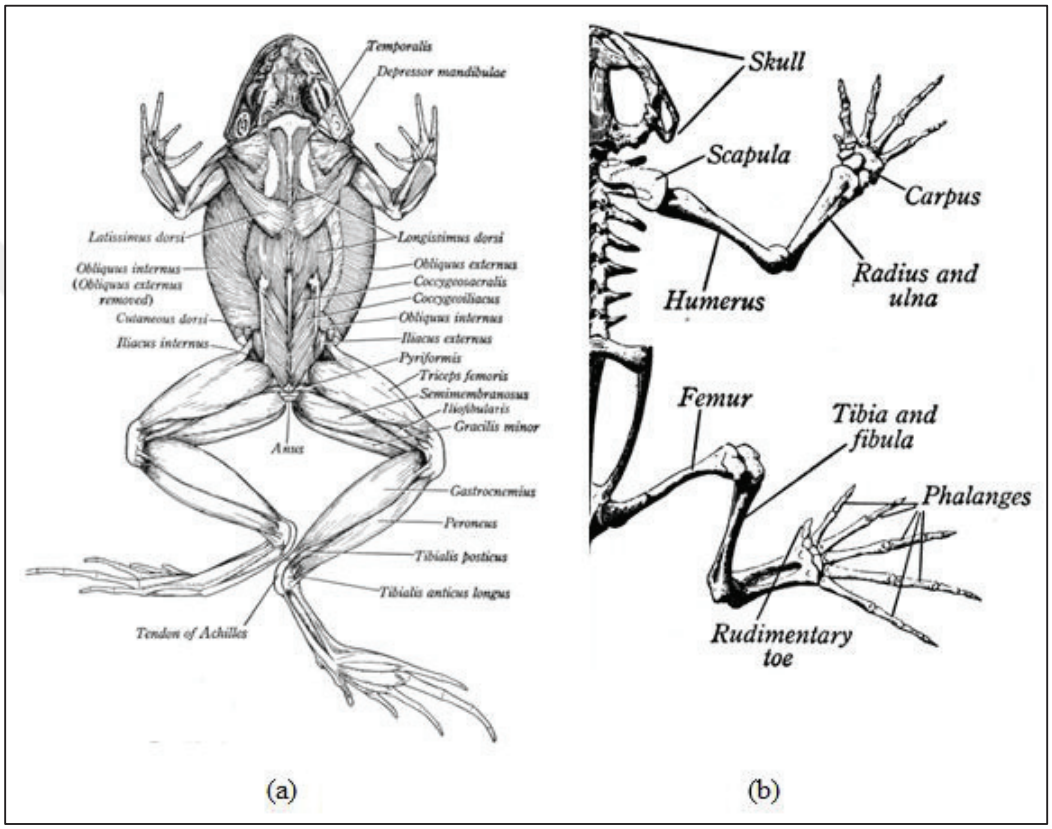

Figure 4.2 (a) Frog Muscular System **[7]**, (b) Frog skeletal system **[7]**

Rana esculenta frogs are obtained regarding the availability, from regional suppliers (1. Sasu, Adana, "http://www.sa-su.com", 2. Froog, Antalya, "http://www.froog.co"). Frogs are maintained in aquariums with water filtering circulating system which has dry platforms inside. Frogs were kept in this facility maximum two weeks during the experiments. All experiments were conducted by the permission of Yeditepe University ethical committee. In Table 4.1 dimensions of *gastrocnemius* muscle of *Rana esculenta* frog is given which the experimental setup designed accordingly.

Table 4.1 Dimensions of Rana Esculenta frog Gastrocnemius muscle. Length is measured between the begining of Aachiles tendon and Femur. Both muscle diameter and length are measured at rest length and muscle length may be 2 mm shorter or longer for compressed and stretched cases.

Animal Mass (gr) ***over***	**Animal Mass (gr)** ***Inc.***	**Length (mm)**	**Stdev. (mm)**	**Diameter (mm)**	**Stdev. (mm)**
20	40	26.14	2.02	8.25	0.9
40	60	31.2	1.51	9.5	0.16
100	130	34.2	1.95	11.88	0.71
130	160	37.56	0.74	11.62	0.89

4.2. Design and Manufacturing of Muscle Testing Apparatus

To investigate the mechanical response of muscle as an actuator and to gain experience on bio-mechatronic device design an experimental setup (muscle testing apparatus) is designed and manufactured. In the course of the project two different experimental setups were designed, however the last revision of the design will be explained in detail. Previous revision of muscle testing apparatus is named as “rev. A” and the recent revision is named as “rev. B”. The experimental setup has three tasks; stimulating muscle, measuring mechanical output, and providing certain *in-vitro* conditions

In Figure. 4.3 a simple schematic for the muscle testing apparatus is given which all revisions are based on the same concept. For an isometric contraction experiment muscle is connected to load cell on one side (*proximal*) and the other side (*distal*) is fixed. For isotonic contraction experiments the fixed side is connected to counterweight and the displacement is measured by an encoder. Muscle is stimulated via different types of electrodes (needle, surface and suction electrodes) and techniques (direct or indirect stimulation) by a signal generator. Muscle is submerged in the pool containing Ringers or Krebs solution during the test that is heated or chilled by a commercial circulating water bath and oxygenated by bubbling.

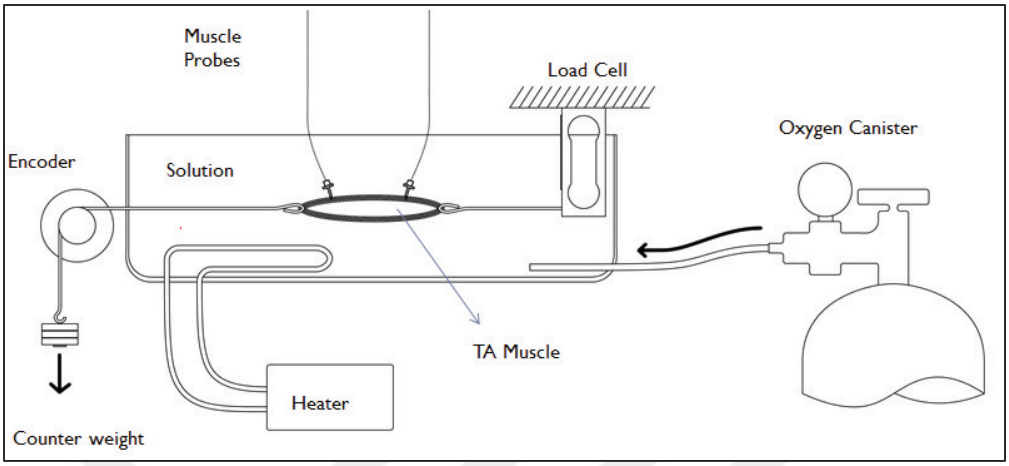

Figure 4.3 Simple schematic of muscle testing apparatus

4.2.1 Mechanical System

Chassis of muscle testing apparatus integrates sensors, electronic hardware and the systems supplying *in-vitro* conditions. It is manufactured from aluminum sigma profile and assembled via special connectors. Chassis is supported by additional L-profile steel elements at the places where more stiffness is needed. Parts are manufactured from stainless steel, aluminum and polyamide by milling, turning and laser cutting.

Muscle is hanged between L-shaped structural elements which are connected to load cell and counter weight at *proximal* and *distal* ends respectively. Structural elements holding muscle are electrically insulated from chassis with polyamide inter-parts. The structural element on the *distal* side is guided via linear guide (SKF linear guide miniature series LZM HS 7) and the linear displacement of the element is measured via contactless magnetic encoder on the top of the linear guide. .In Figure 4.4-4.6 solid model, isometric and isotonic test configurations of muscle testing apparatus are given.

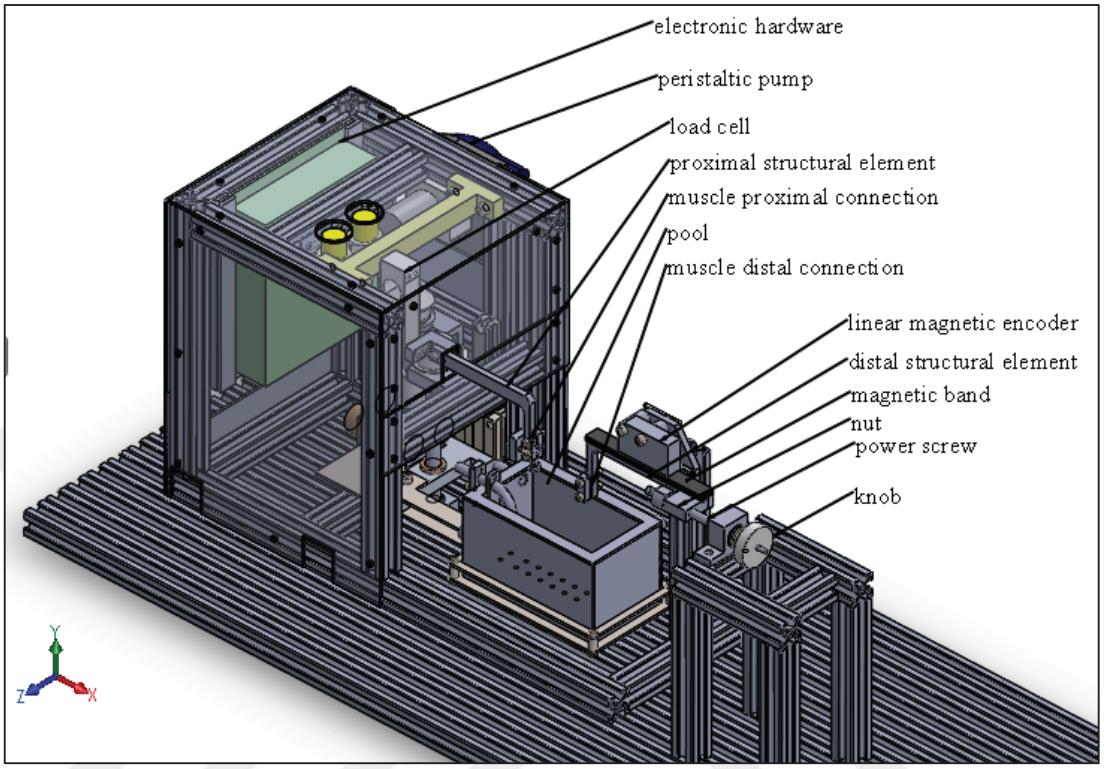

Figure 4.4 Muscle testing apparatus

Isometric test configuration:

For isometric tests a module is connected to the *distal* structural element which is an integration of a power screw, nut, housing and bearings. For isometric testing muscle length must be precisely adjusted thus, the length betwen *proximal* structural element and *distal* structural element is adjusted via rotating the knob manually which rotates power screw and converts rotation into linear motion.

Isotonic test configuration:

For isotonic tests a different module is installed to the setup which connects *distal* structural element to counterweight. Counterweight is connected by a steel wire and directed via pulleys which are supported by ball bearings.

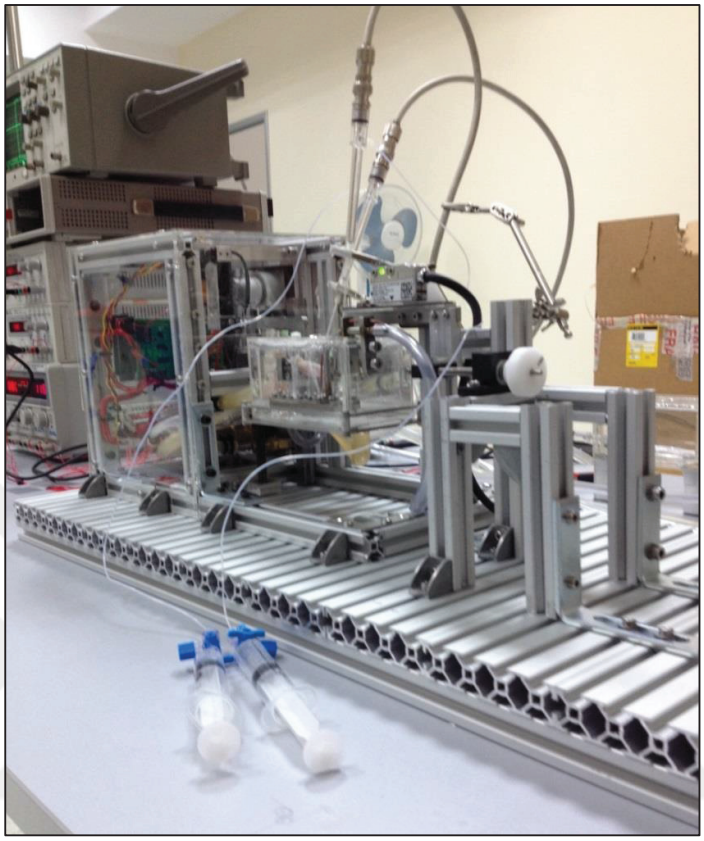

Figure 4.5 Muscle testing apparatus, isometric test configuration (last design revision)

Figure 4.6 Experimental setup at isotonic test configuration

4.2.1.1. Substructure for In-vitro Conditions

As mentioned previously muscle is submerged into aqueous solution (Ringer or Krebs) during the test. A pool is designed and manufactured for this purpose which has an outer cooling/heating water chamber. Water is circulated outside the solution by a commercial heater/cooler water bath (Polyscience). Solution inside the pool is circulated by a peristaltic pump (Welco, WP 1100). Fluids are transferred via silicone tubes. In Figure 4.7 broken view of the pool is given.

Pool can be moved in the vertical direction by a servomotor which is controlled by user interface. To install the muscle, pool is lowered that creates more space for easier installation. For the test, pool raises and muscle submerges in the solution. An identical pool is placed outside the experimental setup to maintain the same *in-vitro* conditions for the muscle which was isolated from other leg while the first isolated muscle specimen is in test.

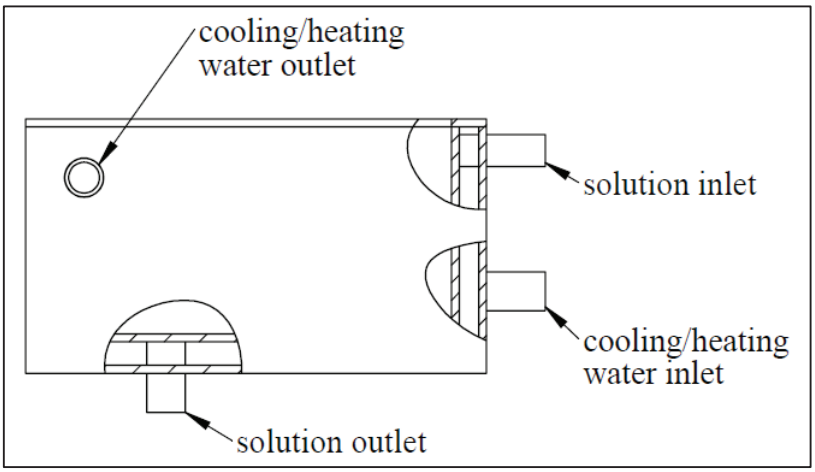

Figure 4.7 Solution pool broken wiev

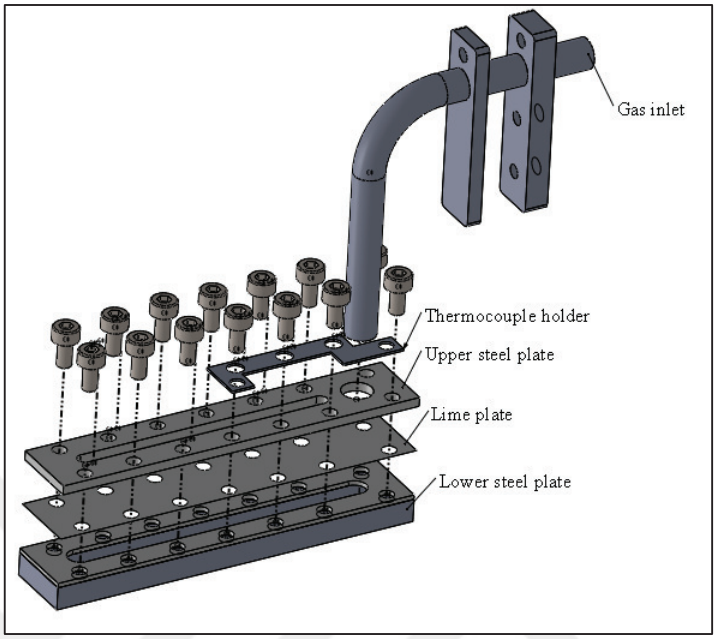

Figure 4.8 Diffuser

Oxygen delivered to the solution by a diffuser which is connected to medical oxygen canister. The diffuser is made of thin wooden (lime) plate clamped between two stainless steel plates. Since lime wood has porous structure oxygen distributed as tiny bubbles. Wooden plate is changed regularly to prevent microbial growth inside the pores. In Figure 4.8 exploded view of the diffuser is given. Oxygen flow is controlled by closing or opening the solenoid valve which is connected to the oxygen line.

4.2.1.2. Muscle to Mechanics Interface

In previous studies muscle is connected to mechanical systems mostly using sutures. In studies [4, 19, 45] tendons are tightly secured to mechanical elements using cotton or silk medical sutures. In study [54] muscle is removed with adjunct bone (*femur*) and drilled on the knee. A nylon suture passed inside the femur and pulled out from the hole on the knee. Tendon on the other end of the muscle is sutured as well. In [47] muscle is hanged to metal hooks vertically. In this thesis work muscles are isolated with the adjunct bones (*femur and tibia)* and knee on *proximal* end and with the *Achilles* tendon at *distal* end to use the advantage of hard connection points. For the earlier revision of muscle testing apparatus

(Rev. A) femur is drilled with 2.5 mm drill bit and metal hook fixed at *proximal* end. For *distal* end *Achilles* tendon is clamped via steel crocodile. In the recent revision of muscle testing apparatus (Rev. B) bones are clamped to the structural element with a mechanism at *proximal* end and *Achilles* tendon is clamped between two steel parts at *distal* end. In Figure 4.9 fixed muscle is shown.

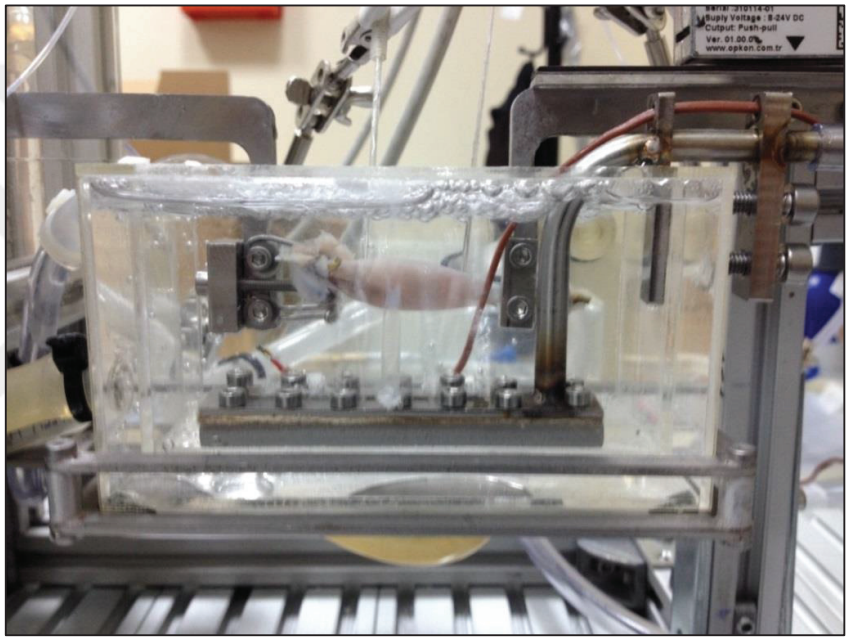

Figure 4.9 Fixed muscle

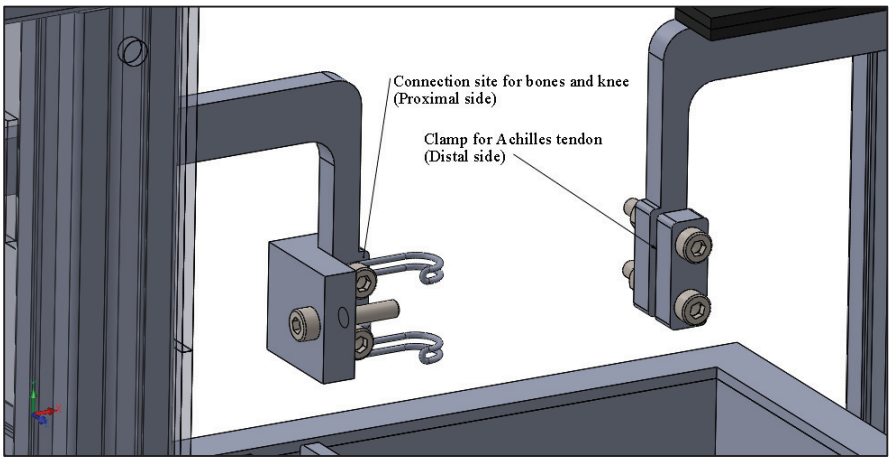

Figure 4.10 Muscle connection sites

4.2.2. Sensors

Contraction force is measured by a commercial full-bridge strain gauge integrated load cell (Puls electronic MT series) which is connected to *proximal* end. Linear displacement of the structural element, thus the displacement of *distal* end of muscle is measured by a contactless magnetic linear encoder (Opkon elektronik MLI magnetic linear encoder) for isotonic experiments. Ambient temperature is measured by a thermocouple (J-type) submerged into the solution. In Figure 4.11 sensors are indicated on the muscle testing apparatus and detailed information about sensors is given in (Appendix B).

Load cell is calibrated by counter weights using isotonic test module. A steel wire is inserted between *proximal* structural element and *distal* structural element (in the place where muscle present during tests) to connect load cell and counter weight. Repeatability and hysteresis error is measured. Hysteresis error is reduced by stiffening the experimental setup chassis. In Figure 4.12 hysteresis error of force measurement is given for three different calibration data.

$$F_L = 1221.1V_L - 63.883 \tag{4.1}$$

Equation 4.1 is the calibration equation, where $\mathbf{F_L}$ (gr) is the force measured by load cell and $\mathbf{V_L}$ (mV) is the voltage output of Wheatstone bridge which is integrated in the load cell.

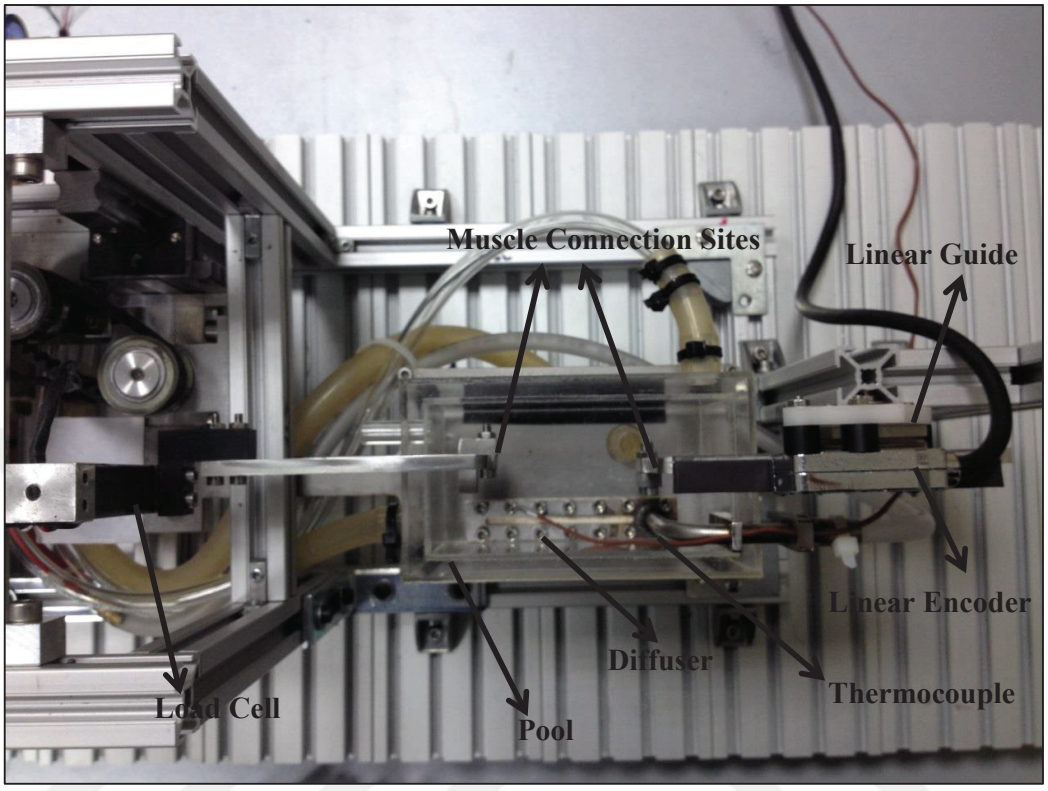

Figure 4.11 Muscle testing apparatus detailed view

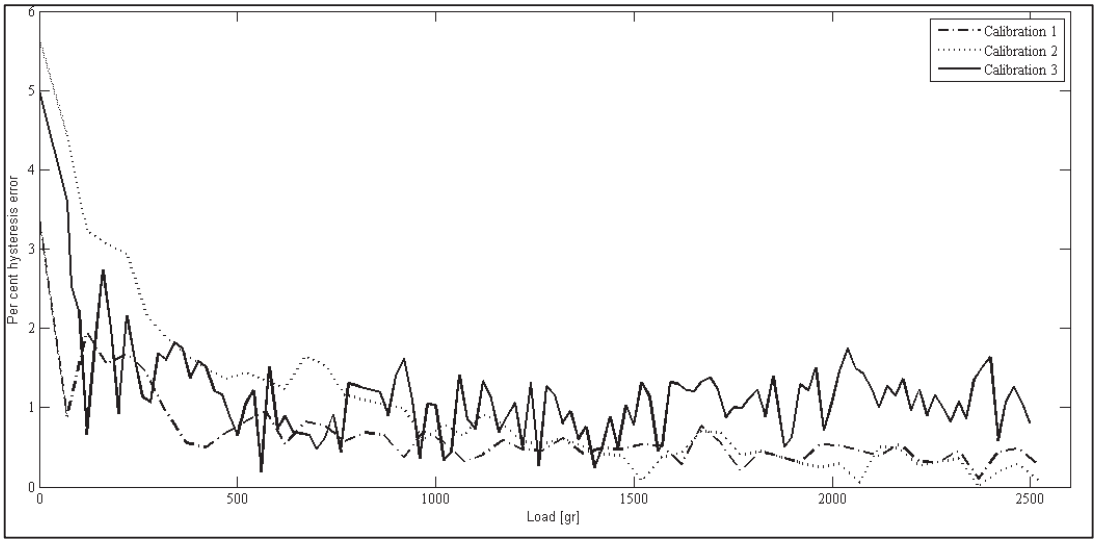

Figure 4.12 Force measurement hysteresis error

4.2.3. Electronic Hardware

4.2.3.1. Stimulation Signal Generation

Muscle may be stimulated via sinusoidal or rectangular profile signals. Since skin and *subcutaneous* fat layer fat tissue creates an RC low pass filter, stimulations with rectangular profile cannot reach the depths of muscle while sine wave stimuli pass easily. Thus, when considering surface stimulation a sine wave stimulus presents an advantage [55] . However in this thesis rectangular wave form stimulation signal is selected since stimulation is not delivered *subcutaneous* and stimulation via rectangular waveform is the most common method in functional electrical stimulus (FES) studies.

The electrical signal may be delivered as voltage or current controlled. In previous studies it is reported that current controlled stimulations has more consistent output hence, induces more predictable forces and voltage controlled stimulations are widely used and suggested as safer method. However considering the amount of stimulation pulse energy delivered to muscle, current-controlled and voltage-controlled stimulations induce same amount of contraction force for same amount of pulse energy [56].

In this thesis work voltage-controlled stimulation is preferred because of the less design effort of hardware. However current controlled stimulation would be advantageous for more robust control and precise characterization. In Table 4.2 rectangular wave electrical stimulus parameters used in various experimental studies are given.

Table 4.2 Rectangular wave electrical stimulus parameters used in several studies, FR: full recruitment, TH threshold

Amplitude (V or A)	**Pulsewidth (µs)**	**Frequency (Hz)**	**Type of signal**	**Animal**	**Target Muscle**	**Reference**
FR V	1000	250	Mono-polar	*Xenoupus laevis* frog	PL	[46]
5.8 V	100	80	Bi-polar	*Rana pipien*	ST	[4]
0-11V	400	100	Bi-polar	Rat	EDL	[57]
Twice TH V	30-1000	20-80	Mono-polar	*Rana proposa* frog	IF	[45]
1 mA	0-100	40	Bi-polar	Adult cat	TA	[48]
2-8 V	10000	90	Mono-polar	Rat	TA	[21]

The stimulation signal may be delivered as mono-polar or bi-polar. In this thesis stimulation signal is selected as bi-polar since uni-polar pulses result in net ion flow, tissue damage and corrosion of the anode electrode surface [57].

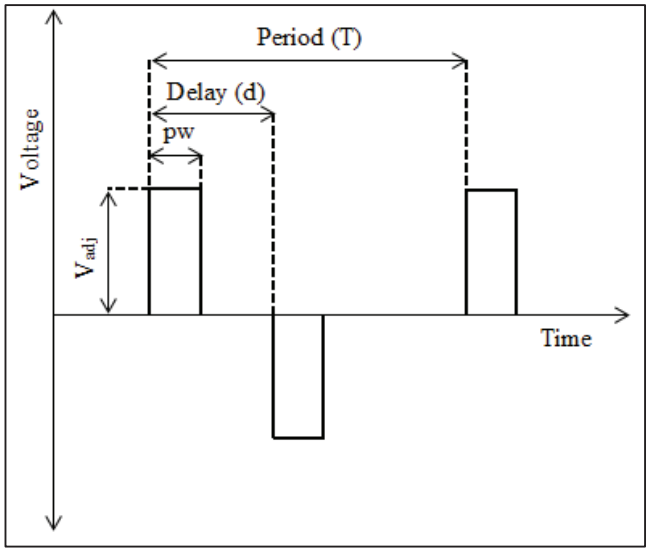

Figure 4.13 Properties of bi-polar rectangular wave signal

A rectangular bi-polar signal is shown in Figure 4.13. Period **(T)** is the duration between pulses of the same polarity. Delay **(d)** is the duration between pulses of positive and negative polarity, $\mathbf{V_{adj}}$ is the adjustable amplitude of the pulse and the pulse-width is denoted by **pw**. In experiments the pulse with reverse polarity is located exactly in the middle of two pulses of positive polarity thus, delay **(d)** is half of the period **(T/2)**. The signal frequency **(f)** is calculated as reciprocal of the period. Since muscle is activated by both positive and negative pulses, activation frequency of muscle is twice the stimulation frequency **(2f)**. In this thesis the expression of "stimulation signal frequency" refers to **2f**, where **f** is the reciprocal of the period **(T)** of a bi-polar rectangular wave signal.

In the previous revision of muscle testing apparatus (rev. A) a signal generator (shown in Figure 4.14) is designed and manufactured to generate stimulation signal. For the recent revision of experimental setup (rev. B) stimulation signal is generated by a commercial multi-purpose DAQ card (NI PCI 6221) and signal amplified by an amplifier (stimulation signal amplifier) shown in Figure 4.16 which is designed and manufactured in the thesis. Schematics for electronic hardware are given in (Appendix B).

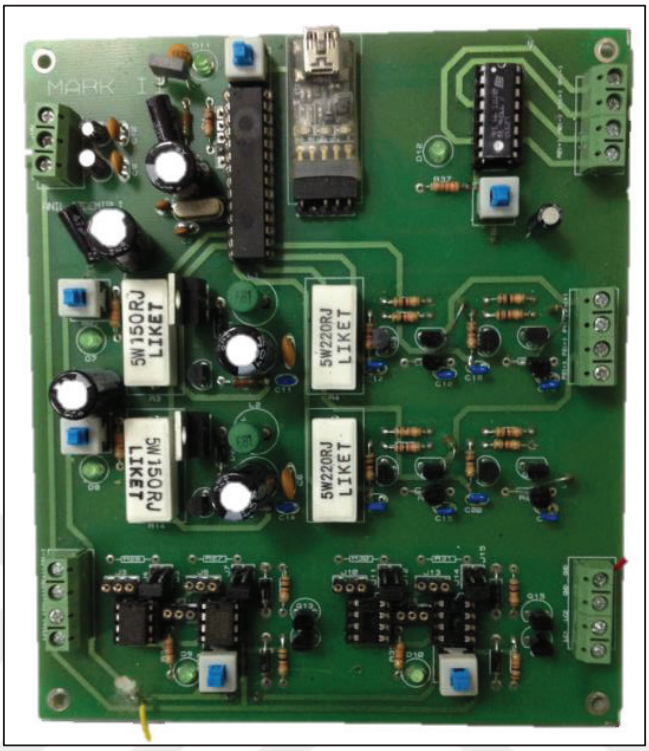

Figure 4.14 Signal generator

Signal generator shown in Figure 4.14 produces a rectangular wave signal with adjustable amplitude **(V_{adj})**, frequency **(f)** and pulse-width **(pw)**. The stimulation amplitude is adjusted by modulating the DC/DC converter which the input of this converter is 10 V. The modulation of DC/DC converter is done via PWM (pulse-width modulation) signal generated by the micro controller (uc). The output voltage of this converter is 10 V times the duty cycle of PWM signal shown in upper left corner in Figure 4.15. The rectangular wave signal is created by switching this constant voltage by four switches which are controlled by the micro controller. If switches controlled by the signal "p1" are closed, muscle is stimulated with $\mathbf{V_{adj}}$ and if switches controlled by the signal "p2" are closed muscle is stimulated with $\mathbf{-V_{adj.}}$ The delay **(d)** is adjusted by adjusting the time between "p1" and "p2" signals and the frequency of switching determines the frequency of stimulation signal.

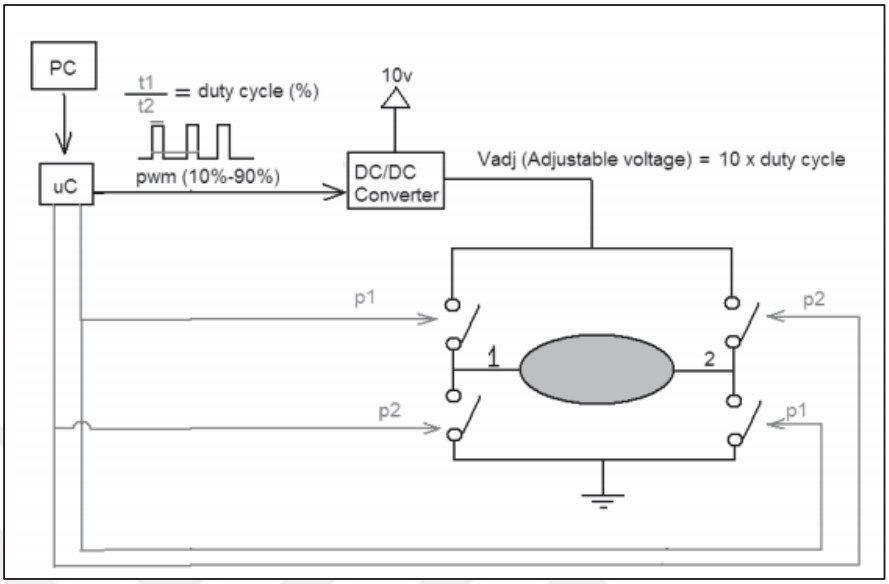

Figure 4.15 Signal flow chart of the signal generator

The signal generator is connected to PC from USB port and stimulation signal parameters are adjusted from a graphical user interface (GUI) on MATLAB. On the PCB shown in Figure 4.14 two separate signal generator circuits are present that may be used to stimulate a pair of antagonistic muscles. The PCB also includes instrumentation amplifier which amplifies the signal from load cell and motor controller that controls the flow rate of solution circulator peristaltic pump.

In the recent revision of experimental setup (rev. B) switching signal is generated by a commercial multi-purpose DAQ card (NI PCI-6221) instead of micro-controller. Switching signals control transistors in the circuit which are integrated in the experimental setup (rev. B) shown in Figure 4.16. DC voltage is supplied to the circuit by a precision laboratory power supply (Aigilent) which has a resolution of 0.1 V and rectangular wave is generated by switching this DC voltage. Topology of the circuit is basically an H-bridge. Stimulation signal parameters are adjusted from a GUI on LabVIEW. In Table 4.3 features and limits of stimulation signal is given for the both signal generation strategies (strategies used in rev A. and rev. B).

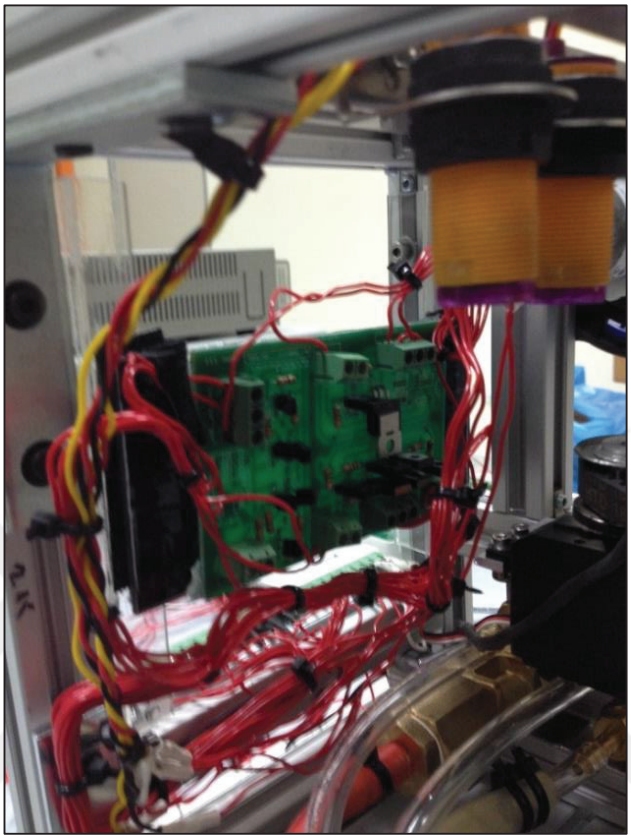

Figure 4.16 Signal amplifier installed in the last revision of muscle testing apparatus

Table 4.3 Signal generator properties and features

	Property	**Min-Max**	**Resolution**
Signal Generator	Amplitude	1-10 V	0.1V
	Frequency	0-not less than 300Hz	1 Hz
	Pulse width	10- NA µs	5 µs
	Signal type	Mono-phase/Bi-phase	
NI 6221 coupled amplifier	**Property**	**Max-Min**	**Resolution**
	Amplitude	0-10 V	0.1 V
	Frequency	0-not less than 300 Hz	1 Hz
	Pulse width	10- NA µs	10 µs
	Signal type	Mono-phase/Bi-phase	

The reason of generating switching signal from DAQ card in the recent revision of experimental setup (rev. B) was to perform signal acquisition and signal generation on the same device to prevent delays during muscle control. Another problem of signal generator designed (used in rev. A) during the thesis work was its lower limit of amplitude. Signals generated by the circuit shown in Figure 4.14 having the amplitude lower than 1 V were in low quality because of the high noise on the signal.

4.2.3.2. Data Acquisition Hardware and Control of Experimental Setup

Data is acquired via DAQ card which also generates the stimulation signal. Signal from load cell is acquired from analog input and encoder signal is acquired from counter input with the acquisition code prepared on LabView.

Signal from load cell is amplified using a strain gauge module (NI, SCC SG 04) which is integrated to connector block of (NI, SCC 68) DAQ card. Load cell excitation voltage of 2.5 V is supplied from the module and input signal is amplified by the module with the gain of 100. Linear encoder is powered by 12 V DC and data acquired from two phases. The encoder is incremental type and one increment corresponds to 10 μm displacement. Stimulation signal is acquired as well to monitor timing between stimulation signal and contraction force. Stimulation signal is measured from isolated voltage input module (NI, SCC AI 00) to prevent noise which was induced on load cell by stimulation signal.

Load cell, encoder and stimulation signals were acquired with 2 kHz sampling rate. For the experiments, where monitoring the timing between the pulse and start of contraction is critical, acquisition is made with 40 kHz and 100 kHz sampling rate not to miss the pulses with 25 and 10 μs pulse width. Data are recorded in ".lvm" file format.

Features of experimental setup such as pool position, solution circulation rate, oxygen flow are controlled using a multi-purpose DAQ card (NI, MyDAQ) from a user interface prepared on LabView. Pool temperatures are also measured from this DAQ card but not recorded. Experimental setup is not controlled from PC which has the tasks to stimulate muscle and record mechanical output, to not to interrupt or slow down the operation. In Figure 4.17 signal flow over the whole experimental setup is summarized in a schematic.

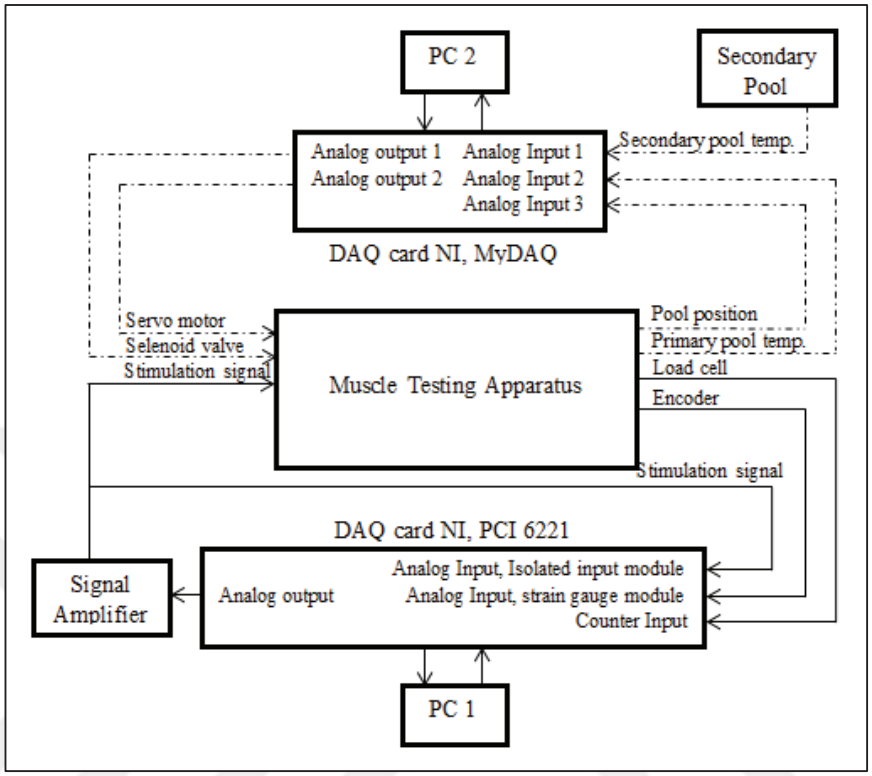

Figure 4.17 Signal flow schematic

4.2.3.3. Muscle to Electronics Interface

Muscle may be stimulated via direct or indirect stimulation. Direct stimulation is defined as delivering electric signal directly in muscle tissue while indirect stimulation encompasses delivering electric signal via nerve. In previous studies both methods are applied for electrical stimulation. In [19, 21, 46, 48] stimulation is delivered as indirect and in [4, 57] as direct. In study [45] force enhancement is compared for indirect and direct stimulation methods via experiments on *Rana brevipoda* frog *illofibularis* muscle. At low temperatures (4, 12 °C) twitch force developed by indirect stimulation is considerably lower than the twitch force generated by direct stimulation (15 per cent of the twitch force generated by direct stimulation). At higher temperatures (22 °C) the difference is lower (80 per cent of the twitch force generated by direct stimulation). For tetanic contractions peak contraction forces generated by direct and indirect stimulation are same for 4, 12 and 22 °C however force is developed with a delay at lower temperatures for indirect stimulation method.

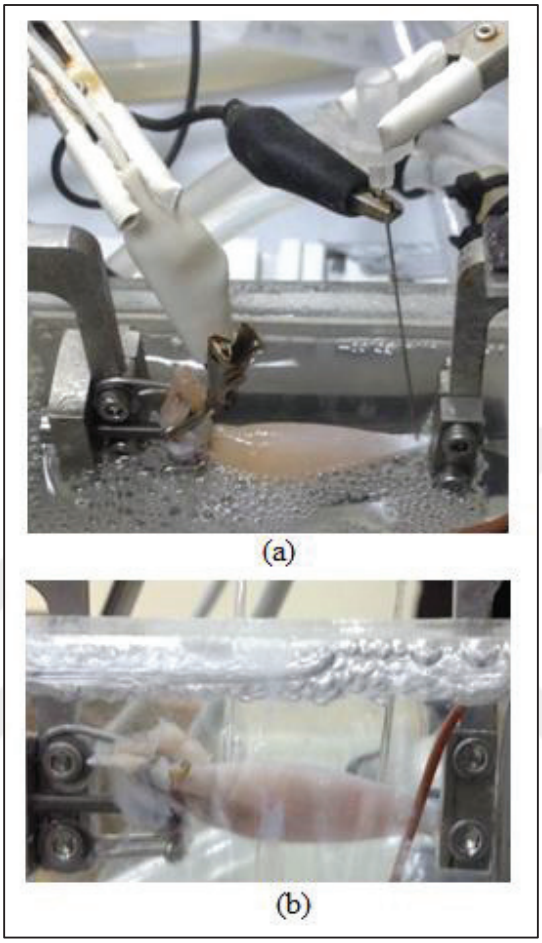

Figure 4.18 (a) Sciatic nerve clamping method, (b) Suction electrode method

In the course of the project both indirect and direct methods are used for muscle stimulation. Direct stimulation is performed using needle electrodes and surface electrodes. Needle electrodes are prepared by cutting the steel tip of a medical syringe and surface electrodes are prepared cutting U-shaped copper sheets. The manufacturing process of surface electrodes is explained in [58]. Indirect stimulation is performed via suction electrode inserted to *sciatic* nerve [19, 46] and by clamping *sciatic* nerve by steel crocodile. Most of the experiments were conducted with indirect stimulation method by clamping *sciatic* nerve and other methods are used for a feasibility assessment for future objectives of developing a muscle actuated bio-mechatronic device. For the method of clamping sciatic nerve, reference electrode was a needle electrode which was inserted in tendon. While stimulating with suction electrodes reference electrode was also a suction electrode which was inserted into muscle tissue. In Figure 4.18 both methods are shown.

4.2.4. User Inerface

The signal generator (Figure 4.14) is controlled from a graphical user interface (GUI) prepared on MATLAB. GUI is prepared in three subsections as state creator, protocol creator and analyzer. Stimulation parameters such as amplitude, frequency, pulse-width, polarity of the signal and stimulation duration are adjusted from state creator interface. In protocol creator a stimulation protocol is prepared by composing stimulations with different properties and placing rest periods between these stimulations if required. For previous design of muscle testing apparatus data acquisition is started and stimulations are applied as the DAQ card records the data. Recorded data is analyzed in the analyzer section of the MATLAB GUI. In Figure 4.19 state creator user interface is shown.

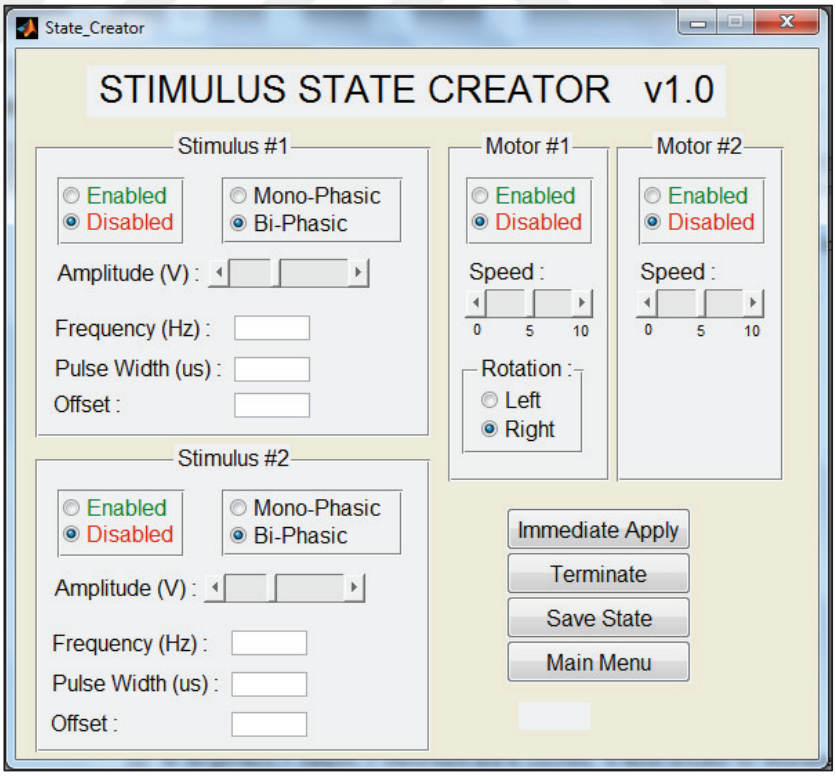

Figure 4.19 State creator user interface on MATLAB

In the recent revision of muscle testing apparatus stimulation parameters and data acquisiton preferences are adjusted on same user interface prepared on LabView since both stimulation signal and data acquisition is made on DAQ card. Three different user interfaces are prepared regarding the type of experiment.

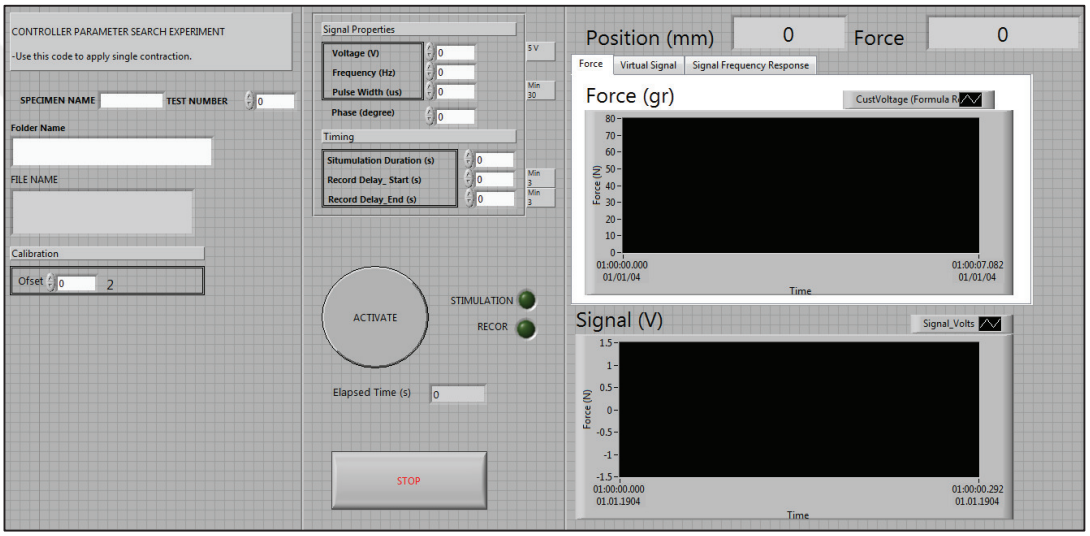

Figure 4.20 User interface for muscle characterization

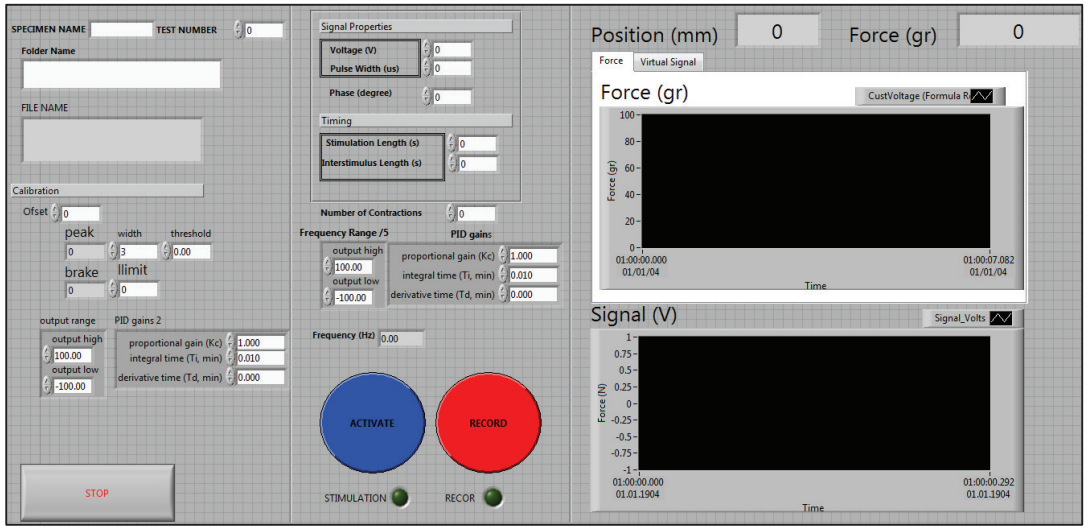

Figure 4.21 User interface for muscle control

In characterization experiments a user interface which prepares open loop stimulation is used to adjust stimulation parameters. Data recording is started just before the activation of muscle and stoped as the activation is over; thus, data is recorded only when the muscle is activated which reduced the size of recording files. For muscle fatigue characterization experiments a different user interface is used which adjusts the properties and number of succesive contractions. Muscle is controlled by a seperate third user interface which allows user to adjust controller parameters. In Figure 4.20 and 4.21 user interface used in characterization experiments and control experiments are shown respectively.

4.3. Experimental Methods

In the project various type of experiments are performed aiming to make an assessment on *in-vitro* performance and feasibility of muscle as an actuator. These experiment types are listed below. In this section experimental methods and procedures for the following experiments are explained.

- Muscle's active and passive response due to initial length.
- Muscle characterization due to various electrical stimulus parameters.
- Fatigue behavior.
- Muscle control for successive short period contractions
- Contraction force control on step and ramp references.

4.3.1. Specimen Isolation Procedure

As mentioned previously *gastrocnemius* muscle of *Rana esculenta* frog is chosen as the specimen target. Here surgical procedure of specimen removal is explained in steps.

1. Frog is put in anesthesia via inhalation using ether. The effect of anesthetics is controlled by moving the jaw and extremities.
2. Euthanasia is applied as decapitating and spinal cord is damaged via needle immediately after which puts animal into spinal shock.

3. Skin is cut around the leg (Figure 4.22.a) and stripped down.
4. Skin covering *gastrocnemius* muscle is stripped as well and the connective tissue between muscle and skin is cut as show in Figure 4.22 b
5. Muscle length and diameter is measured for relaxed, dorsiflexion and plantar flexion positions. In Figure 4.22.d and 4.22.e length and diameter measurement for *plantar flexion* position is given.
6. Connective tissue between muscle and *Tibia* is cut and *Achilles* tendon is separated from *Calcaneus* and *Astragalus*.by cutting the connective tissue in longitudinal direction without damaging the tendon. Shown in Figure 4.22.f.
7. *Tibia* is cut half cm apart the knee for connecting the muscle to mechanical system and muscle is covered with Ringers solution impregnated bandage for the rest of the procedure.
8. *Fascia* between *triceps femoris* and *semimembranosus* is cut to expose *sciatic* nerve. Shown in Figure 4.22.h and 4.22.i.
9. *Sciatic* nerve is separated from surrounding tissue by placing thin stripes under the nerve. Shown in Figure 4.22.j.
10. *Femur* is cut half cm above the knee for mechanical connection to experimental setup shown in Figure 4.22.k and sciatic nerve is cut afterwards.
11. After *gastrocnemius* muscle is completely removed remaining tissue is cleaned.

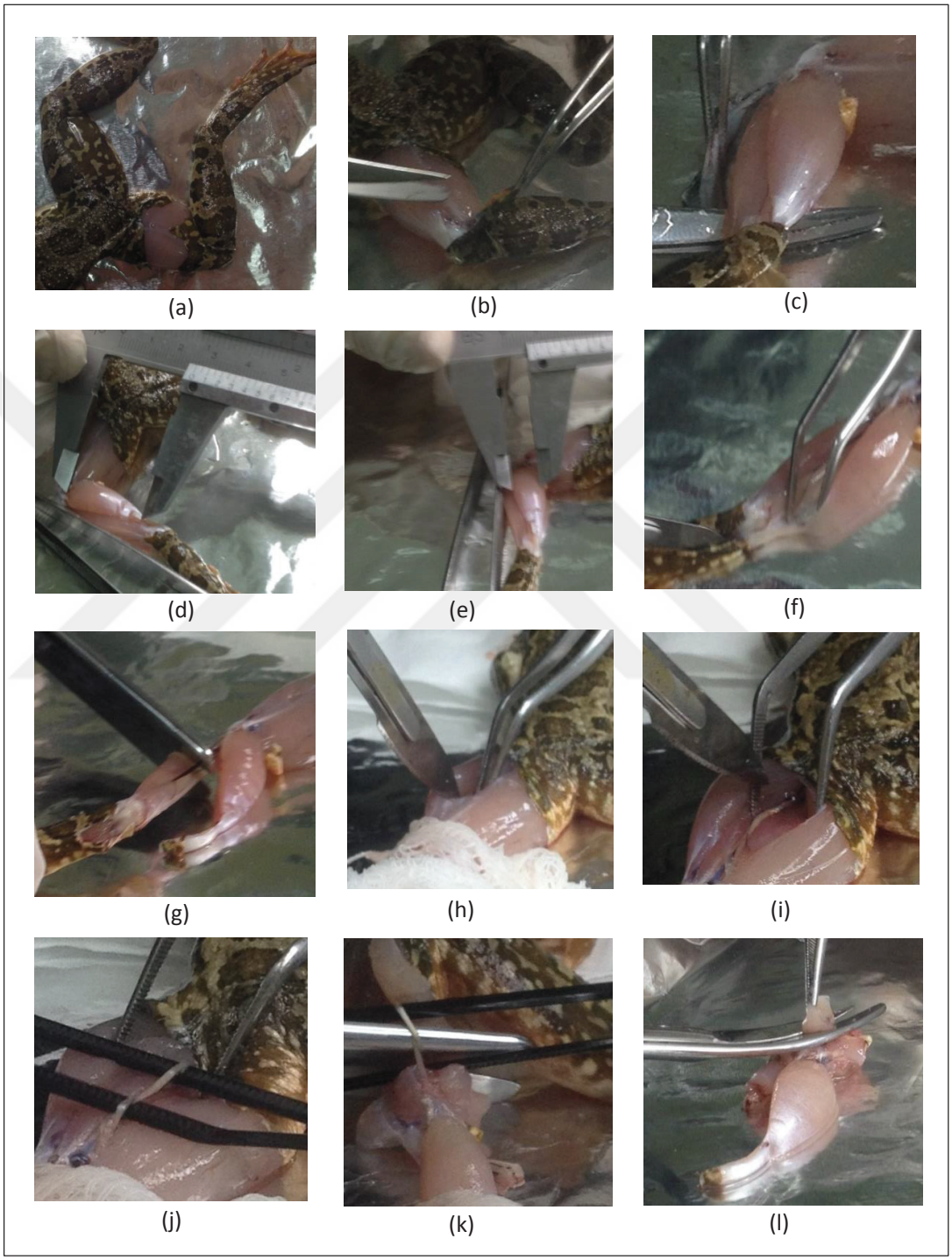

Figure 4.22 Specimen removal process, Rana Esculenta frog, gastrocnemius muscle

4.3.2 Muscle Characterization

Muscle force response changes with some parameters such as; muscle length, stimulation signal parameters and the fatigue condition. Effect of these parameters on force response has to be characterized to use muscle as a mechanical actuator. Muscle is activated for a certain time and some values of this contraction were measured to see effects of the parameters. This values are: peak force, impulse, rise time, fall time and the contraction force magnitude at the end of stimulation.

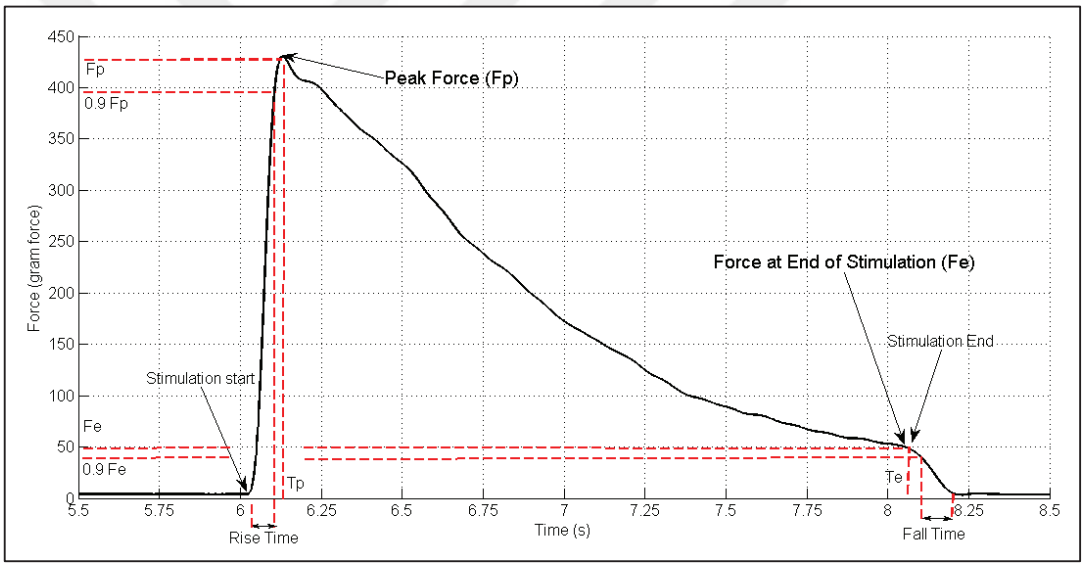

Figure 4.23 Measures of a contraction. A sample result for 2 s long stimulation

In Figure 4.23 a contraction with 2 s stimulation is given. In the figure peak force is denoted as $\mathbf{F_p}$ and the force at end of the stimulation is denoted as $\mathbf{F_e}$. Rise time is between the start time of contraction and the time at 90 per cent of peak force. Fall time is between stimulation end time and the time where force is decreased to its initial value. Although stimulation parameters do not change between stimulation start time and end time, force decreases due to muscle fatigue. Impulse of a contraction is the area under the force-time curve.

In Figure 4.24 contraction with 0.1 s stimulation is given. For shorter stimulations, despite the stimulation ends, force continues to increase for a while. The effect of fatigue is not significant for shorter contractions as it is in the long contractions as shown in Figure 4.23. In Figure 4.24 measures of a short duration contractions are shown which are also applicable for twitch contractions. Peak force is denoted as $\mathbf{F_p}$, stimulation duration is denoted as $\mathbf{T_s}$ and peak time is denoted as $\mathbf{T_p}$. Rise time is betwen stimulation start time and the time where force is 90 per cent of peak force which is located at left hand side of peak force. Fall time is between time where force is 90 per cent of peak force at right hand side of peak force and time where force decreases to its initial value.

These measures were found to characterize the contraction, which characterizes the mechanical response of muscle for different stimulation signal properties, fatigue condition and musle length.

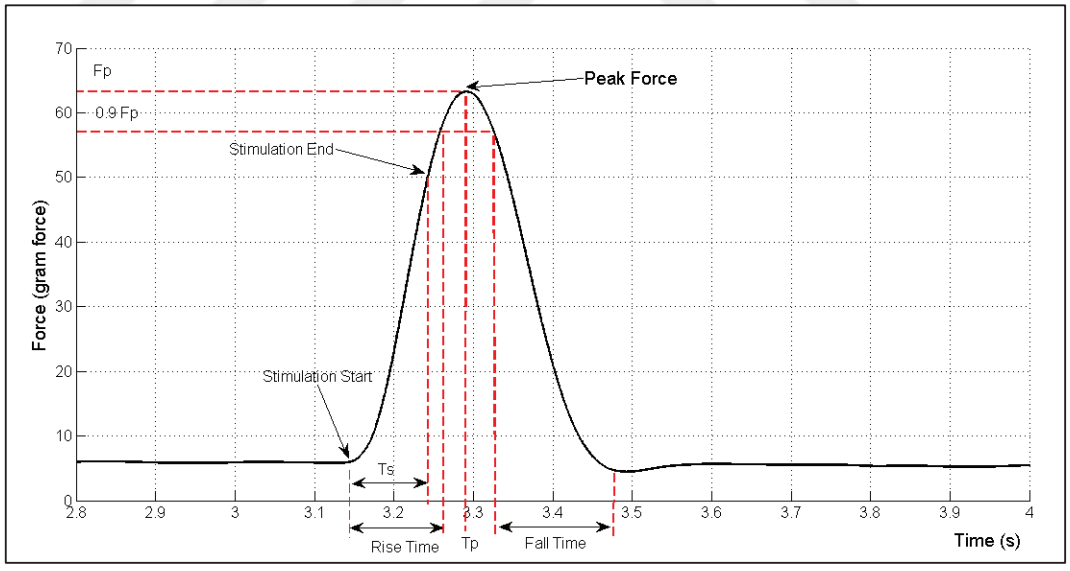

Figure 4.24 Measures of a contraction. A sample result for 0.1 s long stimulation

4.3.2.1. Relationship between Initial Length and Contraction Force

Isometric contraction force of muscle is measured for various muscle lengths. As shown in Figure 2.8 muscle force is varying with the length. It is a prerequisite to measure the stroke and the force profile due to length in order to use muscle as an actuator.

In this experiment previous revision of muscle testing apparatus is used with indirect stimulation method. Ringers solution is prepared before the experiment with the following recipt and stored in 4 ° C refrigerator. For 2L distilled water 13g of NaCl, 0.28g of KCl, 0.3g of $CaCl_2 2H_2O$, 0.4g of $NaHCO_3$.

1. Muscle specimen is isolated. In this experiment *sciatic* nerve is not removed since direct stimulation is applied.
2. Muscle specimen is connected to experimental setup and submerged in Ringers solution. Solution is maintained at 22 ° C.
3. Medical oxygen valve is opened and supplied into solution by bubbling.
4. Muscle length is adjusted in length at *plantar flexion.*
5. Needle electrodes are placed to *proximal* and *distal* ends 1.5 cm apart.
6. Stimulation parameters (pulse-width, amplitude and frequency) are adjusted to constant values and bi-polar stimulation signal is applied.
7. Length is increased by 2 mm and stimulation procedure repeated.
8. Whole experiment is recorded thus; the passive force is measured as well just before the stimulation is delivered.

In the analysis peak total force is plotted versus muscle length. Active and passive forces are calculated separately.

4.3.2.2. Force Response due to Stimulation Signal Parameters

In this type of experiment muscle contraction force is measured for different stimulus variables with isometric boundary conditions. Force response of muscle is characterized for various stimulation signal pulse-width and frequency. Characterization of mechanical response has a vital role to be able to control muscle.

In this experiment recent revision of muscle testing apparatus is used with direct stimulation method. Ringers solution is prepared before the experiment with the receipt described in previous section. Experimental procedure is described in steps.

1. Muscle specimen is isolated with the method described in section 4.3.1.
2. Muscle specimen is connected to experimental setup and submerged in Ringers solution. Solution is maintained at 22 ˚C.
3. Medical oxygen valve is opened and supplied into solution by bubbling.
4. Muscle length is adjusted to rest position.
5. *Distal* electrode is clamped to *sciatic* nerve and *proximal* needle electrode is steeped into the *Achilles* tendon.
6. Stimulation pulse-width and frequency are adjusted to a constant value and stimulation amplitude is adjusted to full recruitment voltage which is found by increasing voltage from 1V with 0.1V increments and analyzing the peak force.
7. Stimulation with 0.1 sec. duration is delivered and contraction force recorded. Data is analyzed afterwards to find the peak contraction force.
8. Amplitude is increased by 0.1 V and step seven is repeated until full recruitment voltage is reached (a threshold which the increment in the amplitude no more causes an increment in the peak contraction force). For the rest of the experiment stimulation amplitude is fixed to full recruitment voltage.
9. In characterization experiments which the effect of variation in pulse-width is measured frequency is fixed to a value which induces tetanic contraction. Pulse-width is set to 25 μs and stimulation is delivered. Pulse-width increased by 25 μs and stimulation is repeated. Pulse-width is increased until 525 μs.
10. In characterization experiments which the effect of variation in frequency is measured pulse-width is fixed to a certain value. Frequency is set to 10 Hz and stimulation is delivered. Frequency increased by 10 Hz and stimulation is repeated. Frequency is increased until 200 Hz.

In the analysis peak contraction force is plotted due to stimulation frequency and pulse-width. Limits for pulse-width and frequency are determined. Later the data obtained from this experiment are used for modeling.

4.3.2.3. Muscle Characteristics due to Fatigue

This type of experiment is performed to characterize the fatigue behavior of the muscle. Muscle fatigue causes a temporary force reduction which changes the system characteristics of the muscle thus; it is needed to be characterized as well. In the

experiment a fatigue protocol is applied and decrease in contraction force of the muscle is observed by comparing the peak forces with the peak force measured at the beginning of the fatigue procedure.

In this experiment recent revision of muscle testing apparatus is used with direct stimulation method. Ringers solution is prepared before the experiment with the following receipt described in Section 4.3.2.1. Experimental procedure is described in steps.

1. Steps 1-8 applied which is described in previous section.
2. Stimulation signal pulse-width and frequency is fixed to a certain value.
3. Fatigue protocol applied which encompasses successive stimulations with 0.1 sec. Contraction and 0.9 sec. rest.
4. Same protocol applied for longer (2 seconds) duration stimulations.

In the analysis rate of force reduction is calculated. For longer stimulations change in the contraction force profile is observed for successive contractions.

4.3.3. Muscle Control Methods

In this thesis two methods of muscle control was performed. The first one is to control contraction force on long duration step and ramp references (longer as 1 to 2 seconds). The other method is to control the peak force of short duration contractions.

A long duration force generation may be required from muscle actuator with a certain profile regarding the needs of mechanism. However it is very likely for a mechanism to require cyclic short duration force generation. For this type of contractions, controlling the peak force of short duration contraction is sufficient since the contraction profile (as shown in Figure 4.24) does not change significantly with stimulation parameters and fatigue condition but the peak force changes.

The strategy for controlling contraction force over ramp and step references is shown in Figure 4.25. Signal generator produces a bi-phase stimulation signal with fixed frequency **(f)** and amplitude **(V)**. Pulse width **(pw)** of the signal is adjusted by PID according to error between reference and force output.

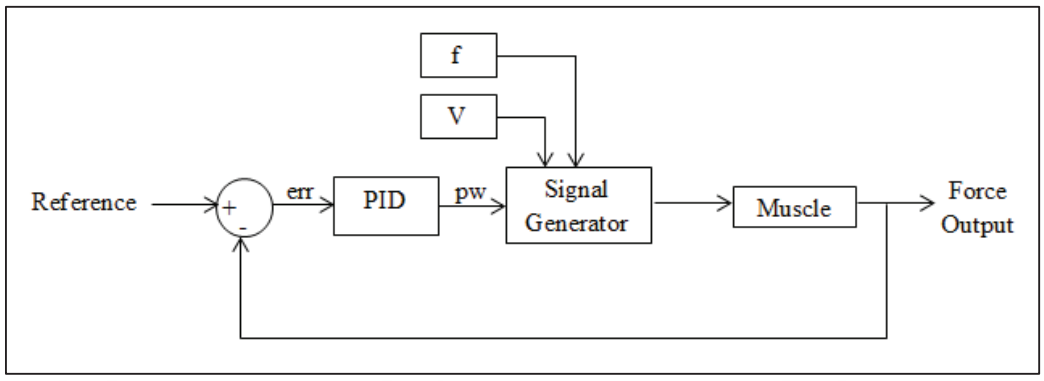

Figure 4.25 Control strategy for controlling muscle force on long duration ramp and step references

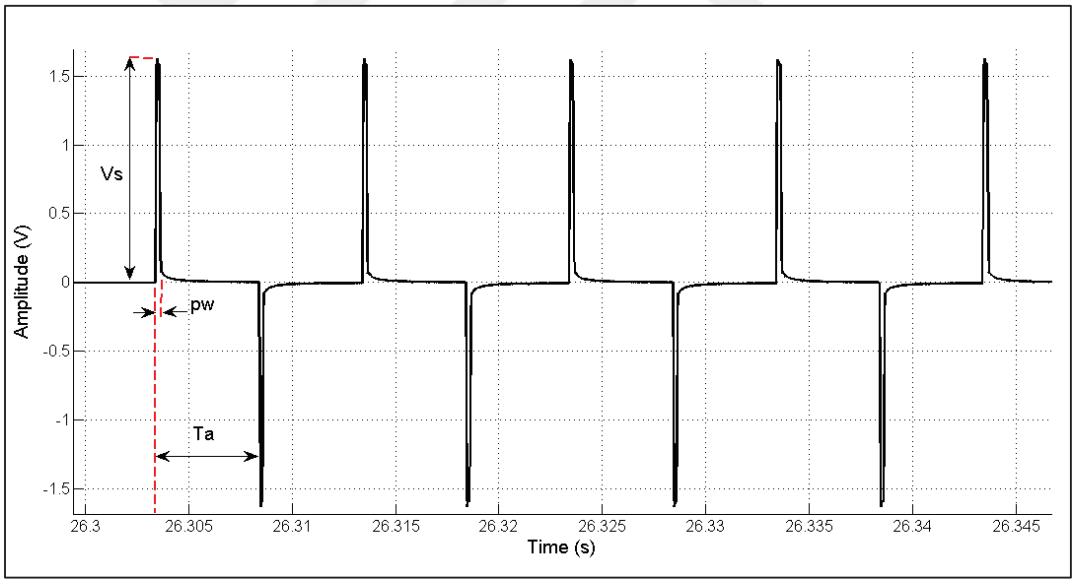

Figure 4.26 Signal generator output. To control muscle force pulse width **(pw)** is adjusted while signal amplitude **(V_s)** and activation period **(T_a)** remained fixed. Activation period **(T_a)** is the half of the signal period

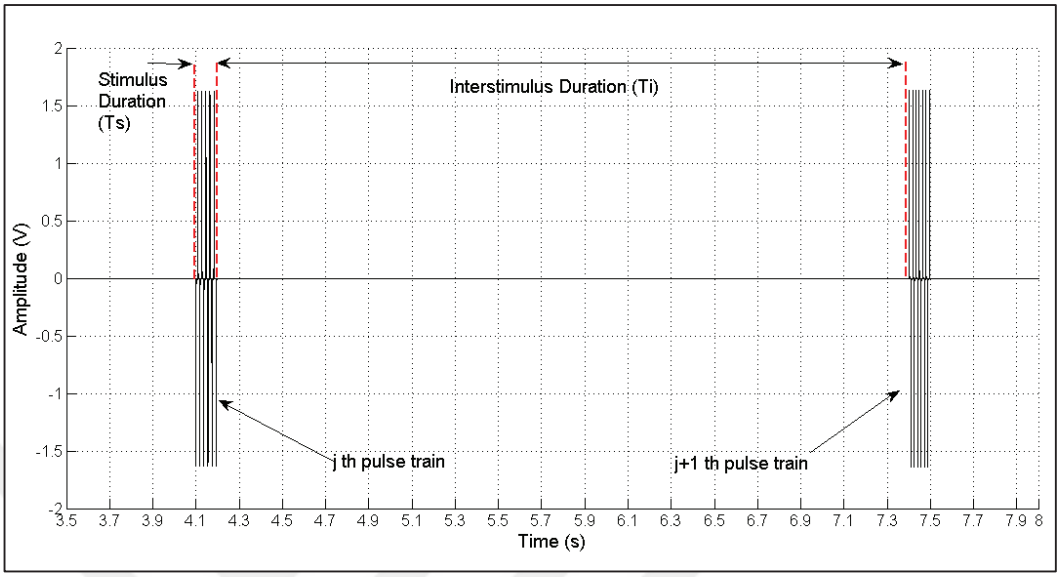

Figure 4.27 Signal generator output for controlling peak force of short duration successive contractions. Pulse-width **(pw)** and signal amplitude **(V_s)** are fixed while frequency **(f)** is changed for each pulse train. Inter-stimulus duration **(T_i)** is increased if recovery of muscle is required.

The stimulation signal created by signal generator is shown in Figure 4.26 for the controlling strategy shown in Figure 4.25. The signal generator output is shown in Figure 4.27 which was used to control peak force of successive short duration contractions.

To control force of successive short duration contractions pulse trains are delivered with certain stimulus duration **(T_s)** and inter-stimulus duration **(T_i).** Each pulse train contains certain number of pulses (depends on stimulation duration T_s) similar to pulses shown in Figure 4.26 and has its own signal properties such as amplitude, frequency and pulse-width. Since stimulation amplitude and pulse-width are not changed while controlling the peak force of contractions, only frequency **(f)** is adjusted for every pulse train. Inter-stimulus duration **(T_i)** is increased if the muscle is fatigued and recovery of force generation capability is required.

In Figure 4.28 strategy for controlling peaks of successive short duration contractions is shown. In the strategy pulse-width **(pw)** and amplitude **(V)** is fixed and stimulation frequency **(f)** is adjusted by PID for the pulse train. As muscle contracts in succession, the

peak force decreases due to fatigue and PID increases the stimulation frequency **(f)** accordingly to maintain the desired force. If the frequency is intended to be increased above a limit **(f_{lim})** another PID increases the inter-stimulus duration **(T_i)** to allow muscle to recover. If muscle recovers inter-stimulus duration is decreased. This strategy prevents reduction in actuator performance (in terms of force generation capability) due to muscle fatigue by reducing the frequency of activation.

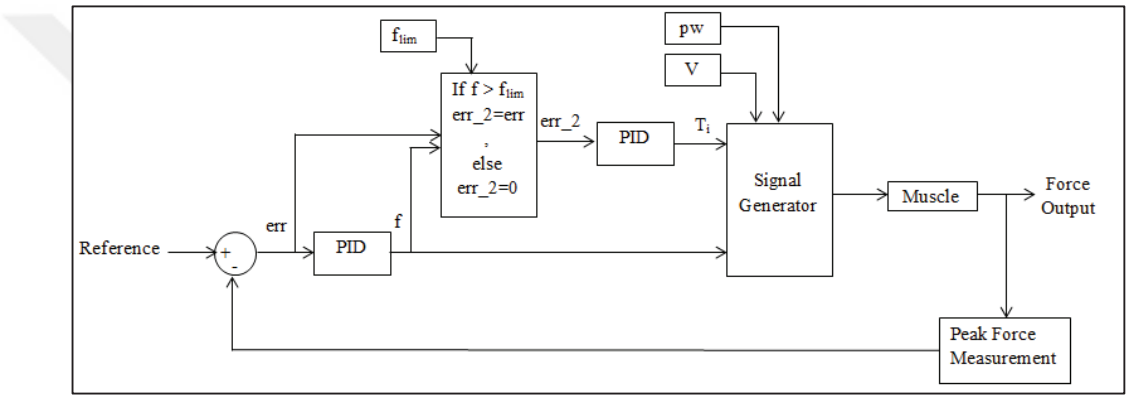

Figure 4.28 Control strategy for controlling peak force of short duration successive contractions

4.3.3.1. Controlling Force over Step and Ramp References

In this experiment contraction force is controlled over a step and ramp force reference with recruitment modulation method. Contraction force is measured and controller variable (pulse-width) is adjusted by PID controller to fit the force on desired reference. Experimental procedure is explained in steps.

1. Steps 1-8 applied which is described in Section 4.3.2.
2. Limits and resolution for controlling variable are adjusted and reference profile is defined.
3. Reference profile is created by controller algorithm and controlling parameter is adjusted by PID while the data is recorded.

4.3.3.2 Muscle Control for Successive Short Duration Contractions

In this experiment peak contraction force is controlled with temporal summation method. If the muscle is fatigued inter-stimulus duration is increased for recovery. This method allows muscle to operate without losing its performance in force generating capability with reducing the stimulation frequency. Here the experimental procedure is explained.
Steps 1-8 applied which is described in Section 4.3.2.

1. Limits and resolution for controlling variable (pulse-width or frequency) and reference value are adjusted.
2. Successive contractions are delivered as 0.1 sec. contraction and 0.9 sec. rest.
3. PID controlled coefficients are tuned by trial and error.
4. Controller code measures the peaks of the contractions and adjusts controller variable and inter-stimulus duration for the next stimulation.

5. MATHEMATICAL MODELLING

In this section three different methods are presented which models the characteristics of muscle. Since the tetanic response is generated by summation of twitches, modeling the twitch response allows the estimation of tetanic response at any stimulation frequency thus, first two models depends on characterization of twitch and calculation of tetanic response. The third model is used to model the fatigue behavior of the muscle. These models are used to test control algorithms and making assessments on certain aspects such as fatigue condition of muscle.

The first modeling method gives a relation between twitch properties and tetanic force enhancement which is proposed in [33]. In the model force response of an activated fiber is calculated and bridged to macro scale response of whole muscle via FEM. Second model is based on predicting the transfer function of twitch response and calculating the tetanic contraction force which is developed in this thesis. The fatigue model is applied according to the modeling idea given in [13]. By using the fatigue model, an assessment on fatigue behavior of muscle is made in Section 6.4.

5.1. Models Based on Twitch Characterization

The twitch response of muscle is the basic component of tetanic contraction since tetanic contraction is the sum of twitches as explained in Section 2.3.2. Twitch response of whole muscle as an organ is dependent on the number of fibers activated thus, it varies with stimulation signal amplitude, pulse-width (these stimulation parameters directly effect number of fibers activated as explained in Section 3.2) and fatigue condition of muscle.

Assuming a muscle which is stimulated with same stimulation signal amplitude and pulse-width and none of the fibers are not going into fatigue, a twitch response of this muscle would represent the behaviour through the entire operational life. However if the stimulation signal amplitude or pulse-width changes characteristics of twitch changes and the model parameters must be re-calculated to represent the behaviour of muscle under

these conditions. Another factor that changes the characteristics of twitch is the fatigue condition of muscle. A muscle stimulated with succesive pulse trains experiences fatigue and the characteristics of twitch changes after every stimulation. For such conditions at which the muscle experiences fatigue, the twitch response only represents the tetanic contraction if the fatigue condition is same for both twitch and tetanic responses. In the thesis twitch response is modelled with two different methods and tetanic response is calculated. Calculations are validated with the experimental data.

An experimental procedure is applied on a single specimen for model verification purposes. A single pulse applied on the muscle with a certain pulse-width and amplitude and the twitch response is measured. Just after the single pulse excitation a high frequency pulse train is sent and tetanic response is measured. To estimate the tetanic response, this twitch response is modeled and the estimated tetanic response is compared with the experimental tetanic response which is measured just after the single pulse excitation.

In Figure 5.1 the twitch response is modeled shown as dashed line and the tetanic response is estimated accordingly. Then, this estimation is compared with the experimentally measured tetanic response shown as solid line which is measured just after measuring the twitch response. Both twitch and tetanic responses are generated with same stimulation signal amplitude and pulse-width.

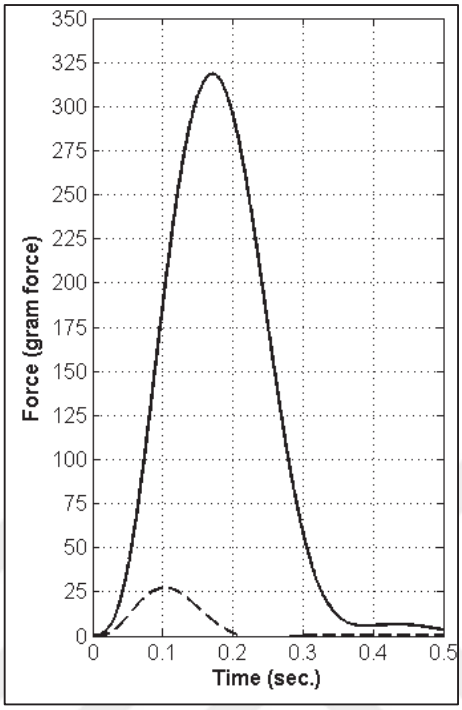

Figure 5.1 Twitch contraction and induced tetanic contraction for 200 Hz stimulation frequency, twitch response (dashed line) is modeled, tetanic response (solid line) was measured just after measuring the twitch response and used to validate the model estimation.

5.1.1. Modelling the Twitch with a Sigmoid Function

In the model presented by [33] the force generation of a muscle is divided into two parts as active and passive response. Active force response is generated by contractile element as the muscle is activated. Passive response of muscle is the force induced by stretching the connective collagen tissue in muscle which behaves like a spring. However in this thesis only active part of the force is calculated using this model since no isotonic experiments are performed for model validation. Thus, initial passive forces in isometric experiments are considered as the datum.

The model calculates the force response of a fiber and macro scale behavior is predicted via FEM by modeling the fibers in 3D according to the fiber architecture of muscle. Since the fiber architecture of muscle specimens are not obtained in this thesis a different

approach is proposed for this model as applying the model for whole muscle instead of fibers. This approach assumes whole muscle as a single fiber. In the model, first twitch response of fiber is modeled and tetanic contraction behavior is calculated accordingly. In this proposed case twitch response of whole muscle is modeled and tetanic contraction force is calculated using this method.

The model defines the properties of twitch in terms of twitch contraction time ($\mathbf{T_1}$) and peak force ($\mathbf{P_1}$). In Figure 5.2 measures of twitch contraction are shown. Here, $\mathbf{T_1}$ is defined as the time elapsed until the peak force is reached. For fiber based modeling twitch contraction time and peak force are assumed as constant for the same type of fibers. However for the approach presented in this thesis the twitch properties of whole muscle is taken into account which represents the behavior of all fibers in the muscle. Thus, measures of twitch varies for different stimulation conditions such as stimulation signal amplitude and pulse-width and fatigue condition of muscle which are determining the number of activated fibers in the muscle.

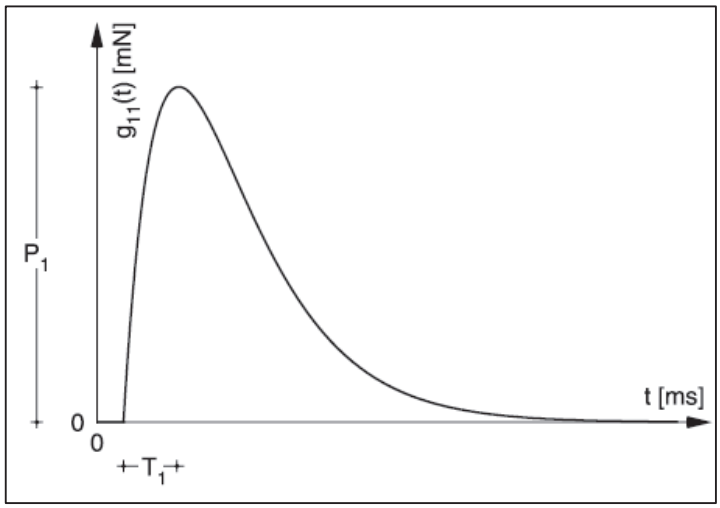

Figure 5.2 Froce profile of a single twitch peak twitch force (P1), contraction time (T1) **[33]**

Contraction force of a twitch is calculated with Equation 5.1 as a function of time assuming the muscle is a single fiber driven by single motor unit. Where; $\mathbf{F_{active}}$ is the active force generated by muscle, **t** is time, $\mathbf{t_j}$ is the start time of the j^{th} action potential (or pulse excitation) and n_{IMP} is the number of pulse excitation with j=1,2,3,…,n_{IMP}. The active force is calculated by summing twitch forces.

$$F_{Active} = \sum_{j=1}^{n_{IMP}} G\,(T_1/I_1) g_j(t - t_j) \tag{5.1}$$

Here term $\mathbf{G(T_1/I_1)}$ is defined as the gain function and $\mathbf{g_j(t-t_j)}$ term is defined as the time-dependent function. Equations for gain function and time-dependent functions are Equation 5.2 and 5.3 respectively.

$$G_1(T_1/I_1) = \frac{S_1(T_1/I_1)}{T_1/I_1} = \frac{1 - e^{-2(T_i/I_i)^3}}{T_1/I_1} \tag{5.2}$$

$$g_j(t - t_j) = \frac{P_1(t - t_j)}{T_1} e^{1-((t-t_j)/T_1)} \tag{5.3}$$

The relationship between $\mathbf{F_{active}}$ and normalized stimulus rate ($\mathbf{T_1/I_1}$) is nonlinear which can be described via sigmoid relationship [33] as given in Equation 5.4.

$$S_1(T_1/I_1) = 1 - e^{-2(T_i/I_i)^3} \tag{5.4}$$

In Figure 5.3 the non-linear relationship between normalized stimulus rate and sigmoid behavior $\mathbf{S(T_1/I_1)}$ and gain function $\mathbf{G(T_1/I_1)}$ is given.

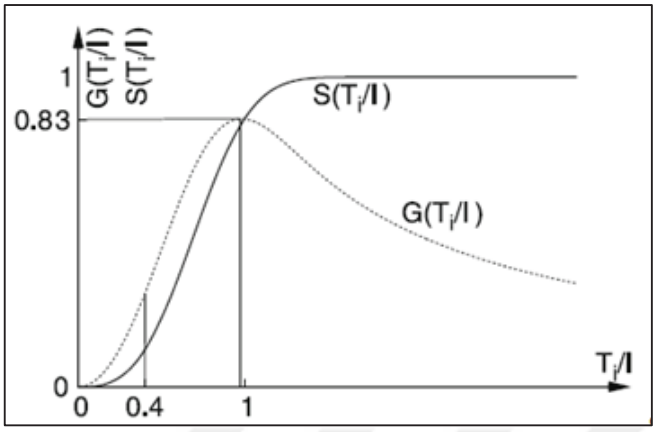

Figure 5.3 Non-linear relationship between gain (dotted line)/sigmoid (solid line) and stimulus rate

This modeling method is used to test control algorithms for temporal summation control method. If the twitch properties for different recruitment states (due to stimulation amplitude, pulse-width and fatigue) are supplied, model can also be used in modeling for recruitment modulation.

To add the fatigue effect to model $\mathbf{F_{active}}$ may be multiplied by and exponential function $\mathbf{e^{\tau t}}$ **(**Equation 5.5) which the fatigue time constant τ is calculated due to experimental data. Values for $\mathbf{P_1}$ and $\mathbf{T_1}$ are calculated due to experimental data as well. Time constant τ is calculated by fitting an exponential equation between peak point (A) and stimulation end (B) shown in Figure 5.4.

$$F_{Active,f} = \left(\sum_{j=1}^{n_{IMP}} G\,(T_1/I_1) g_j\left(t - t_j\right) \right) e^{\tau t} \qquad (5.5)$$

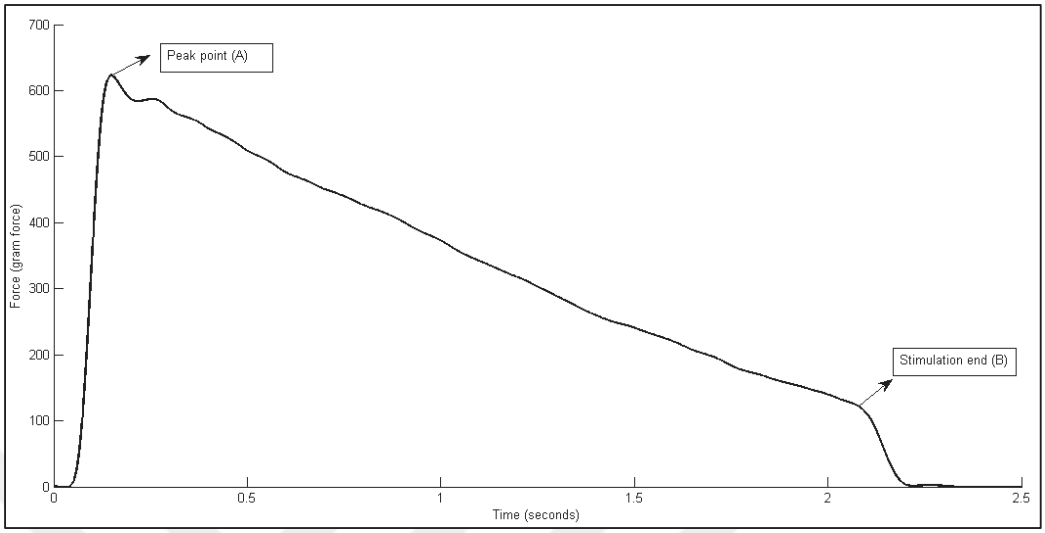

Figure 5.4 Experimental data for isometric contraction with two seconds stimulation, point "A" is peak and point "B" is end of stimulation

5.1.2. Modelling the Twitch by Predicting the Transfer Function

In this section a different approach is proposed for muscle modeling which also based on chacterizing the twitch response. Here the transfer function of single twitch is predicted and tetanic response is calculated accordingly. As stated in section 5.1 twitch response of whole muscle varies due to number of activated fibers specified by stimulation amplitude, pulse-width and fatigue condition. In Equation 5.6 definition of transfer function is given in s domain where **X(s)** is the electrical input signal and **Y(s)** is the force output signal.

$$H(s) = \frac{Y(s)}{X(s)} \tag{5.6}$$

The transfer function H(s) is the Laplace transform of the response of the system to a unit impulse excitation. An impulse signal may be approximated with a very short duration pulse of unit area. The contraction force caused by such a pulse is a twitch. Such an experiment was done on one specimen at four different times at different fatigue levels during an experimental procedure. In Figure 5.5 the input of the transfer function is shown which is a single pulse having an amplitude of V_s and duration of Δt. For the calculations V_s is unity since the voltage level of the pulse was selected as the full-recruitment voltage of the specimen in the experiment and Δt is 100μs which is the pulse-width of the stimulation signal.

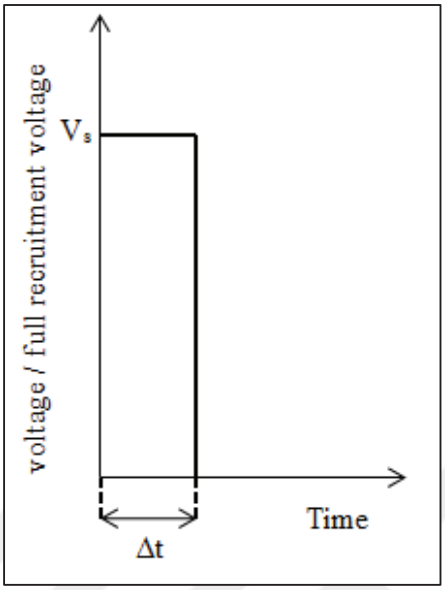

Figure 5.5 Single pulse excitation for twitch characterization

The twitch response (similar to twitch as shown as dashed lines in Figure 5.1) in the time domain was analyzed using MATLAB system identification toolbox. The transfer function of the order shown in Equation 5.7 was determined by trial-and-error and the coefficients were predicted and results are given in Appendix C. Poles and zeroes of H(s) at the four time instances are also given in Appendix C.

$$H(s) = \frac{c_1 s + c_2}{c_3 s^4 + c_4 s^3 + c_5 s^2 + c_6 s + c_7} \tag{5.7}$$

In this model a muscle which is generating twitch response is assumed as a linear system thus, Laplace transform is performed for the system response to a single pulse excitation normalized by full recruitment voltage. However the relationship between stimulation frequency and force is non-linear as shown in Figure 5.3 and in Section 6.2 (experimental results). Thus, output in time domain **y(t)** must be multiplied by the gain function given in Equation 5.2 to include the non-linearity between excitation frequency and force output which results in Equation 5.8. Where $\mathbf{F_{active}}$ is the contraction force. The tetanic response of

muscle is calculated and compared with the experimental tetanic contraction data (similar to tetanic contraction as shown as solid lines in Figure 5.1).

$$F_{Active,f} = y(t)G(T_1/I_1) \tag{5.8}$$

Ones the transfer function is estimated force response of muscle at any frequency is calculated for the certain fiber recuitment state. If twitch can be characterized for all possible fiber recuitment states and the model is updated as recruitment state changes a robust prediction of force enhancement thus, muscle control would be obtained without complex muscle models.

5.2. Modeling the Fatigue Behavior

In this section a modeling technique presented based on the idea given in [59]. This model is coupled with the model presented above [33] in the study [9]. The concept is explained as dividing fibers of functioning muscle into three groups which are active fibers, fatigued fibers and fibers currently resting. The number of fibers of each group are shown as $N_i^{fib\ A}$, $N_i^{fib\ F}$, $N_i^{fib\ R}$ and named as number of active, fatigued fibers and fibers in the resting state, respectively where **i** is the number of fiber types. Regarding the concept of the model these fibers are able to switch between different groups with the rates of $A_i(t)$, $F_i(t)$ and $R_i(t)$. Transfer of fibers from resting to active state is controlled by activation rate Ai(t). After certain time some of the active fibers are fatigued and switched to fatigued state which is controlled by fatigue rate $F_i(t)$. After a while these fibers are recovered and activated again with the recovery rate of $R_i(t)$. Although, these rates time-variant, here they are assumed as constant for simplification. In Figure 5.4 the concept is shown.

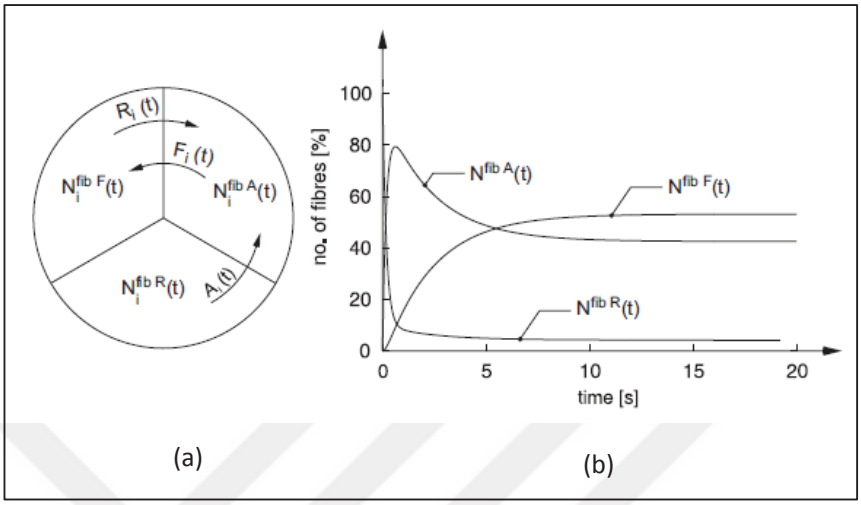

Figure 5.6 Pool of fibers divided into three different groups (a), Number of fibers in groups due to time for certain rates (b) **[9]**

Equations 5.9-5.11 are the differential equations which represents the change of number of fibers with time. The total number of fibers is denoted as $\mathbf{N^{fib\ 0}}$. In this model whole muscle is considered as a single fiber as in the modeling method presented in Section 5.1.1. Regarding the assumption numbers of fibers in each group are normalized with total number of fibers to achieve $\mathbf{N^{fib\ 0}}$ as unity. Since there is one fiber (whole muscle is a single fiber) indices **i** is removed from variables.

$$\frac{dN^{fib\ A}(t)}{dt} = A(t)N^{fib\ R}(t) + R(t)N^{fib\ F}(t) - F(t)N^{fib\ A}(t) \tag{5.9}$$

$$\frac{dN^{fib\ F}(t)}{dt} = F(t)N^{fib\ A}(t) - R(t)N^{fib\ F}(t) \tag{5.10}$$

$$N^{fib\ R}(t) = N^{fib\ 0} - N^{fib\ A}(t) - N^{fib\ F}(t) \tag{5.11}$$

Equations 5.12-5.14 are solutions of Equations 5.9-511 with following initial conditions.
$N^{fib\ A}(t=0) = N^{fib\ F}(t=0)$, $N^{fib\ R}(t=0) = N^{fib\ 0}$

$$\frac{N^{fib\ A}(t)}{N^{fib\ 0}} = \frac{e^{-At}(A-R)}{R-A+F} - \frac{e^{-(F+R)t}FA}{F^2+R^2+2RF-FA-RA} + \frac{R}{F+R} \tag{5.12}$$

$$\frac{N^{fib\ F}(t)}{N^{fib\ 0}} = \frac{-e^{-At}F}{R-A+F} - \frac{e^{-(F+R)t}FA}{F^2+R^2+2RF-FA-RA} + \frac{F}{F+R} \tag{5.13}$$

$$\frac{N^{fib\ R}(t)}{N^{fib\ 0}} = -e^{-At} \tag{5.14}$$

Since only active fibers are in charge of force development, normalized number of active fibers is multiplied by $\mathbf{F}_{max}$ which is defined as the peak contraction force if all fibers were activated.

$$F_{Active,f} = F_{max}\frac{N^{fib\ A}(t)}{N^{fib\ 0}} \tag{5.15}$$

Peak force $\mathbf{F}_{max}$ is measured from experimental data and fiber transition rates are predicted by using genetic algorithm for which the model output fits to experimental data. These fiber transition rates of different contractions measured from same muscle specimen at different times are compared. Number of fibers in each section and transition rates identifies the fatigue condition of the muscle.

6. RESULTS

6.1. Force Length Relationship

Here the experimental data regarding contraction force and muscle length relationship is given. As mentioned before in Hills model, a muscle is the integration of passive and active components: Active and passive response of a muscle is measured as a function of pre-applied muscle elongation with the experimental procedure explained in Section 4.3.2.1. This type of experiment is a quasi-static type measurement and data presented here can be used while calculating isometric contraction response of a shortening muscle. Sample result for a specimen is given in Figure 6.1. Active force is maximum at optimum point which is at zero displacement. Here peak forces of contractions with duration of one second are plotted at different positions. As the displacement increases or decreases active force decreases due to reduced number cross-bridges formed during contraction (as shown in Figure 2.8). Passive force increases due to increasing displacement for the lengths greater than the length at optimum point. Total force is the summation of these two components.

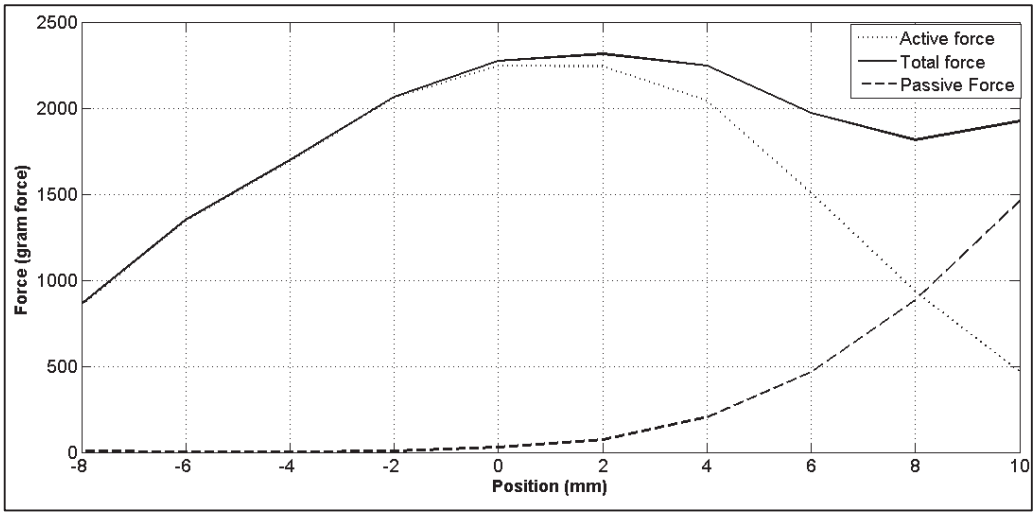

Figure 6.1 Total, active and passive force response of muscle due to displacement. Optimum point is at zero. Signal amplitude 10V, frequency 40 Hz and pulse-width 10 ms

In Figure 6.2 active response of each specimen is normalized due to peak active force to be able to make an assessment of active force profile due to displacement. Figure 6.2 gives the active response of muscle for 30 specimens. Although all specimens have the same trend differences between specimens increases as the initial length goes towards extremities. Passive force of each specimen is normalized due to their peak passive force and plotted in Figure 6.3 due to position with 95.4 per cent confidence bounds. Muscle behaves like a strain stiffening, non-linear spring. Regarding the data specimens have a wide range of stiffness.

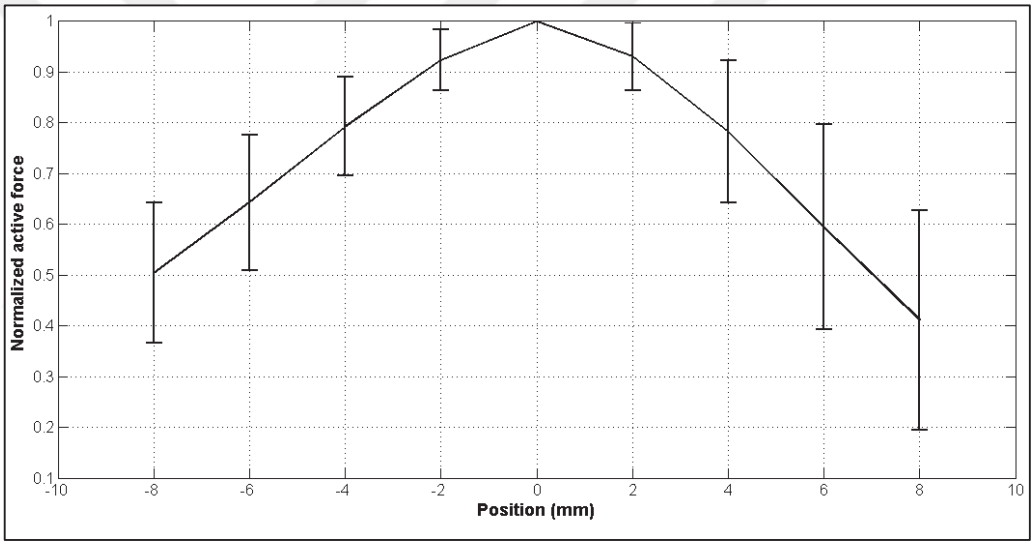

Figure 6.2 Normalized active force due to position according to data from 30 specimens. Optimum point is placed at position zero. Error bars indicate ±σ

Although specimens have the same passive response, estimating the exact stiffness of the particular muscle which is going to be implemented in mechanical system may be critical. As a solution, the force-length curve may be expressed with a simple exponential function (Equation 6.1) and the coefficients of the function may be found by measuring passive force at three different muscle lengths.

$$F_{passive} = ae^{bx} \tag{6.1}$$

In the trials first muscle length (**x)** is selected as position zero, second selected as maximum length of the working stroke and third is selected in the middle of these two. Rest of the force-position curve is predicted with RMS error between 0.02-0.05 per cent.

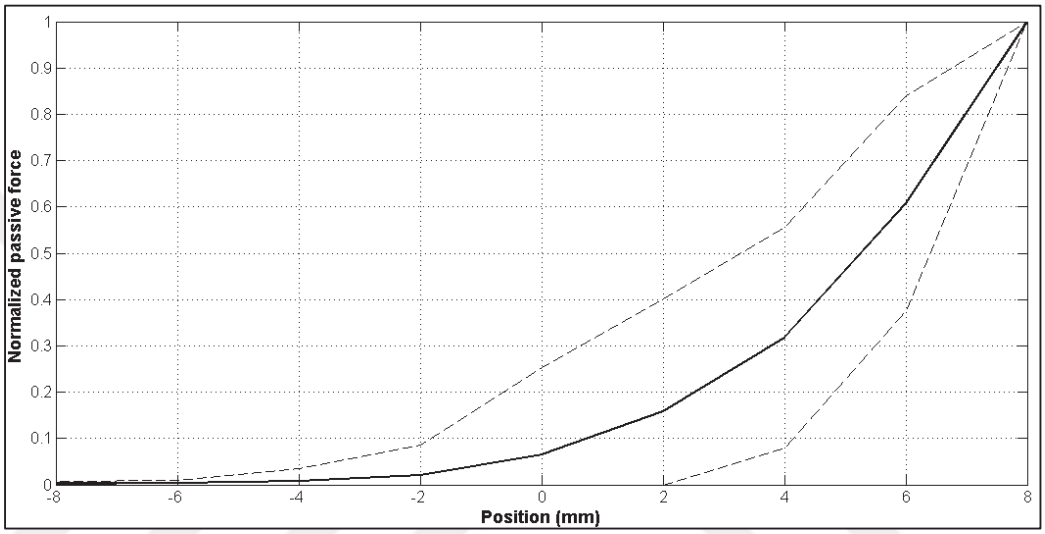

Figure 6.3 Normalized passive force due to position according to data from 30 specimens with 95.4 per cent confidence bounds. Optimum point is placed at position zero.

6.2. Mechanical Response due to Stimulation Parameters

Active force response of muscle is measured for various stimulations such as (frequency and duty cycle). As mentioned in experimental procedure in section 4.3.2.2 amplitude is fixed to a constant value during the experiment. This value is called as full recruitment voltage and differs due to specimen and stimulation method. Procedure for finding full recruitment voltage is described in section 4.3.2.2. With suction electrode stimulation (described in section 4.2.3.3) full recruitment voltage is found as 1.69 ±0.18 V for number of experiments (N=11). For nerve clamping stimulation method full recruitment voltage is found as 1.43±0.17 for N=8.

Peak active force of contraction with duration of 0.1 s is plotted for various pulse-widths with constant frequency (40 Hz) in Figure 6.4. Activation limit for pulse-width is 25 or 50

μs and the force reaches its maximum at around 150 μs. For higher pulse-widths (above 200 μs) force remains constant or decreases. Some specimens generated highly random forces for pulse-widths above 300 μs. As shown in data from individual seven left specimen, random forces are generated for pulse-widths above 350 μs.

In Figure 6.5 similar data is given for 100 Hz stimulation frequency with smaller pulse-width steps (10 μs). As shown activation pulse-width threshold is 20 and 30 μs and maximum force is reached at around 150 μs as in Figure 6.4. However forces in Figure 6.5 are higher than the ones in Figure 6.4 since the stimulation frequency is higher.

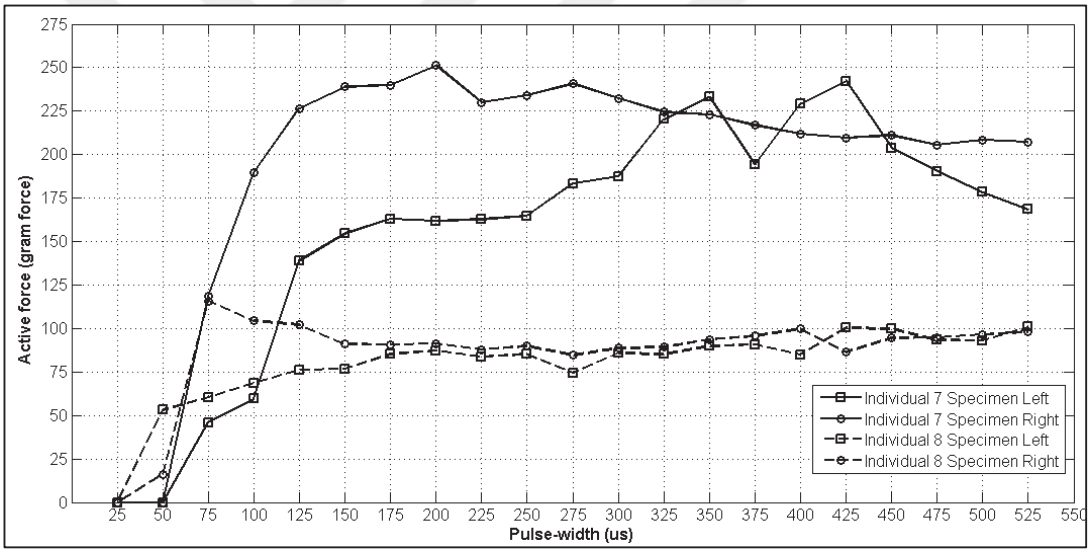

Figure 6.4 Pulse-width effect on active response, data plotted for two individuals with specimens isolated from left and right legs. Stimulation frequency is 40 Hz and pulse-width step is 25 μs at full recruitment voltage

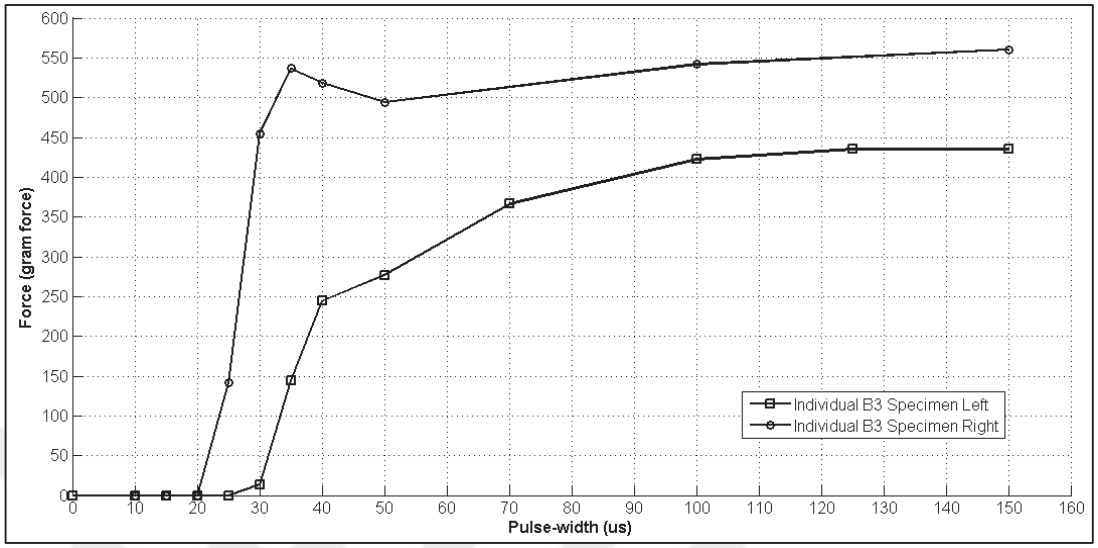

Figure 6.5 Pulse-width effect on active response with smaller pulse-width steps. Data plotted for one individual with specimens isolated from left and right legs. Stimulation frequency is 100 Hz and pulse-width step is 10 µs at full recruitment voltage

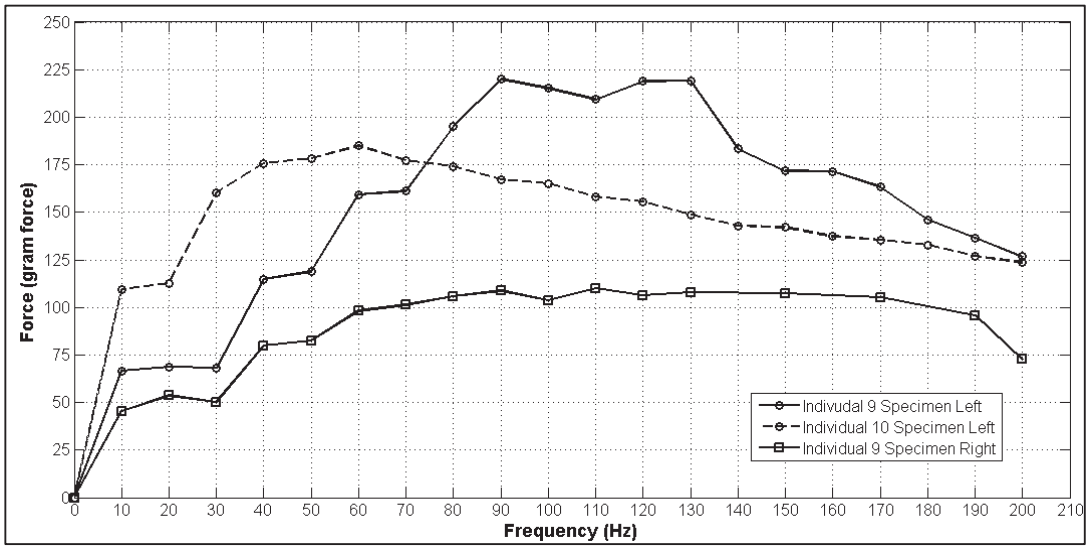

Figure 6.6 Frequency effect on active response. Data plotted for two individuals with isolated from left and right legs for individual nine and from left leg for individual ten. Right specimen of individual ten is discarded due to its problematic function. Stimulation pulse-width is 175 µs and frequency step is 10 Hz at full recruitment voltage.

Using a method similar to the method which is described above, force response of muscle due to frequency is measured. Experiments were made according to the experimental procedure described in section 4.3.2.2. However in this type of experiment pulse-width is set to a constant value (175 μs) and frequency is changed between 10-200 with 10Hz increments. As shown in Figure 6.6 active force increases as frequency increases until a threshold (60 Hz for individual 9 right specimen and individual 10 left specimen, 90 Hz for individual 9 left specimen). Muscles are activated even at 1 Hz (twitch response).

Although behavior of specimens for stimulation parameters are similar, there is no coherence between specimens isolated from separate individuals and even between specimens isolated from same individual. Thus, characterizing the muscle specimen in individual basis would be the solution to have accurate behavior. The relationship between contraction force and stimulation frequency is non-linear which is coherent with the modeling idea presented in Section 5.1.1 particularly with Figure 5.2.

6.3. Characterization due to Twitch Response

Twitch is the basic element of the tetanic contraction and a tetanic contraction may be fully explained by the twitch response. Twitch response is measured for specific stimulation signal properties and tetanic response of the muscle is calculated via models presented in sections 5.1 and 5.2. In Figure 5.1 twitch response of a specimen is given with induced tetanus for 200 Hz stimulation frequency.

Due to twitch response of muscle tetanic behavior is calculated by two modeling methods for 200 Hz stimulation frequency and compared with the experimental tetanic contraction data at 200 Hz. Here model described in section 5.1 is named as “Model A” and model in section 5.3 is named as “Model B”. Sample results for four different contraction data is plotted in Figure 6.11-6.14 which belong to same specimen at different fatigue conditions.

For sample calculations peak twitch force **(P)** and contraction time **(T)** are given in Table 6.1 which are the inputs of model A. An assessment for fatigue condition of muscle can be made with the magnitude of peak twitch force. Transfer functions of the twitch responses due to single pulse excitation are given in Equations C.1-C.4. Zero and pole locations of

these transfer functions are plotted in Figures C.1-C.4. In Figures 6.7-6.10 output of estimated transfer functions and the experimental data (true data) are plotted. Figures 6.11-6.14 gives the resultant tetanic force and compares them with the experimental tetanic force (true data).

Table 6.1 Twitch peak force and contraction times found for four different sample calculations.

Calculation Number	Twitch Peak Force **(P)** mN	Contraction Time **(T)** s
1	488	0.0822
2	284	0.09
3	272	0.0885
4	258	0.0963

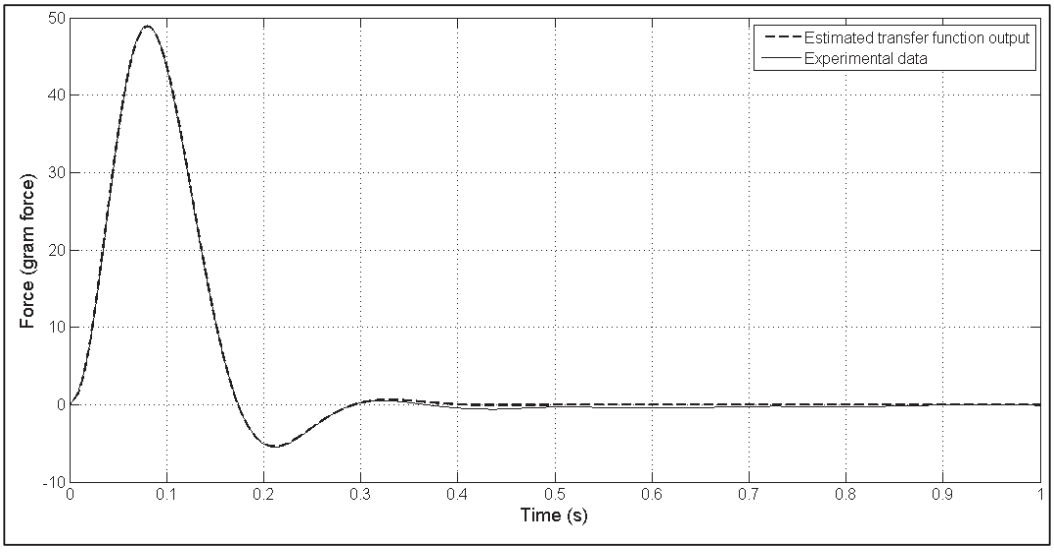

Figure 6.7 Comparison of the output of estimated transfer function and experimental data for sample calculation 1. Transfer function is given in Equation C.1

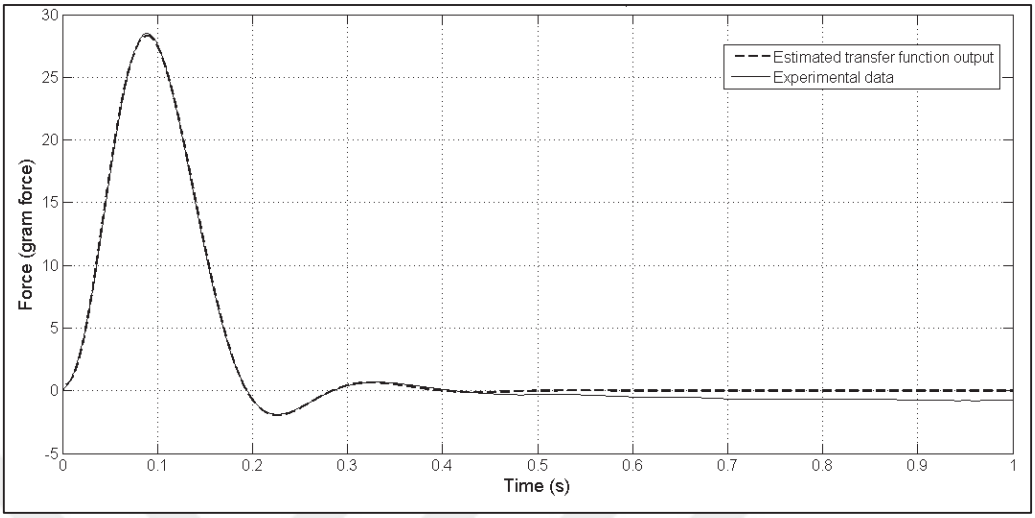

Figure 6.8 Comparison of the output of estimated transfer function and experimental data for sample calculation 2. Transfer function is given in Equation C.2

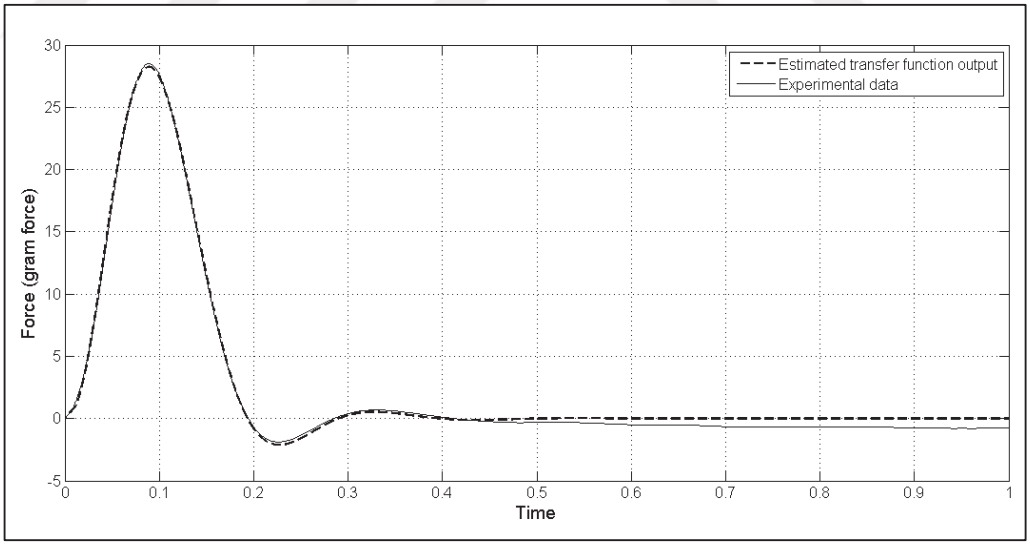

Figure 6.9 Comparison of the output of estimated transfer function and experimental data for sample calculation 3. Transfer function is given in Equation C.3

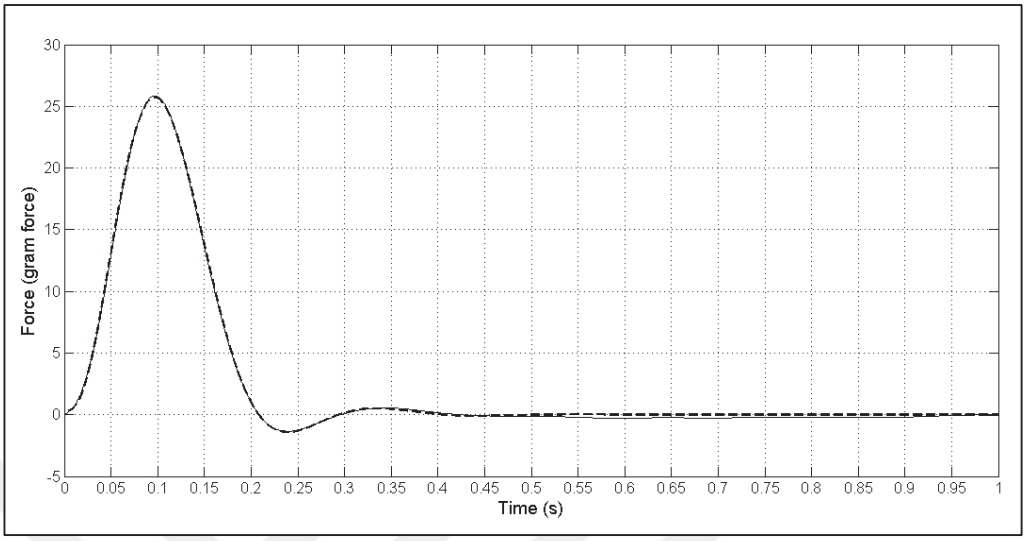

Figure 6.10 Comparison of the output of estimated transfer function and experimental data for sample calculation 4. Transfer function is given in Equation C.4

As shown, model A results in larger impulse (area under the force-time curve) while model B results in smaller impulse than the experimental data. Peak forces are calculated with 9 per cent error for model A and with 10.5 per cent error for model B in average. No data presented for different frequencies since no adequate experimental data acquired for comparison.

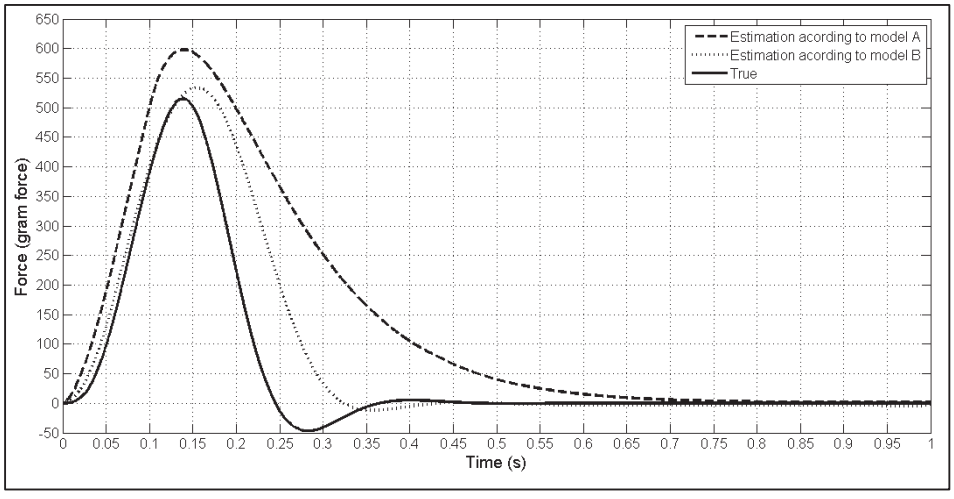

Figure 6.11 Comparison of calculations with experimental data due to twitch response. Sample result 1

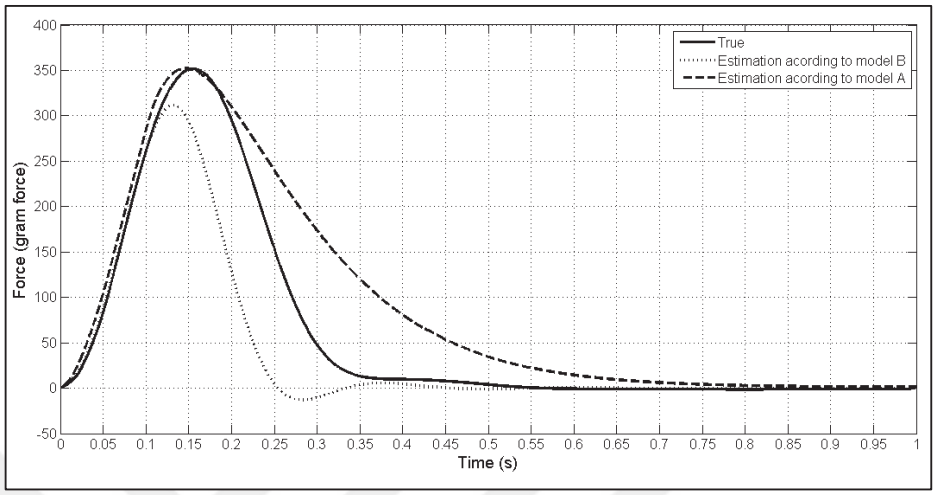

Figure 6.12 Comparison of calculations with experimental data due to twitch response. Sample result 2

As shown in Figure 6.11 model B estimated the tetanic response than model A which calculated a higher peak force. For second sample calculation model A has a better estimation as shown in Figure 6.12 while model B calculated lower contraction forces for tetanic response.

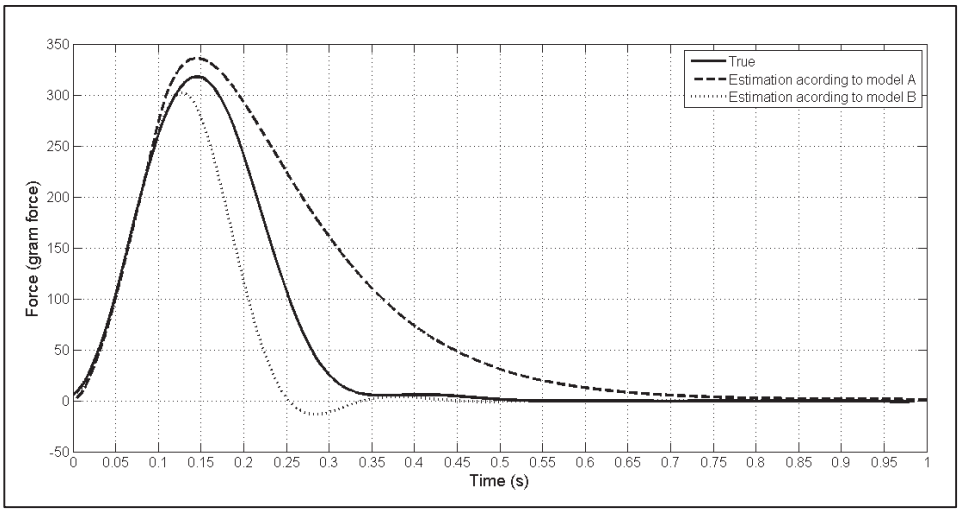

Figure 6.13 Comparison of calculations with experimental data due to twitch response. Sample result 3

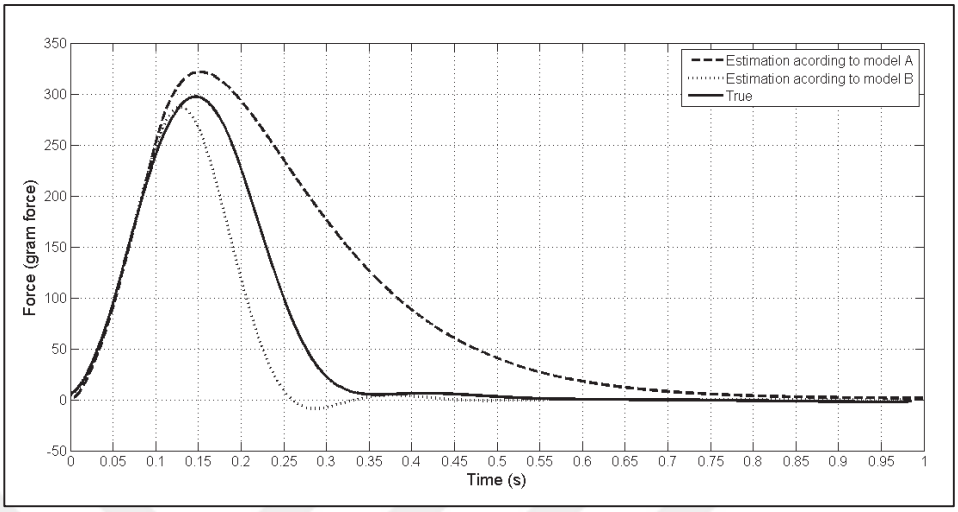

Figure 6.14 Comparison of calculations with experimental data due to twitch response. Sample result 4

As shown in Figures 6.13 and 6.14 both models made better estimations compared to the results shown in Figures 6.12 and 6.13. However as stated previously magnitudes of impulses (the area under force-time curve) of calculated data are still different than the magnitude of experimental data.

6.4. Fatigue Characteristics

One of the most significant parameter that effect force enhancement is the fatigue condition of muscle besides stimulation parameters. A fatigued muscle loses its capability of force generation temporarily and recovers within a certain time. However the fatigue rate and recovery time is critical for the muscle used as an actuator and this effect must be included in the control strategy. As an example for fatigue behavior peak contraction force are plotted for successive contractions of a specimen. Peak active forces of 100 successive contractions with 0.1 seconds contraction followed by 0.9 seconds rest are plotted in Figure 6.11. Although stimulation parameters are fixed (frequency: 200 Hz, pulse-width: 100 μs and amplitude: full recruitment voltage) contraction force decreases with decreasing rate since fibers are losing their capability of force production due to fatigue.

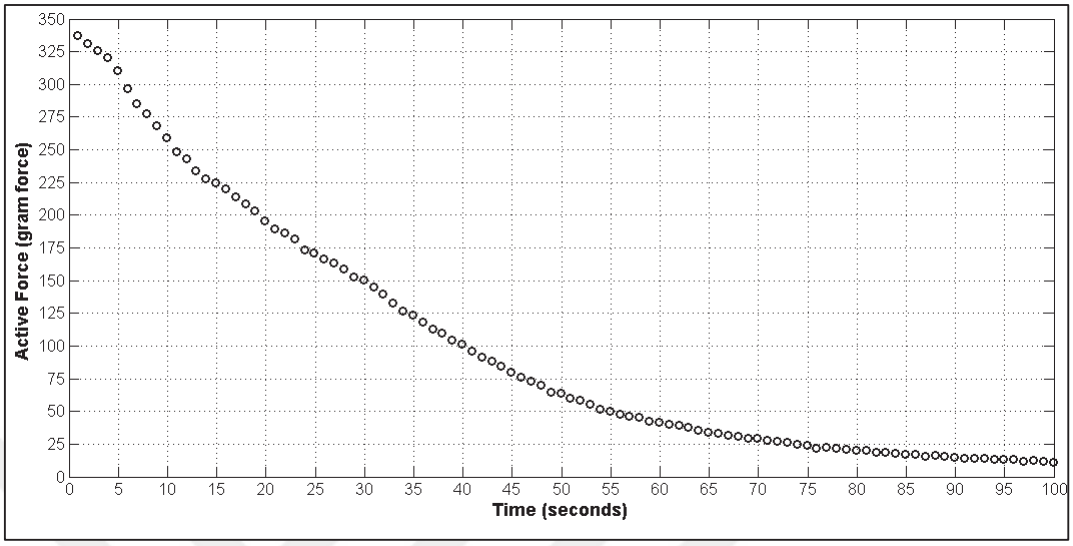

Figure 6.15 Peak forces of 100 successive contractions with 0.1 seconds stimulation and 0.9 seconds rest. For stimulation frequency 200 Hz , pulse-width 100 us and amplitude full recruitment voltage

Using the modeling idea explained in section 5.2 fatigue condition of the muscle may be characterized by three coefficients (transition rates); $A_i(t)$, $F_i(t)$ and $R_i(t)$. Thus model fitted on contractions with different fatigue conditions. Fiber transition rates are found due to experimental data using genetic algorithm. Here three contractions from different specimens are modeled and potted in Figure 6.16-6.18 with the experimental data. Number of active, fatigued fibers and number of fibers in rest normalized due to total number of fibers are plotted due to time.

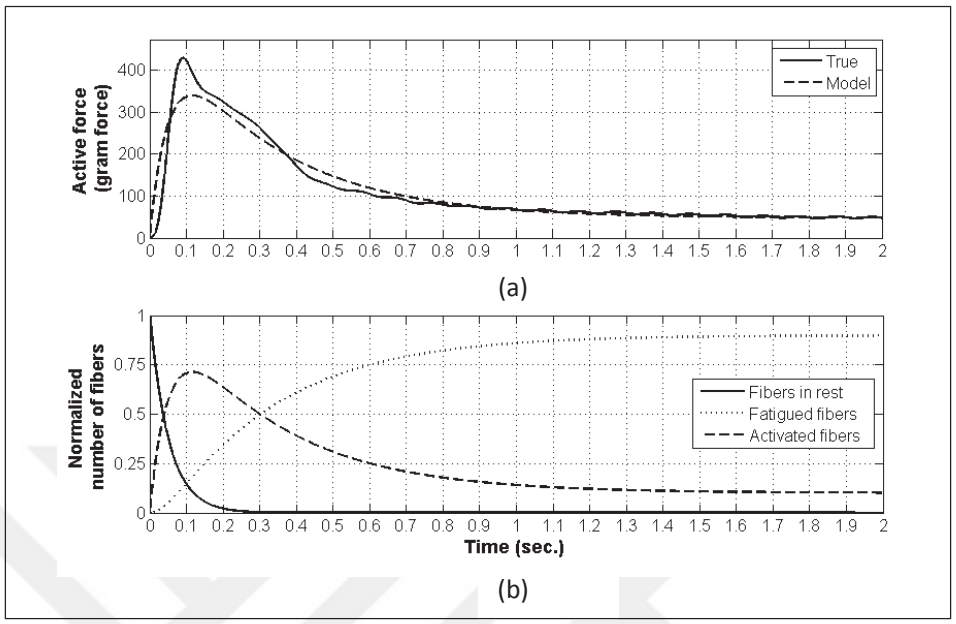

Figure 6.16 Experimental data and fitted model (a), normalized number of activated, fatigued and fibers at rest due to contraction time (b). For fiber transition rates A=19.26, R=0.332, F=2.971

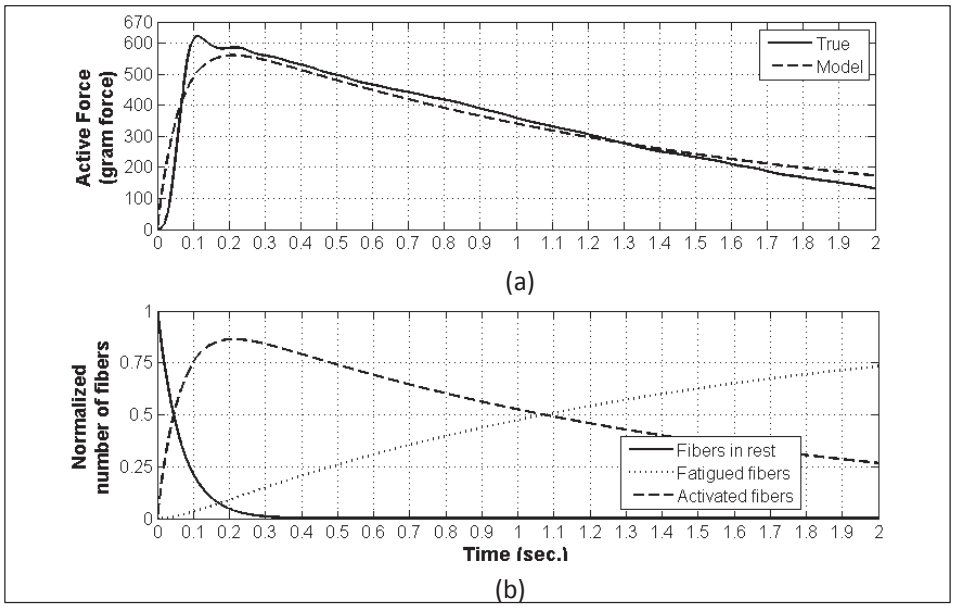

Figure 6.17 Experimental data and fitted model (a), normalized number of activated, fatigued and fibers at rest due to contraction time (b). For fiber transition rates A=16.133, R=0.342, F=0.915

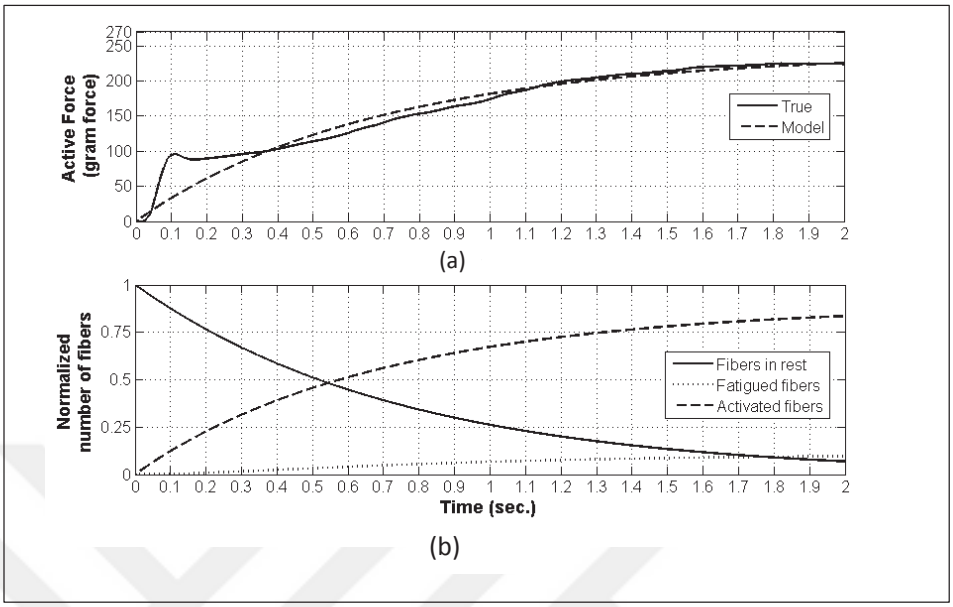

Figure 6.18 Experimental data and fitted model (a), normalized number of activated, fatigued and fibers at rest due to contraction time (b). For fiber transition rates A=1.657, R=5.682, F=0.744

In Figure 6.16 contraction data from highly fatigued muscle is given. After the force reaches its maximum it decreases considerably and remains steady afterwards. Nnumber of fatigued fibers is the highest (90 per cent) while activated fiber numbers is 10 per cent. In Figure 6.17 muscle experiences less fatigue and has more activated fibers. In Figure 6.18.a resting fibers are recruited gradually not like the contraction in Figure 6.16 and 6.17. The fatigue transition rate is higher in Figure 6.16 while data in Figure 6.17 and 6.18 have higher activation rate and hıgher resting rate respectively. These methods allow characterizing the fatigue behavior and to acquire an assessment on fatigue condition of muscle.

6.5. Muscle Control

In the thesis two types of control experiments are conducted. In the first one presented here muscle force is controlled over long duration step and ramp references by adjusting the pulse-width with fixed stimulation frequency (100 Hz) and constant amplitude (full recruitment voltage). In the second method peak active forces of frequent successive contractions are controlled.

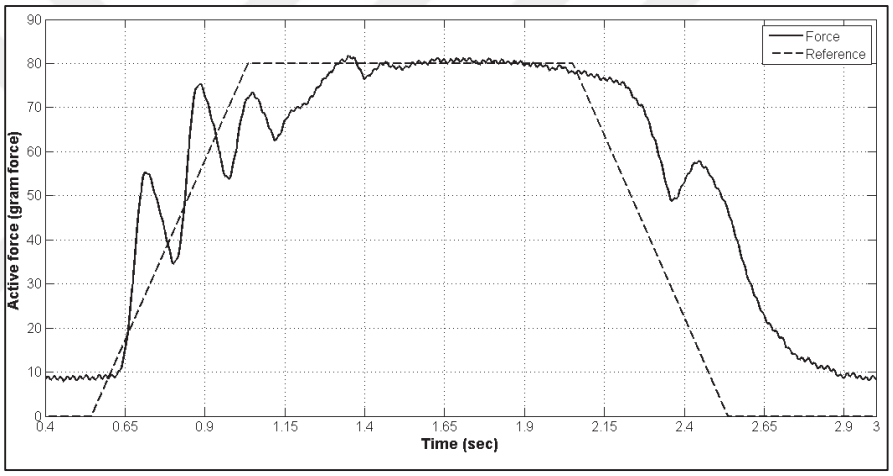

Figure 6.19 Contraction force control over ramp reference. Result 1

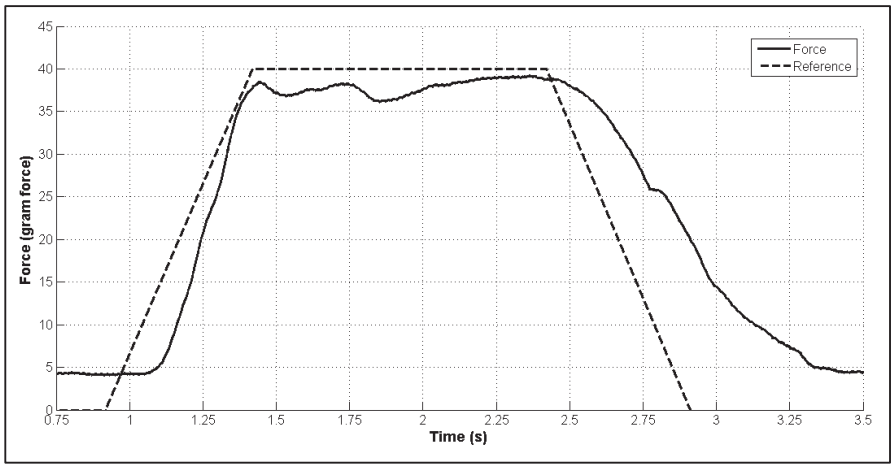

Figure 6.20 Contraction force control over ramp reference. Result 2

In Figure 6.19 and Figure 6.20 force responses of muscle are given for the control over ramp reference. In Figure 6.19, although muscle has instability on the ramp it reaches the plateau with a minor error. Force decays with a delay and does not track the reference as the reference ramps down. In Figure 6.20 delay is observed at the beginning of contraction, however the performance is better for tracking ramps for this result. The contraction force makes an undershoot at the plateau.

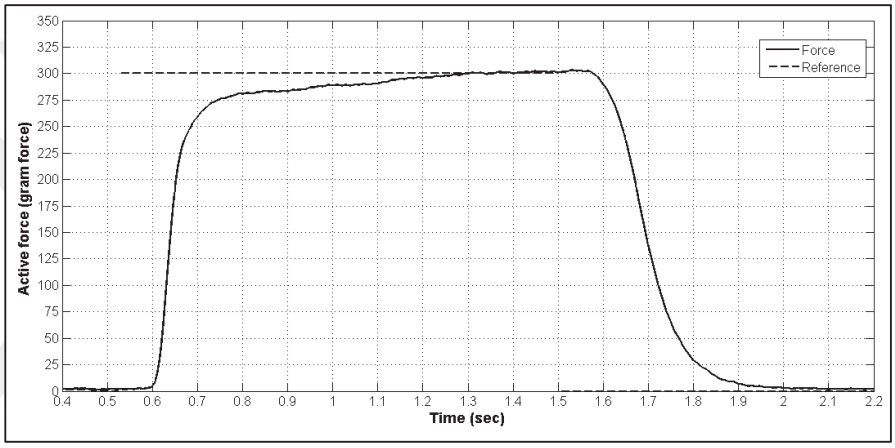

Figure 6.21 Contraction force control over step response

In Figure 6.21 force response for the control over step function is given. The force increases with a delay but reaches the target force. It generates force at reference level slightly longer than the desired duration. Some of the control trials are not succeeded regarding the unstable response of muscle (data not given here).

Peak forces of short duration successive contractions are controlled. Results for one specimen are given in Figures 6.22-6.23. As muscle fatigues the controlling parameter (frequency) is increased by PID up to a limit. If controller cannot maintain the reference force (shown as dashed line, 400 mN) with the highest stimulation frequency a second PID loop increases the inter-stimulus duration for recovery. After recovery, frequency is reduced below the threshold and inter-stimulus duration is decreased to the desired value. In this experiment smallest inter-stimulus duration is one second and the contraction duration is 0.1 s.

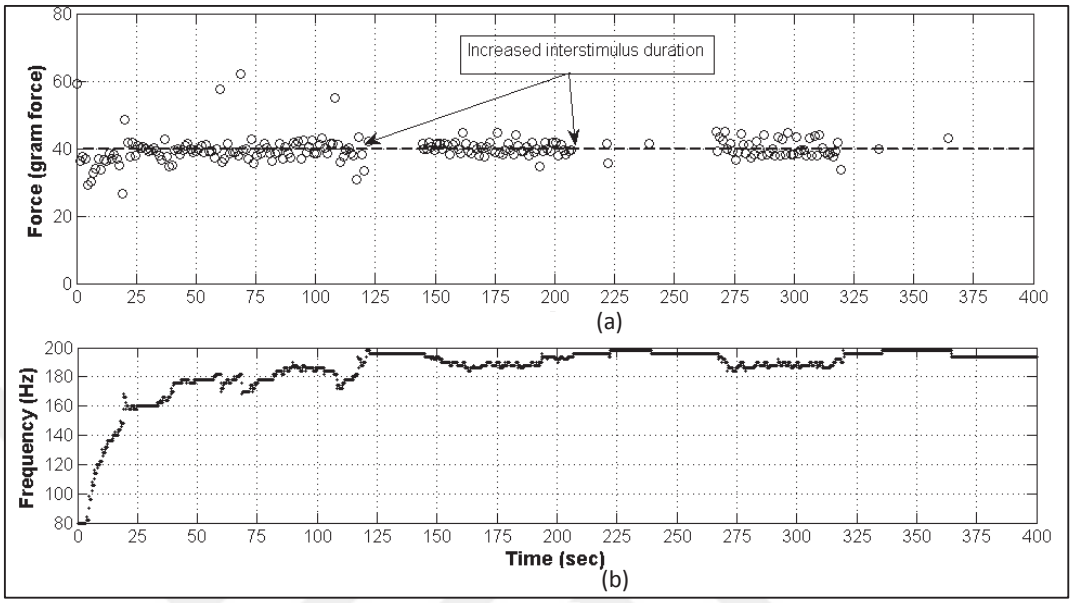

Figure 6.22 Control of peak force of contraction with a stimulus duration 0.1 s followed by 0.9 s rest applied in succession, result 1. Inter-stimulus duration is increased if required. Stimulation signal frequency is varied between 80 and 200 Hz with fixed pulse-width (100 us) and amplitude (0.7 V)

In Figure 6.23 another result of control experiment is presented which was performed on the same specimen (the specimen whom the result in Figure 6.22 belongs to). In this experiment controller is activated after a certain time to emphasize the effect of controller on peak force of contraction. Before the controller is activated, muscle is stimulated with constant frequency of 80 Hz (lower limit of PID) and the peak force decreases due to fatigue (effect of fatigue is similar to shown in Figure 6.15). As the controller is activated, peak force increases to reference (400 mN, shown as dashed line in Figure 6.23) and controller maintains peak force close to the reference afterwards.

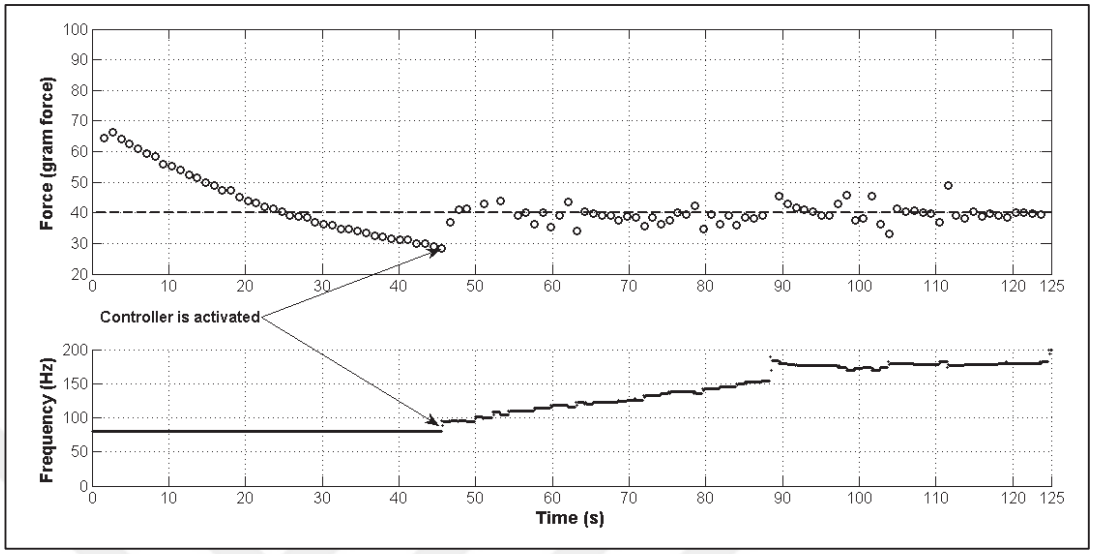

Figure 6.23 Control of peak force of contraction with a stimulus duration 0.1 s followed by 0.9 s rest applied in succession, result 2. Stimulation signal frequency is varied between 80 and 200 Hz with fixed pulse-width (100 us) and amplitude (0.7 V). Controller is activated after a certain time to emphasize the effect of controller on peak contraction force.

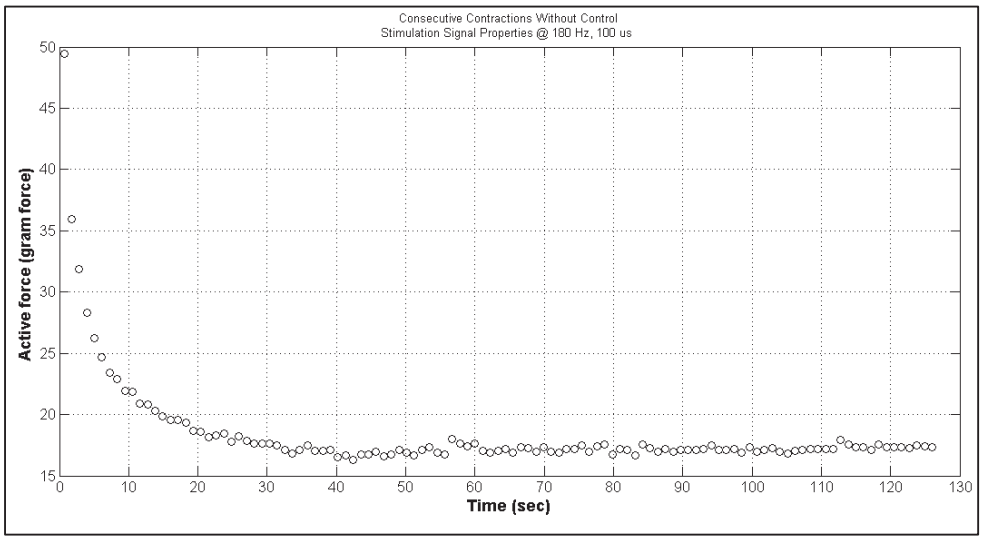

Figure 6.24 Stimulation in succession without control with 0.1 sec. stimulation and 0.9 sec. rest period. Stimulation signal frequency is 180 Hz, pulse-width 100 us and amplitude is 0.7 V

In Figure 6.24 magnitudes of peaks are plotted for the same specimen on which the control experiment is performed. This time peak force is not controlled, only open loop stimulation protocols are delivered (frequency: 180 Hz, pulse-width: 100 μs, amplitude: full recruitment voltage). As shown in Figure 6.23 reference force cannot be maintained with open loop stimulations (fixed stimulation frequency and inter-stimulus duration). Force decreases rapidly due to muscle fatigue in 15-20 contractions while the reference is maintained for 200 contractions if the proposed controller is activated (as shown in Figures 6.22-6.23).

7. DISCUSSION AND CONCLUSIONS

In this section a perspective on performance and feasibility of a muscle is given which is used as an actuator in mechanical system. Discussion is presented under three main titles addressing bio-mechatronic applications. In the first one muscle characteristics are discussed and experimental findings are compared with the literature. Secondly developed and applied methods are discussed for muscle characterization and for bio-mechatronic integration. Finally feasibility of the idea is discussed and performance of the application is discussed for certain circumstances.

7.1. Muscle Characteristics

In the thesis mechanical output characteristics of muscle is investigated for various stimulation signal parameters and fatigue conditions. Although different specimens showed similar behavior under the same conditions, the level of force generation was not coherent. Different specimens isolated from different individuals, and even different specimens isolated from the same individual (i.e. from left and right legs) showed, at times, a large difference in the force level generated. As an example, in Figures 6.4-6.6, contraction forces are given for various stimulation signal parameters. As shown, forces have significant differences even between the specimens isolated from the same individual. Thus, presenting a general conclusion on contraction forces is not possible with the data presented in this thesis. One of the main reasons for this varience may be due to differences in muscle fiber architecture.

It is well known that muscles have different fiber architectures such as number of fibers and fiber orientations. In references [9, 31] models are validated accurately by 3D construction of muscle architecture. However some simple methods also may reduce the variation among specimens such as normalizing forces by their mass or cross section area since they are directly related with the amount of parallel fibers. However due to the methods applied in this thesis, weight and diameter measurements of specimens are not accurate enough to make such calculations. Here muscle weight is measured as the

specimen is isolated from the body and at the end of the test by cutting off the bone and tendon (net muscle weight) which are used to attach the muscle to the test setup. If the bone or tendon is cut at different lengths during the surgical procedure the initial weight measurement varies. Final weight measurement is the wet weight of the muscle since it remained in the solution for few hours and it is not the actual weight of the muscle as well. Diameter of the muscle is measured with a caliper. The measurement is not accurate since muscle is a soft material and it is very likely to have large measurement errors due to the caliper clamping force.

Another reason for variations may be due to the specimen isolation procedure and the condition of animals. Although the same isolation procedure was applied to the specimens which belong to the same experimental procedure group, some different responses were observed. The most critical phase of the isolation procedure is the removal of the sciatic nerve. For the situations in which the nerve may have been damaged during removal, the contraction forces were well below the expectations. During the experiments some specimens could not be activated or gave relatively low force response. The number of such situations increased as the duration for maintenance of frogs in aquariums increased, which may be due to the maintenance conditions.

However, the general behavior of specimens is consistent with each other and with the literature. In Figure 6.1 force vs. initial length relationship of a muscle is given. The active force makes a peak at optimum point and decreases as the initial length increases as shown in Figure 2.8. The concept is explained with the sliding filament theory [10, 11]. Passive force increases as the length of muscle increases over the optimum length as shown in [9]. Normalized active response of 30 different specimens is given in Figure 6.2. The variance between specimens is increased as the muscle length increases or decreases from the optimum point as shown in [21]. Force length relationship is an important aspect for the design of a mechanism driven by a muscle. For isotonic contractions active and passive force output of a muscle varies with initial muscle length and the force requirements of the mechanism must be adjusted accordingly.

Active force response of muscles is measured for various stimulation signal parameters shown in Figures 6.4-6.6. Peak contraction force increases with increasing number of recruited fibers, which, in turn, happens as the pulse-width increases as shown in Figures 6.4 and 6.5. Similar results are given in [20, 48]. However activation and saturation pulse-

width thresholds vary with stimulation amplitude, fiber composition, and source of muscle specimen. In this thesis, experiments to measure the effect of pulse-width are conducted at full recruitment voltage and for stimulation frequencies of 40 and 100 Hz. The activation threshold is found between 25 and 50 μs and the force completely saturates at around 150 μs for trials on different specimens. In Figure 6.6 force response is given for various stimulation frequencies which is similar to the results given in [60]. The lowest threshold for activation frequency is 1 Hz which induces a twitch response. As the frequency increases to 90-100 Hz the force saturates and does not increase any further. Recruitment characteristics of muscles define the limits actuation and accurate characteristics of an actuator muscle must be determined before integrating it into the bio-mechatronic system. Special attention is necessary regarding the properties which vary among muscle specimens.

Successive contractions induce fatigue in muscles. As shown in Figure 6.15 muscle force decreases due to fatigue which reduces actuation performance considerably. A similar result is given in [61, 62] for human subjects. Although experiments were performed to characterize fatigue of muscle specimens, a general conclusion could not be achieved since muscle specimens had their own individual fatigue rate. Fatigue behavior of contraction is modeled as described in section 6.4; however the relation between stimulation parameters and fatigue is not given.

7.2. Methods for Bio-mechatronic System Integration

7.2.1. Mechanics and Electronics Interfaces

As described in Sections 4.2.1.3 and 4.2.3.3 a muscle is connected to the mechanical and electronic systems in the experimental setup. The most feasible solution for mechanical connection is found to be connection via clamping at *proximal* and *distal* ends of a muscle. This method is the most practical way to securely fix a muscle since it does not require as much effort such as in fixing via surgical sutures [4, 19, 45]. It is a non-invasive method since the muscle is clamped at *femur* on the *proximal* side and at *Achilles* tendon on the *distal* side. However, a better solution may be fixing muscle ends through disposable

apparatuses which are adhered to biological tissue (bone and tendon) using medical adhesives without applying any clamping stress on *Achilles* tendon and *femur*. Stimulation signal is delivered via direct and indirect stimulation. For the direct stimulation, needle electrodes were used which were inserted into muscle tissue. However this method may damage the tissue as needles move inside the muscle as muscle contracts and changes the shape [4]. Indirect stimulation is delivered with two methods as; nerve stimulation via suction electrodes and nerve stimulation via clamping. Although suction electrodes remove the risk of short circuit of stimulation signal through the solution it requires much effort to insert the nerve into suction electrode. Clamping the nerve is more straight-forward solution but it may damage the nerve. As a result slightly lower full recruitment voltage values are measured with nerve clamping method (section 6.2) which may reduce the tissue damage induced by electrical stimulation.

7.2.2. Maintaning *In-Vitro* Conditions

To maintain *in-vitro* conditions muscle is submerged into ringers solution (recipe is described in section 4.3) which is maintained at 22 $^{\circ}$ C and oxygen is supplied by bubbling into solution from a medical oxygen source. Some muscle specimens are tested for longer periods to test their *in-vitro* life span. Specimens remained functioning for 36 hours. To achieve higher *in-vitro* lives a solution is proposed by [4] which includes antibiotics to prevent sepsis. In some studies a mixture of CO_2 and O_2 is proposed as the supply gas since CO_2 adjusts the pH of the solution. These methods would increase the quality of *in-vitro* conditions and, thus, the service life of the proposed actuator.

7.2.3. Methods for Modeling

Since muscle specimens have differences as explained in previous section a better solution for robust control of a muscle actuator is to characterize muscles on an individual basis. Regarding the data acquired from characterization experiments the twitch response of muscle is modeled with the modeling idea based on [33] (model A) and by estimating the transfer function (model B). Tetanic response of a muscle is calculated based on these

models and compared with the experimental data. As shown in Figures 6.11-6.14 model A and model B predicted the peak force of tetanic response with 9 per cent and 10.5 per cent average errors respectively. However model A calculated a response with a higher impulse amplitude (area under the contraction force-time curve) and model B calculated with lower impulse amplitude while the true value is in between.

Model B identifies both the muscle and the response of the experimental setup. Actually experimental setup is a spring, and mass damper system driven by the contraction force. Thus, the force measured by the load cell is actually the indication of the displacement at the tip of the load cell. Contraction force makes an undershoot as it drops down to zero which is explained by this mechanism (shown in Figures 6.7-6.10). On the other hand model A does not model the dynamics of the measurement systems but only identifies the twitch response with two parameters namely, contraction peak force and time. The differences in the impulse magnitude yielded by the two models may be explained with this mechanism. As shown in Figure 4.12 measurement system has high hysteresis errors (around 4 per cent) at low forces. Since twitch responses had peak forces of 250 to 400 mN, measurements may have significant errors. Consequently, error in tetanic force calculations was higher since the measurement error summed as twitches are added up. More accurate calculations for force enhancement may be achieved with the same modeling techniques if aforementioned problems are solved.

In the thesis system identification is performed for short duration pulses (0.1 s of stimulation) for which the fatigue effect is not added to the model. For contractions with longer durations a fatigue model must be coupled. Another case may be operating a muscle actuator for successive short contractions, which will induce fatigue in the muscle as shown in Figure 6.15. In this case characteristics of twitch response changes and, therefore, the transfer function (for model B) or the model parameters (for model A) have to be updated as the fatigue state changes.

A fatigue model is fit to the long duration (2 s) contractions based on [59]. Fatigue state of contractions is characterized by three transition rates. The magnitudes of the rates calculated are in the expected range. In Figures 6.12-6.14, model output and experimental data are plotted. As shown, using this modeling idea, the profile of contractions is calculated by estimating the transition rates from the experimental data. However the relation between variations of these parameters and stimulation protocol or stimulation

parameters are not presented in this thesis. To take advantage of this model the variation of rates has to be predicted for the subsequent contractions so, that variation in force profile could be estimated.

7.2.4. Methods for Muscle Control

Two types of muscle control experiments are conducted using PID control. Firstly it was aimed to induce force histories of ramp and step type in response to such reference signals by pulse-width modulation. In Figures 6.19-6.21 performance of the controller is shown. In ramp reference muscle had instability while it reached to the plateau with minimum error. The step reference gave a better result as shown in Figure 6.21. In most of the control experiments abrupt changes in muscle characteristics were observed and PID coefficients were adjusted manually to fit to the changing conditions. These changes may be due to muscle fatigue or tissue necrosis. A robust controller may be designed by characterizing the fatigue behavior of successive contractions for certain stimulation parameters and applying an adaptive control strategy. In study [20] muscles are controlled more accurately than here.

One of the main reasons for the difference between the reference and the actual force value may be due to the nature of *in-vitro* testing. In [20] muscles are tested *in-vivo* thus, accumulation of byproducts is reduced by blood flow and oxygen is delivered to the whole of the muscle. Another reason may be the low resolution of pulse-width (25 μs) used for control since it was limited with the DAQ equipment used in the experiments. Recruitment curve of a muscle (shown in Figure 7.1) has three regions namely; deadzone, high-slope and saturation. At the high-slope region of a recruitment curve, muscle force increases rapidly with small changes in pulse-width. In study [20] a higher resolution is used for control (10 μs). This may explain the low performance of controller in ramp responses as shown in Figures 6.19-6.20. A reason for low performance in accuracy may be because of the controller equipment (multi-purpose DAQ card) was not a real-time (RT) device. Since these type of devices operate on Windows they may experience delays while controlling which reduces the controller accuracy. Better performance may be achieved by using a real-time device which has its dedicated RTOS (Real Time Operating System).

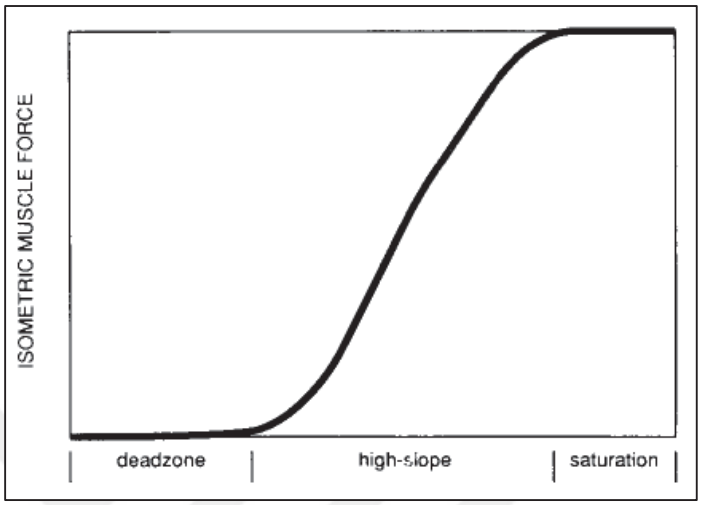

Figure 7.1 Phases of recruitment curve **[48]**

In the second type of control experiments, peak force of short duration successive contractions were controlled. Here, 0.1 s of stimulation is applied followed by 0.9 s of rest period. Since the stimulation duration is very short, profile of the contraction curve does not change much, but the peak force changes due to stimulation parameters or fatigue condition. The profile for longer stimulations may have different shapes regarding the fatigue condition as shown in Figures 6.16-6.18 and requires a control strategy as mentioned above. Since a muscle actuated mechanism will more likely require short cyclic contractions controlling the peak force of such short duration contractions is effective and simpler.

Although force output decreases for a set of 100 succesive contractions due to muscle fatigue, force profile shows a small change as shown in the isoplot (Figure 7.2). Thus for contractions with short duration, controlling the peak force instead of controlling the whole force profile is a simpler solution since changing electrical parameters does not affect the profile significantly in short-duration contractions. Likewise the trend in the force profile does not influenced by fatigue in such contractions eventhough the magnitudes may differ. For this type of control experiment the peak force of contraction is measured and the frequency of the stimulation signal is adjusted for the subsequent contraction. If the muscle is fatigued and the reference cannot be reached for the saturated muscle inter-stimulus

duration is increased to allow muscle to recover. Results are given in Figures 6.22-6.23. This method is based on slowing down or pausing the motion of actuator temporarily rather than losing the force generation performance. Control strategy for controlling peak magnitude of short duration contractions succeeded, by maintaining contraction force at desired level although muscle experiences severe fatigue.

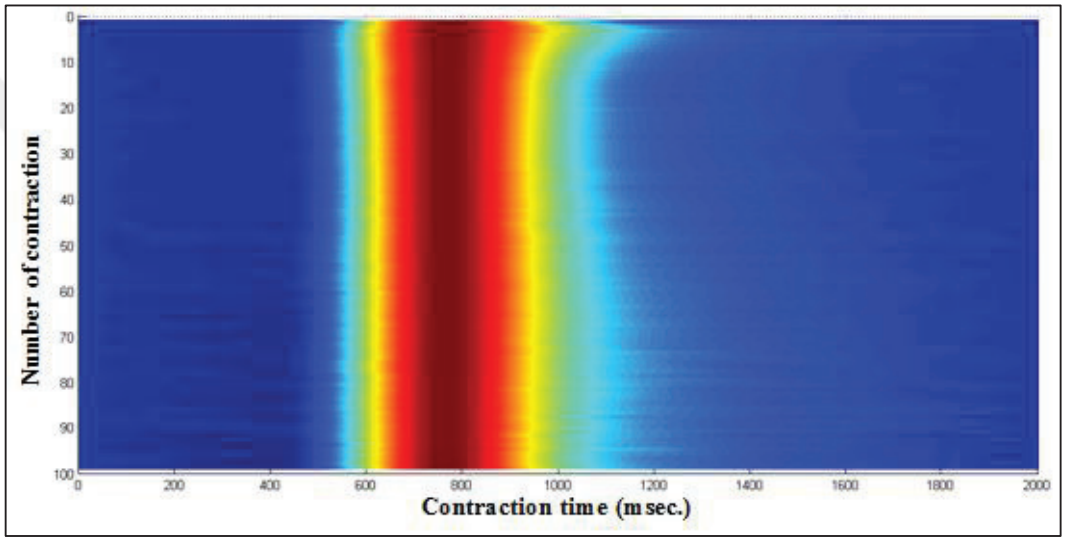

Figure 7.2 Successive contractions with 0.1 s stimulation and 0.9 s rest period normalized by the peak force. Horizontal axis is time for a single contraction, vertical axis is the number of contraction and the third axis (out of the paper) is the contraction magnitude for each contraction which is normalized by its maximum.

7.3. Performance and Feasibility Assessment

In this thesis, a preliminary investigation of feasibility and performance of live muscles is carried out as possible actuators in mechanical systems and methods are developed or applied with the hope of enabling their use as mechanical systems. As mentioned in [5] muscle based actuation may present better performance concerning inertia, back-drivability, stiffness control and power consumption. Muscle tissue is able to adapt to changes in power needs [4, 5] and has the highest efficiency among artificial actuators as

shown in Table 1.1. Thus, muscles may be a good solution for mechanical actuation problems to be used in the future.

A critical aspect in using a muscle as an actuator is the ability to control the mechanical output. Previous studies [20, 24, 36, 37, 38, 41, 43, 44] and the experimental results obtained in this thesis show that muscle can be controlled with a reasonable accuracy. However accuracy and robustness of a control process are dependent on the control strategy. Methods presented in this thesis seem effective in controlling muscle output however, the performance may be improved by solving the problems mentioned in section 7.2.4.

One of the significant drawbacks of a muscle actuated *in-vitro* systems is the short life cycle of muscle. A life-cycle experiment was performed in this study wherein the active force of a specimen was measured at certain times; the results are plotted in Figure 7.3. The muscle had gone through another experimental procedure and, when it was over, muscle was allowed to passive sit in its solution. The active force measured at different discrete times grew until the 13^{th} hour at which time 100 per cent recovery of its initial state was achieved due to recovery (the forces measured at very beginning of the first experimental procedure and the force at the 13^{th} hour beyond the end of the first experimental procedure were the same). However, the force decreased beyond that time even if no stimulation was applied.

Each discrete electrical stimulation consisted of a pulse train (with a duration of 0.1 s) and generated force was measured while maintaining *in-vitro* conditions as described in the regular experimental procedure (except for the temperature which was decreased to 17 $^{\circ}$C to provide a longer muscle life).

Muscle force decreased due to core necrosis (caused by less diffusion of oxygen to the core of the muscle) and sepsis occurred whose signs were observed at 35.5^{th} hour. These were signs that appeared to point to muscle disintegration as observed in the quality of solution and *rigor mortis*. With the solution used in [4] it is reported that specimens functioned for 42 hours before their performance decreased to 75 per cent. In study [63] frog muscles are maintained for 2-3 weeks with normal action-potential properties. In that study a more complex solution and isolation procedures (aseptic methods) are applied while muscle is maintained at lower temperatures (6 $^{\circ}$C). Two days later neuromuscular transmission was

still normal after which motor endings denigrate. Hence direct stimulation may be considered for applications where longer lifecycle is required.

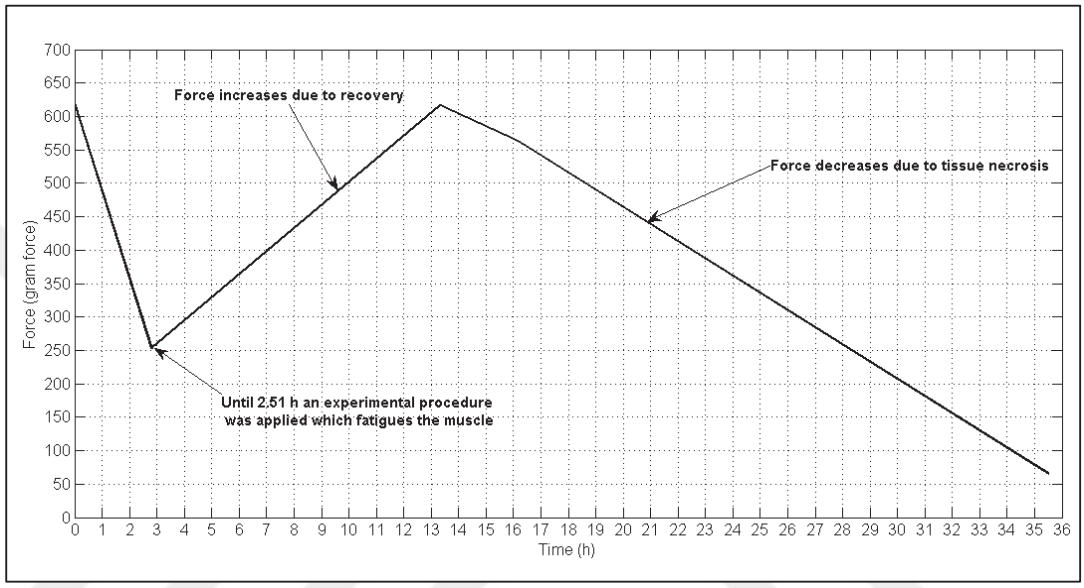

Figure 7.3 Decrement of active force due to in-vitro conditions caused by tisse necrosis and sepsis. In the experimental procedure that fatigues muscle, a total number of 120 stimulation pulse-trains were delivered. Each pulse train has a duration of 0.1 seconds followed by 0.9 seconds rest period with stimulation frequency of 200 Hz. After 10 pulse trains were delivered muscle is unactivated for 2 minutes and 10 pulse trains were sent again.

In conclusion this thesis shows that muscle is able to be integrated in electro-mechanical systems as a controllable mechanical actuator. *Gastrocnemius* muscle of *Rana Esculenta* muscle is isolated and installed into the experimental setup through mechanics and electronics interfaces. Integration of muscle in such experimental setup may be a proof of concept for a bio-mechatronic device. Muscle is stimulated with rectangular wave electric signal and the force output is controlled by adjusting stimulation signal parameters such as pulse-width and frequency. Results reported in the literature and experimental study in this thesis show that muscle force is controllable. Thus, muscle is able to generate the force profile required by the mechanism with a proper controller. One of the greatest problems is

the short *in-vitro* life-cycle of muscle that hinders the widespread of bio-mechatronic machines. If problems related with the service life of muscle are solved muscles may be used as efficient actuators which present promising solutions to certain mechanical actuation problems. This thesis is one of the few studies that consider muscle in such perspective and further studies on this topic may allow rise of new generation machines with life-like movements.

REFERENCES

1. M. Bergamasco, F. Salsedo, S. Mandreschi and N. Lucchesi, "A Novel Actuator for Wearable Robots with Improved Torque Density and Mechanical Efficiency,," *Advanced Robotics,* vol. 24, no. 1, pp. 2019-2014, 2010.

2. M. Pilarek, P. Neubauer and U. Marx, "Biological cardio-micro-pumps for microbioreactors and analytical micro-systems," *Sensors and Actuators,* vol. 156, no. B, pp. 517-526, 2011.

3. W. I. Hunter, *A comparison of muscle with artificial actuators,* Montreal, McGill Univ.: Solid-State Sensor and Actuator Workshop 5th Technical Digest, IEEE, 1992.

4. H. Herr and R. G. Dennis, "A swimming robot actuated by living muscle tissue," *Journal of NeuroEngineering and Rehabilitation,* vol. 6, no. 1, 2004.

5. L. Ricotti and A. Menciassi, "Bio-hybrid muscle cell-based actuators," *Biomedical Microdevices,* pp. 987-998, 2012.

6. T. Fukunoga, Y. Kawakami, S. Kuno, K. Funato and S. Fukashiro, "Muscle Architecture and Function in Humans," *Journal of Biomechanics,* vol. 30, no. 5, pp. 457-463, 1997.

7. Wiki, en.wikipedia.com, "Encyclopedia, en.wikipedia.com," [Online].

8. C. Yücesoy, "Skeletal Muscle Mechanics," Boğaziçi Univ. Institute of Biomedical Engineering , Istanbul, 2012.

9. M. Böl, R. Weikert and C. Weichert, "A coupled electromechanical model for the excitation-dependent contraction of skeletal muscle," *Journal of the Mechanical Behaviour of Biomedical Materials,* vol. 4, pp. 1299-1310, 2011.

10. A. F. Huxley and R. Niedergerke, "Structural Changes in Muscle during Contraction," *Nature,* vol. 172, pp. 530-532, 1953.

11. H. E. Huxley and J. Hanson, "Changes in the Cross-Striations of Muscle during Contraction and Srech and their Structural Interpretation," *Nature,* vol. 172, pp. 530-532, 1953.

12. C. A. Yücesoy, "Intra-, Inter- and Extramuscular Myofascial Force Transmission," DPP-Utrecht B.V, Utrecth, 2003.

13. M. Böll, H. Stark and N. Schilling, "On a phenomenological model for fatigue effects in skeletal muscles," *Journal of Theoretical Biology,* vol. 281, pp. 122-132, 2011.

14. Y. Tanaka, Y. Yanagisawa and T. Hitamori, "Fluid actuation for a bio-micropump powered by previously frozen cardiomyocytes directly seeded on a diagonally streched thin membrane," *Sensors and Actuators ,* vol. 156, no. B, pp. 494-498, 2011.

15. C. Cvetkovi, R. Raman, V. Chan, B. J. Williams, M. Tolish, P. Bajaj, M. S. Sakar, H. H. Asada, M. Taher, A. Saif and R. Bashir, "Three-dimensionally printed biological machines powered by skeletal muscle," *Proceedings of National Academy of Sciences,* vol. 111, no. 28, pp. 10125-10130, 2014.

16. A. Heidland, G. Fazeli, A. Klassen, K. Sebekova, H. Hennemann, U. Bahner and B. Dilorio, "Neuromuscular electrostimulation techniques: historical aspects and current possibilities in treatment of pain and muscle waisting," *Clinical Neohrology,* vol. 79, no. 1, pp. 12-23, 2013.

17. F. J. Teixeira, W. N. McDonell, W. D. Black, W. Harris and L. Grovum, "Effects of muscarinic receptor antagonist on acetylcholine-induced contractions of jejunal smooth muscle in horses," *Journal of Veterinary Pharmacology and Therapeutics,* vol. 35, pp. 313-318, 2011.

18. Y. Akiyama, K. Odaira, K. Sakiyama, T. Hoshino, K. Iwabuchi and K. Morishima, "Rapidly-moving insect muscle-powered microrobot and its chemical acceleration," *Biomed Microdevices,* vol. 14, pp. 976-986, 2012.

19. W. Farahat and H. Herr, "An Apparatus for Characterization and Control of Isolated Muscle," *IEEE Transactions on Neural Systems and Rehabilitation Engineering,* vol. 13, no. 4, 2005.

20. H. J. Chizeck, P. E. Crago and L. S. Kofman, "Robust Closed-Loop Control of Isometrci Muscle Force Using Pulsewidth Modulation," *IEEE Transactions on biomedical engineering ,* vol. 35, no. 7, 1988.

21. A. Ramirez, J. Grasa, F. Soteras, R. Osta, M. J. Munoz and B. Calvo, "Active response of skeletal muscle: In vivo experimental results and model formulation," *Journal of Theoretical Biology,* vol. 267, pp. 546-553, 2010.

22. P. R. Shorten, P. O'Callaghan, J. B. Davidson and T. K. Soboleva, "A mathematical model of fatigue in skeletal muscle force contraction," *Journal of Muscle Research and Cell Motility,* vol. 28, pp. 293-313, 2007.

23. M. Tanaka, Y. Hirayama, N. Fujita and H. Fujino, "Electrical stimulation using sine waveform prevents unloading-induced muscle atrophy in the deep calf muscles of rat,"

Acta Histochemica, vol. 116, pp. 1192-1198, 2014.

24. L. A. Bernotas, P. E. Crago and H. J. Chizeck, "Adaptive Control of Electrically Stimulated Muscle," *IEEE Transactions on Biomedical Engineering ,* vol. 34, no. 2, pp. 140-147, 1987.

25. A. V. Hill, "The heat of shotening and the dynamic constants of muscle," *Proceedings of the Royal Society of London,* vol. 126, no. B, pp. 136-195, 1938.

26. A. V. Hill, "The maximum work and mechanical efficiency of human muscles, and their most economical speed," *Journal of Physiology,* vol. 56, pp. 19-41, 1922.

27. A. E. Ehret, M. Böl and M. Itskov, "A continuum cınstitutive model for active behaviour of skeletal muscle," *Journal of the Mechanics and Physics of Solids,* vol. 59, pp. 625-636, 2011.

28. B. Sharifimajd and J. Stalhand, "A continuum model for excitation-contraction of smooth muscle under finite deformations," *Journal of Theoretical Biology,* vol. 355, pp. 1-9, 2014.

29. O. Röhrle, "Simulating the Electro-Mechanical Behaviour of Skeletal Muscles," *Computational Biomechanics,* 2010.

30. A. F. Huxley, "Muscle contraction and theories of contraction," *Progress in Biophysics and Biochemistry,* vol. 7, pp. 225-318, 1957.

31. J. Weickenmeier, M. Itskov, E. Mazza and M. Jabareen, "A physically motivated constitutive model for 3D numerical simulation of skeletal muscles," *International journal for numerical methods in biomedical engineering,* vol. 30, pp. 545-562, 2014.

32. M. Böl, "Micromechanical modelling of skeletal muscles:from the single fibre to the whole muscle," *Archive of Applied Mechanics,* vol. 80, pp. 557-567, 2010.

33. M. Böl and S. Reese, "Micromechanical modelling of skeletal muscle based on finite element method," *Computer Methods in Biomechanics and Biomedical Engineering,* 2008.

34. O. Röhrle, J. B. Davidson and A. J. Pullan, "Bridging scales: A three-dimensional electromechanical finite element model of skeletal muscle," *SIAM Journal of Scientific Computing,* vol. 30, no. 6, pp. 2882-2904, 2008.

35. D. A. Lansdown, Z. Ding, M. Wadington and J. L. Hornberger, "Quantitative diffusion tensor MRI-based fiber tracking of human skeletal muscle," *Journal of Applied Physiology ,* vol. 103, pp. 673-681, 2007.

36. J. P. Giuffrida and P. E. Crago, "Reciprocal EMG Control of Elbow Extension by FES," *IEEE Transactions on Biomedical Engineering,* vol. 9, no. 4, 2001.

37. S. Jezermik, R. G. Wassink and T. Keller, "Sliding Mode Closed-Loop Control of FES: Controlling the Shank Movement," *IEEE Transactions on Biomedical Enigneering ,* vol. 51, no. 2, 2004.

38. H. Gollee, K. J. Hunt and D. E. Wood, "New Results in Feedback Control of Unsupported Standing in Paraplegia," *IEEE Transactions on neural systems and rehabilitation engineering,* vol. 12, no. 1, 2004.

39. W. A. Farahat and H. M. Herr, "Optimal Workloop Energetics of Muscle-Actuated Systems: An Impadence Matching View," *PLOS Computational Biology,* vol. 6, no. 6, 2010.

40. F. G. Wilhere, P. E. Crago and H. J. Chizeck, "Design and Evaluation of a Digital Closed-Loop Controller for the Regulation of Muscle Force by Recruitment Modulation," *IEEE Transactions on Biomedical Engineeing ,* vol. 32, no. 9, 1985.

41. P. H. Veltink, H. J. Chizeck, P. E. Crago and A. El-Bialy, "Nonlinear Joint Angle Control for Artificially Stimulated Muscle," *IEEE Transactions on Biomedical Engineering ,* vol. 39, no. 4, 1992.

42. P. E. Crago, J. T. Mortimer and P. H. Peckham, "Closed-Loop Control of Force During Electrical Stimulation of Muscle," *IEEE Transactions on Biomedical Engineering ,* vol. 27, no. 6, 1980.

43. H. J. Chizeck, N. Lan, L. S. Palmien and P. E. Crago, "Feedback Control of Electrically Stimulated Muscle Using Simultaneous Pulse Width and Stimulus Period Modulation," *IEEE Transactions on Biomedical Engineering ,* vol. 38, no. 12, 1991.

44. P. E. Crago, R. J. Nakai and H. J. Chizeck, "Feedback Regulation of Hand Grasp Opening and Contact Force During Stimulation of Paralyzed Muscle," *IEEE Transactions on Biomedical Engineering,* vol. 38, no. 1, 1991.

45. Y. Ishii, T. Watari and T. Tsuchiya, "Enhancement of twitch force by stretch in a nerve-skeletal muscle preperation of the forg Rana proposa brevipoda and the effects of temperature on it," *The Journal of Experimental Biology,* vol. 207, pp. 4505-4513, 2004.

46. C. T. Richards, "Building a robotic link between muscle dynamics and hydrodynamics," *The Journal of Experimental Biology ,* vol. 214, pp. 2381-2389, 2011.

47. C. Y. Tanga, C. P. Tsuia, B. Stojanovicb and M. Kojicb, "Finite element modeling of skeletal muscles coupled with fatigue," *International Journal of Mechanical Sciences ,*

vol. 49, pp. 1179-1191, 2007.

48. W. K. Durfee and K. E. Maclean, "Methods for Estimating Isometric Recruitment Curves of Electrically Stimulated Muscle," *IEEE Transactions on Biomedical Engineering ,* vol. 36, no. 7, 1989.

49. D.-H. Kim, J. Park, K. Y. Suh, P. Kim, S. K. Choi, S. Ryu, S. Park, S. H. Lee and B. Kim, "Fabrication of patterned micromuscles with high activity for powering biohybrid microdevices," *Sensors and Actuators,* vol. 117, no. B, pp. 391-400, 2006.

50. Y. Akiyama, R. Terada, M. Hashimoto, T. Hoshino, Y. Furukawa and K. Morishima, "Rod-shaped Tissue Engineered Skeletal Muscle with Artificial Anchors to Utilize as a Bio-Actuator," *Journal of Biomechanical Science and Engineering,* vol. 5, no. 3, 2010.

51. K. Shimizu, H. Fujita and E. Nagamori, "Evaluation systems of generated forces of skeletal muscle cell-based bio-actuators," *Journal of Bioscience and Bioengineering,* vol. 155, no. 2, pp. 115-121, 2013.

52. R. G. Dennis, "Engineered Muscle Actuators: Cells and Tissues," Capel Hill, 2007.

53. G. Vassilakos, R. S. James and V. M. Cox, "Effect of stimulation frequency on force, net power output, and fatigue in mouse soleus muscle in vitro," *Canadian Journal of Physiology and Pharmacology,* vol. 87, pp. 203-210, 2009.

54. C. T. Richards, "Building a robotic link between muscle dynamics and hydrodynamics," *The Journal of Experimental Biology ,* vol. 214, pp. 2381-2389, 2011.

55. J. Petrofsky, "The effect of the subcutaneous fat on the transfer of current through skin and into muscle," *Medical Engineering and Physics ,* vol. 30, pp. 1168-1176, 2008.

56. C.-F. Chen, W.-S. Chen, L.-W. Chou, Y.-J. Chang, S.-C. Chen, T.-S. Kuo and J.-S. Lai, "Pulse Energy as a Reliable Reference for Twitch Forces Induced by Transcutaneous Neuromuscular Electrical Stimulation," *IEEE Transactions on Neural Systems and Rehabilitation Engineering ,* vol. 20, no. 4, 2012.

57. R. G. Dennis, D. E. Dow and J. A. Faulkner, "An implantable device for stimulation of denervated muscles in rats," *Medical Engineering and Physiscs,* vol. 25, pp. 239-253, 2003.

58. Ş. Turaç, "Development of a Novel Electrode for In-vitro Muscle Stimulation," Yeditepe University, Istanbul, 2014.

59. J. Z. Liu, T. H. Dai, T. H. Elster, V. Sahgal, R. W. Brown and G. H. Yue, "Simultaneous measurement of human joint force, surface electromyograms, and functional MRI-measured brain activation," *Journal of Neuroscience Methods,* vol.

101, pp. 49-57, 2000.

60. K. Trisha, C. Li-Wie and B.-M. A. Stuart, "Effects of stimulation frequency versus pulse duration modulation on muscle fatigue," *Journal of Electromyography and Kinesiology,* vol. 18, pp. 662-671, 2008.

61. C. Li-Wei and B.-M. A. Stuart, "The effectd of stimulation frequency and fatigue on the force-intensity relationship for human skeletal muscle," *Clinical Neurophysiology,* vol. 118, pp. 1387-1396, 2007.

62. D. Jun, A. S. Wexler and B.-M. A. Stuart, "Mathematical models for fatigue minimization during functional stimulation," *Journal of Electromyography and Kinesiology,* vol. 13, pp. 575-588, 2003.

63. A. J. Harris and R. Miledi, "A study of frog muscle maintained in organ culture," *Journal of Physiology,* vol. 221, pp. 207-226, 1972.

64. Medi, "Medical Dictionary, www.thefreedictionary.com".

65. B. R. Macintosh, P. F. Gardiner and A. J. McComas, "Skeletal Muscle: Form and Function," in *Human Kinetics*, ISBN 978-0-7360-4517-9, 2006.

66. A. Ito, Y. Yamamoto, M. Sato, K. Ikeda, M. Yamamoto, H. Fujita, E. Nagamori, Y. Kawabe and M. Kamihira, "Induction of functional tissue-engineered skeletal muscle constructs by defined electrical stimulation," *Scientific Reports,* 2014.

67. W. K. Durfee and K. I. Palmer, "Estimation of Force- Activation, Force-Length, and Force-Velocity Properties in Isolated, Electrically Stimulated Muscle," *IEEE Transactions on Biomedical Engineering ,* vol. 41, no. 3, 1994.

,

APPENDIX A: MEDICAL TERMS

A.1 Medical Jargon

In this section a list for medical jargon is given as following [64].

Acetilcholine:
Acetilcoline is an organic molecule that acts as a neurotransmitter in many organisms including humans

Actin:
A protein found in muscle that together with myosin which functions in muscle contraction.

Cardiomyocyte:
The specialized striated muscle tissue of the heart; the myocardium.

Cytoplasm:
The protoplasm of a cell contained within the cell membrane contains organelles, vesicles, and other inclusions but excluding the nucleus.

Endoplasmic Reticulum :
A membrane network within the cytoplasm cells involved in the synthesis modification, and transport of cellular materials.

Epimysium:
The external sheath of connective tissue surrounding a muscle.

Distal:
Away from the referenced point. Extremity of appendage that joins bodies.

In-vitro:

In an artificial environment outside the living organism.

In-vivo :

Within a living organism.

Isometric Contraction:

Isometric contraction is a type of contraction which the joint angle and muscle length do not change during contraction.

Isotonic Contraction:

In an isotonic contraction, tension remains unchanged and the muscle's length changes. Lifting and object at a constant speed is an example of isotonic contractions.

Myosin:

A protein found in muscle tissue as a thick filament made up of an aggregate of similar proteins

Myoglobin:

Myoglobin is an iron- and oxygen binding protein found in the muscle tissue of vertebrates in general and in almost all mammals.

Perimysium:

The sheath of connective tissue enveloping bundles of muscle fibers.

Proximal:

A close point or the point referenced. Point at which appendage joins bodies.

Sarcoplasm:

The cytoplasm of a muscle fiber.

Sarcoplasmic Reticulum:

The form of endoplasmic reticulum found in striated muscle fibers.

Sarcomere:

One of the segments into which a fibril of striated muscle is divided

Titin:

Titin is a giant protein that functions as a molecular spring which is responsible for the passive elasticity of muscle

Troponin:

Troponin is a complex of three regulatory proteins (troponin C, troponin I and troponin T) that is integral to muscle contraction in skeletal muscle, but not smooth muscle.

A.2 Anatomical Basics

In this section basic anatomical knowledge is given to the reader with the medical jargon for assistance to read this thesis.

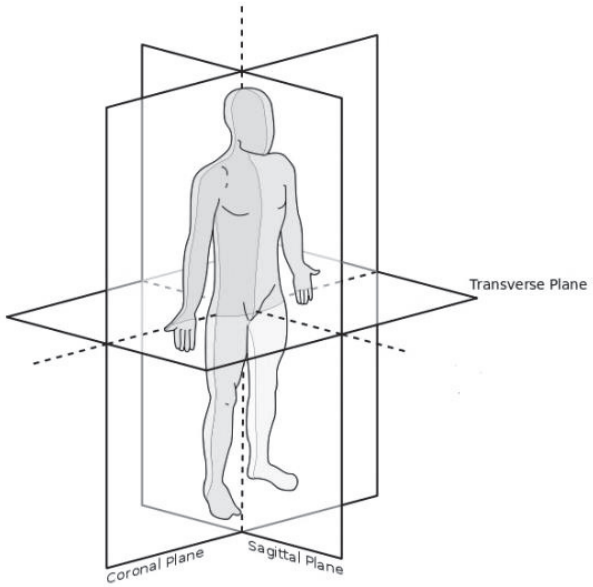

Figure A.1 Anatomical Planes

Transverse plane divides body or body parts into upper and lower parts. Median plane is a vertical plane that passes in the middle that divides into left and right halves. *Sagital* plane is a vertical plane parallel to the median plane, but does not have to be in the middle. *Corronal* (Frontal) plane is a vertical plane which is perpendicular to sagittal and median planes. Anatomical planes for human body are given in Fig. 1.1. Anatomical directions are given as following.

Anterior: Toward the front
Posterior: Toward the back
Lateral: Away from the midline
Medial: Toward the midline
Superior: Above
Inferior: Below

APPENDIX B: ELECTRONIC HARDWARE

B.1 Load Cell

The load cell used in the experimental setup is bending beam type. It is fixed on one end as cantilevered beam and the force applied on other end which is shown by arrow in Figure B.1. It generaes an analog output signal. The properties of load cell is given in Table B.1.

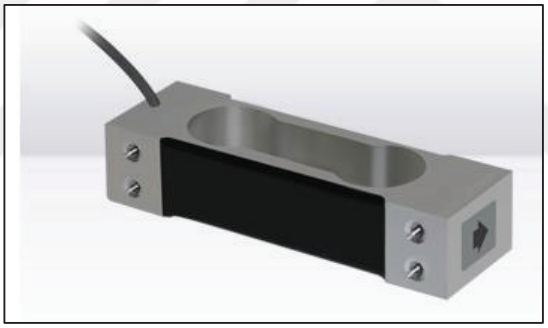

Figure B.1 Load cell, puls elektronik MT series, bending beam type.

Table B.1 Load cell properties

Property	**Value/Explanation**
Accuracy Class	C1
Capacity	3 kg
Output signal	2 mV/V
Resolution	1 gr
Input voltage	5 V
Total Error	0.03 %

Load cell has four strain gauges located on upper and lower fibers of load cell as couples. Strain gauges are connected eachother forming a full Wheatstone bridge. In Figure B.2

schematic of Wheatstone bridge is given. The voltage between points A and C is the excitation voltage (Vs) and the output voltage (V_G) is measured between points D and B. Resistors are indicated with "R". In Equation B.1 the relation between excitation voltage (Vs) and output voltage (V_G) is given.

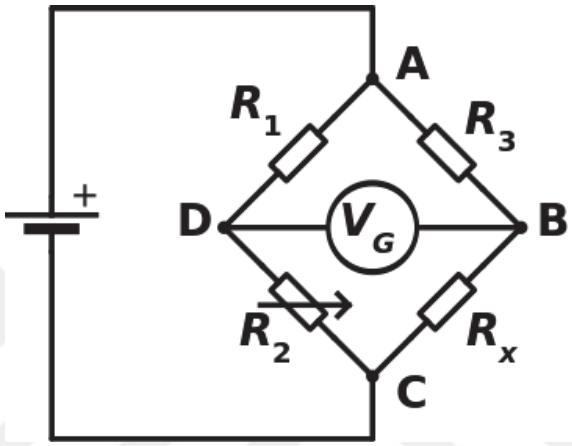

Figure B.2 Wheatstone bridge schematic

$$V_G = \left(\frac{R_2}{R_1 + R_2} - \frac{R_x}{R_x + R_3}\right) \tag{B.1}$$

B.2 Linear Encoder

Magnetic contactless linear encoder is used with the magnetic band. It generates pulses after the reading head passes on divisions. Pulses acquired from two channels which provide the information of position according to a reference. Properties of the linear encoder in Table B.2.

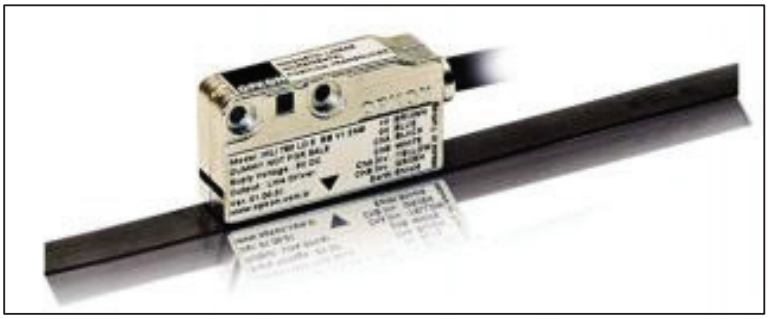

Figure B.3 Contactless magnetic linear encoder, OPKON

Table B2 Linear encoder properties

Property	**Value/Explanation**
Sensing distance	1 mm max.
Max. speed	3 m/s
Output signal	Two channel
Resolution	10 µm
Input voltage	8-24 V
Accuracy	±40 µm

B.3 Data Acquisition and Signal Generation Equipment

This multi-purpose DAQ card is used to acquire analog and digital data via connector port SCC-68. Here two modules (strain gauge module and isolated input module) is integrated into connector block for data signal amplification and isolation respectively.

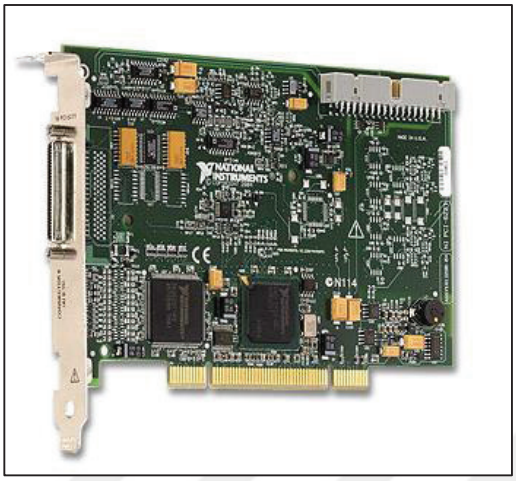

Figure B.4 DAQ card, NI PCI-6221

Table B.3 DAQ card properties, NI PCI 6221

Property	**Value/Explanation**
Number of channels	8 differential 16 single ended
ACD resolution	16 bits
Sampling rate	250 kS/s single channel, 250 kS/s multi-channel
Timing accuracy	50 ppm of sample rate
Timing resolution	50 ns
Maximum working voltage for analog inputs	±11 V
Input FIFO size	4095 samples

Figure B.5 Strain gauge input module, SCC68-SG

A strain gauge module (NI SG series analog input module) is used for amplifying the load cell signal and excitation of Wethson Bridge. SG series input modules include (shown in Figure B5) a 1.6 kHz low-pass filter and an instrumentation amplifier. The excitation signal is produced by the module between 0-2.5 V. Isolated analog input modules (NI SCC-68 AI series) have a low pass filter and are working safely up to 60 V with module-to-module isolation.

In Figures B.6-B.10 schematic for circuits are shown which are integrated in the PCB shown in Figure 4.14. This circuit is used in the previous revision of the experimental setup. In Figure B.6 schematic of stimulation generator circuit is shown. In Figure B.7 the schematic of the amplifier circuit which was used to amplify load cell signal is given. The load cell signal is acquired after amplification. In Figure B.8 schematic of motor driver circuit is given. This motor driver circuit controls the flow rate of peristaltic pump with an open loop control strategy which circulates the solution in the test pool. In Figure B.9 the controller circuit of pulse generator and motor driver is given. In Figure B.10 input and output terminals of the PCB are shown.

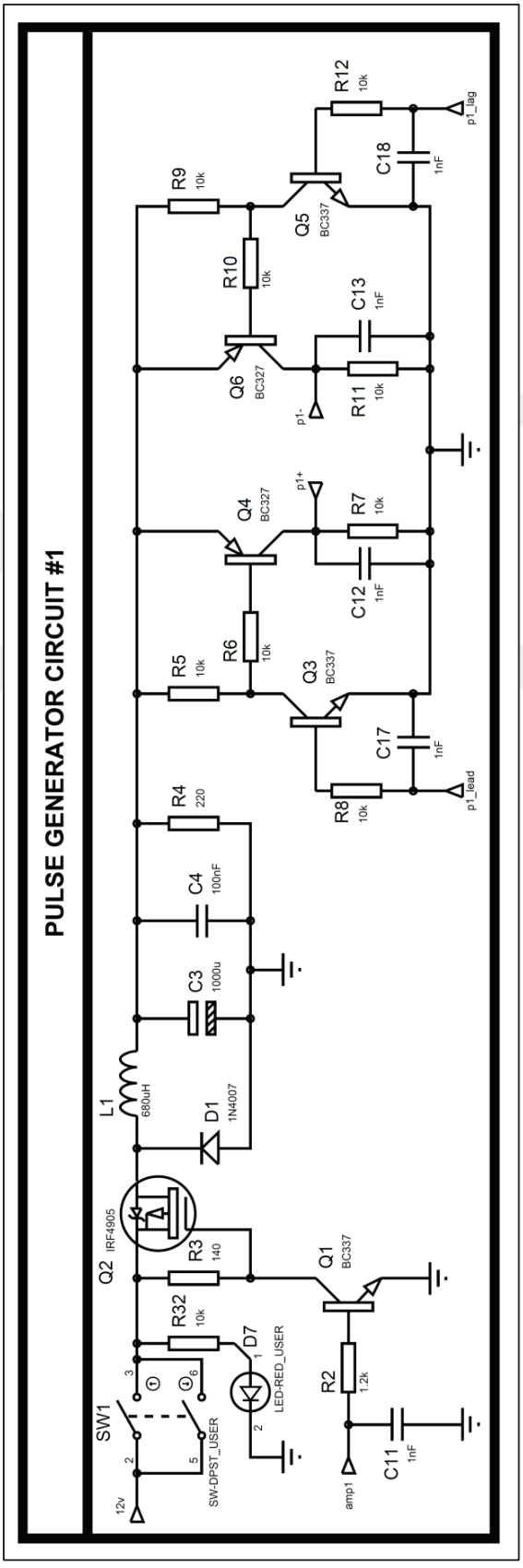

Figure B.6 Pulse generator circuit integrated in the PCB shown in Figure 4.14

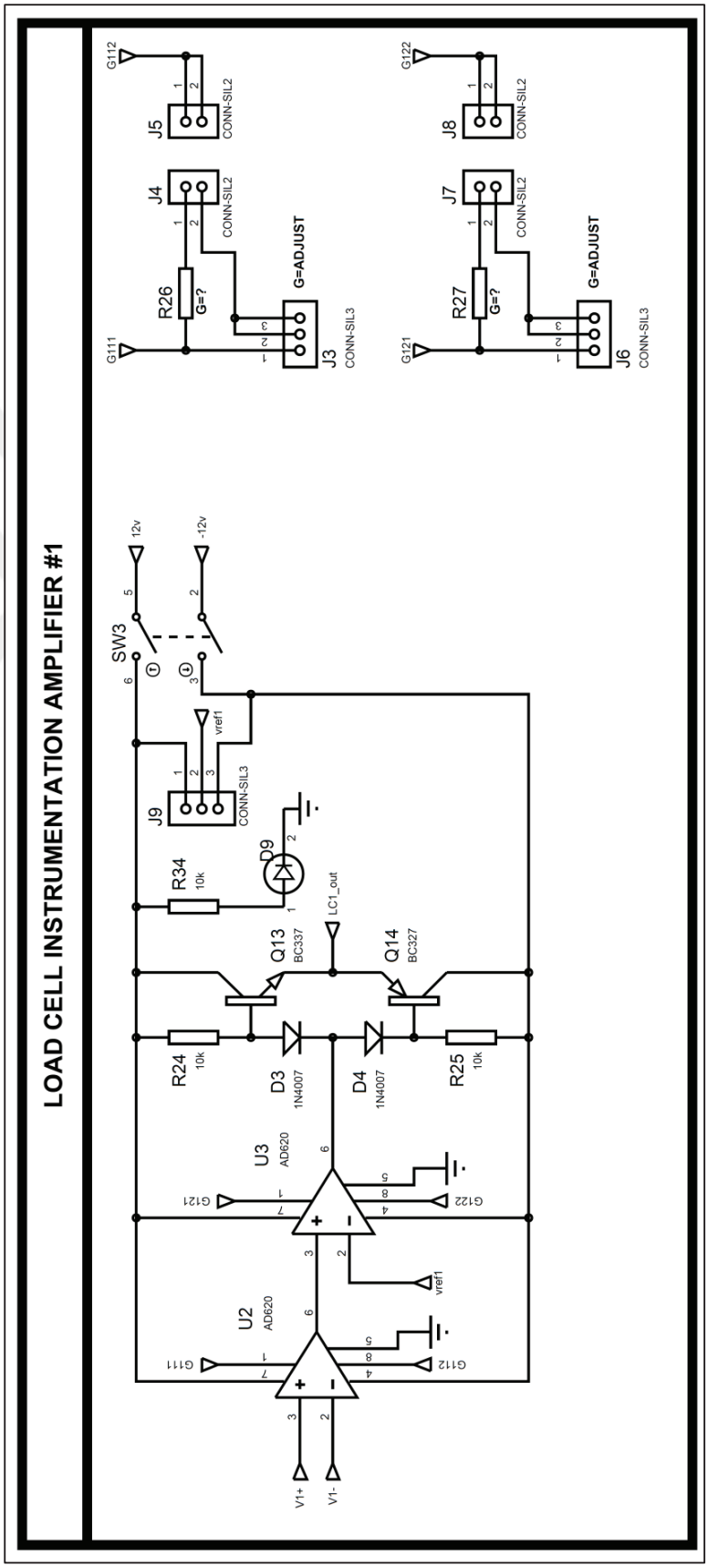

Figure B.7 Instrumentation amplifier for load cell signal integrated in the PCB shown in Figure 4.14

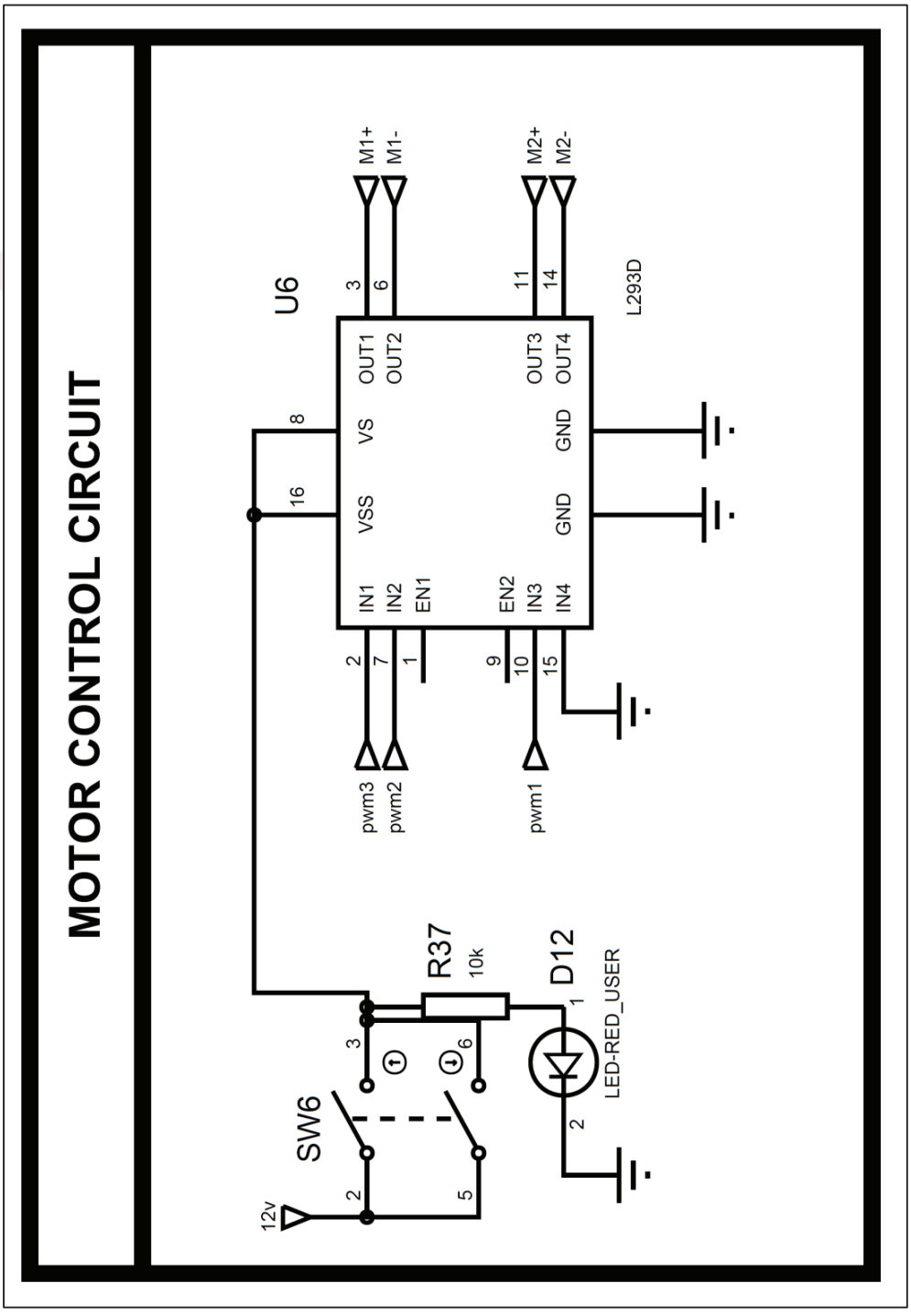

Figure B.8 Motor controller to control peristaltic pump integrated in the PCB shown in Figure 4.14

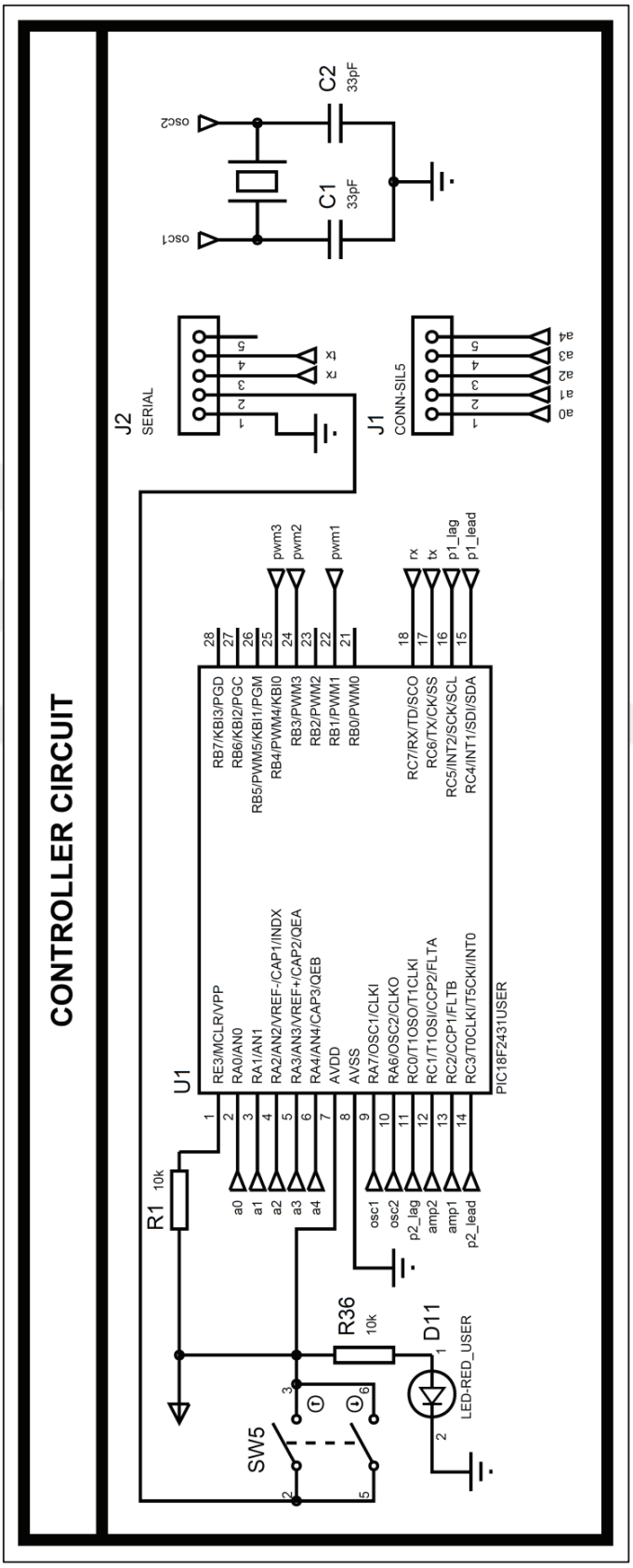

Figure B.9 Controller circut that adjusts the stimulation signal parameters integrated in the PCB shown in Figure 4.14

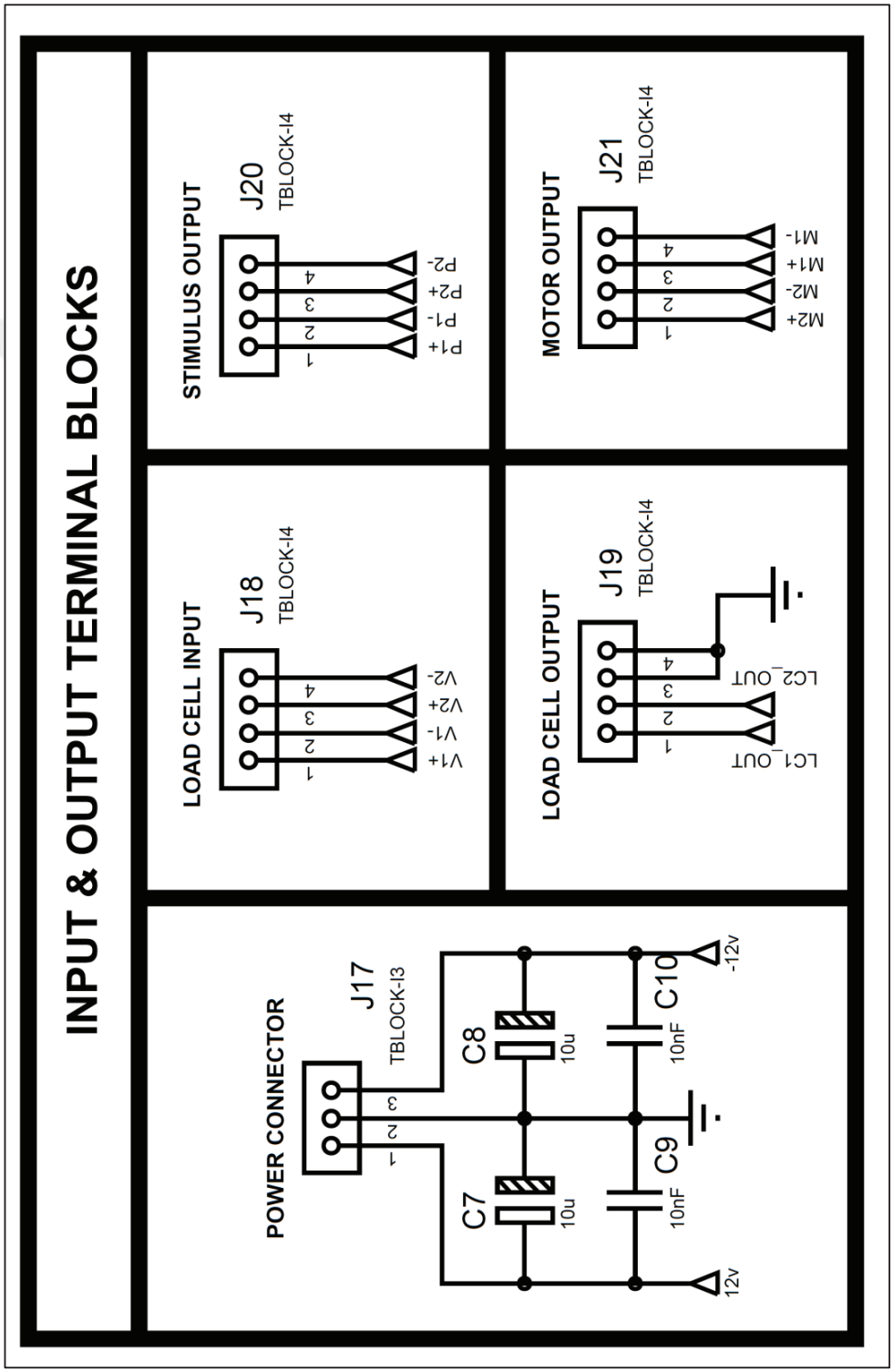

Figure B.10 Input and output terminals of the PCB shown in Figure 4.14

APPENDIX C: ADDITIONAL INFORMATION FOR MODELING

Zero and pole locaions of transfer functions of twitch responses given in Section 6.3 are shown in Figures C.1-C.4. Equations C.1-C.4 are the transfer functions given respectively. Theese all belong to same specific muscle at different fatigue levels.

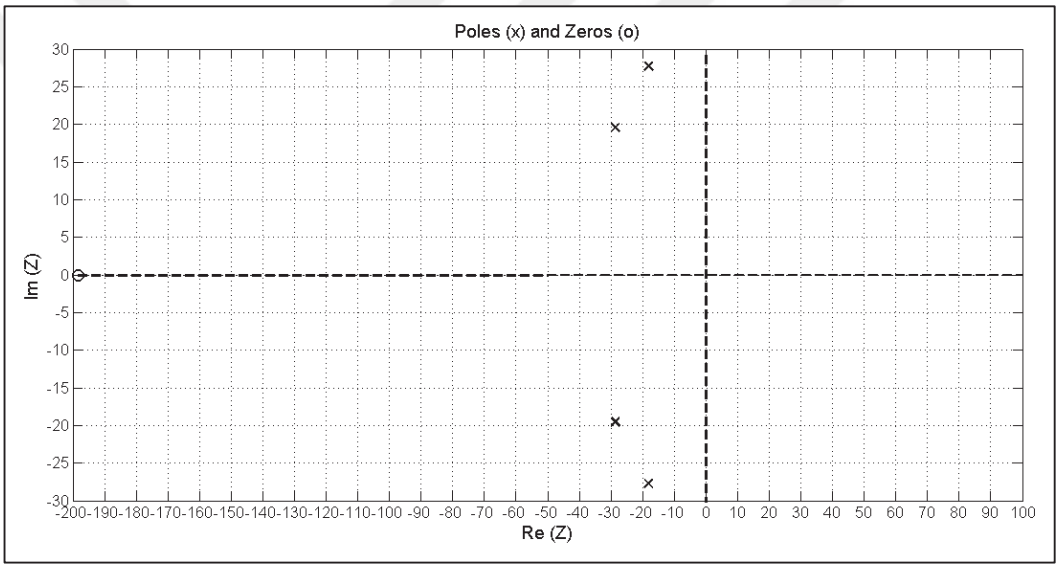

Figure C.1 Zero and pole locations of twitch transfer function 1

$$H(s) = \frac{2.722e08s + 5.401e10}{s^4 + 93.51s^3 + 4374s^2 + 1.064e05s + 1.318e06} \quad \text{(C.1)}$$

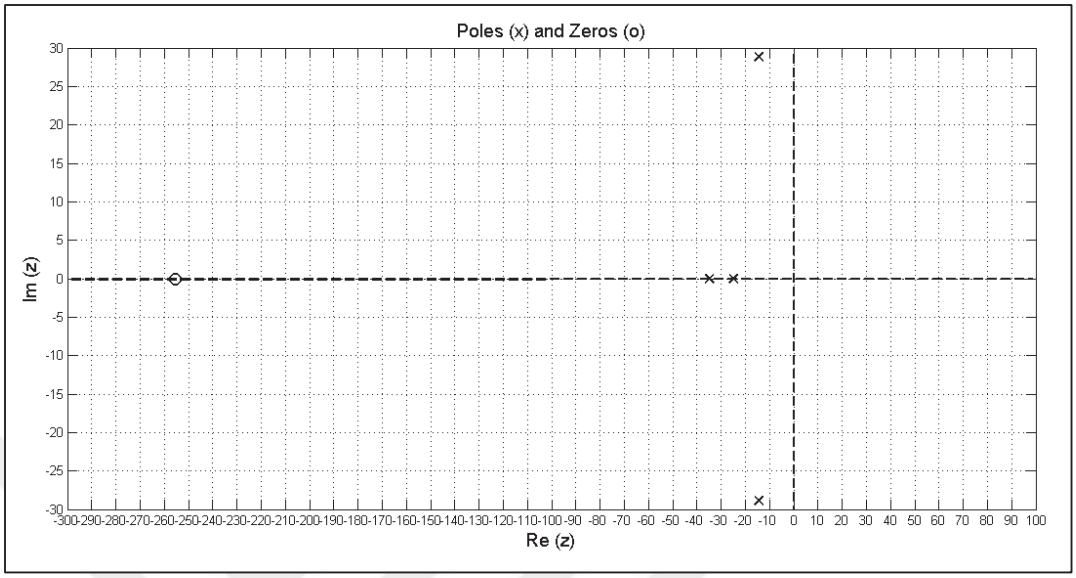

Figure C.2 Zero and pole locations of twitch transfer function 2

$$H(s) = \frac{9.672e07s + 2.471e10}{s^4 + 88.61s^3 + 3636s^2 + 8.729e04s + 9.022e05} \quad \text{(C.2)}$$

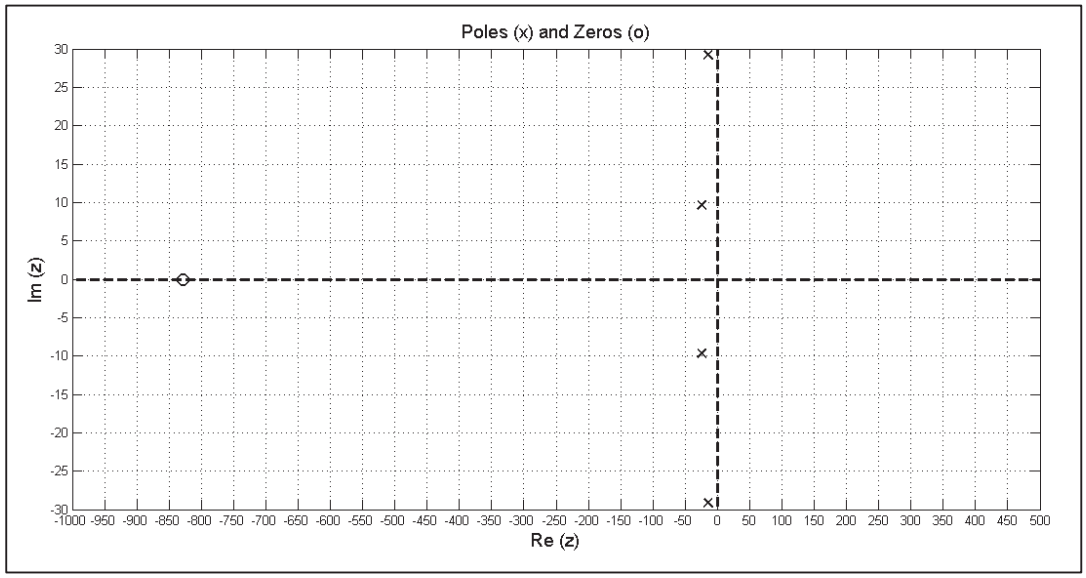

Figure C.3 Zero and pole locations of twitch transfer function 3

$$H(s) = \frac{2.299e07s + 1.906e10}{s^4 + 77.04s^3 + 3125s^2 + 7.041e04s + 1.106e05} \quad \text{(C.3)}$$

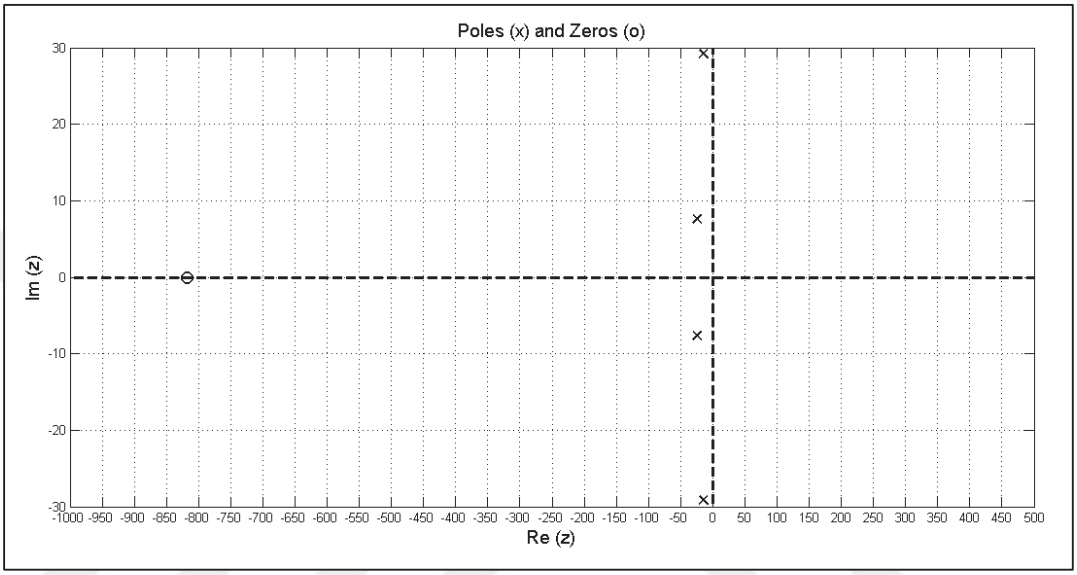

Figure C.4 Zero and pole locations of twitch transfer function 4

$$H(s) = \frac{2.156e07s + 1.765e10}{s^4 + 76.7s^3 + 3069s^2 + 6.902e04s + 6.727e05} \quad \text{(C.4)}$$

APPENDIX D: CODES FOR ANALYSIS AND MODELLING

In this section some of the MATLAB codes used for analysis and modeling are given. Algorithm D.1 is used to crop the acquired data between desired time interval. It finds the contraction start time and places the start point of contraction to the origin. Algorithm D.2 finds the peaks of data and Algorithm D.3 finds the contraction start time and the time of global maximum. Algorithm D.1 is the function which imports data from Algorithm D.2 and Algorithm D.3. Algorithms written in LabView for data acquisition are not given here, however softcopy of these algorithms are given to Yeditepe University Institute of Natural Sciences.

Algorithm D.1Data crop algorithm

```
function []=datacrop(s_rate,data_length)
global x3                                   % Raw data
global data_c                               % Cropped data
[ivdc_1 ivdc_2]=findtiming;                 % Contraction start and peak time
data_c=x3(ivdc_1:(ivdc_1+(s_rate*data_length)),[1 2 3 4]);
data_c(:,1)=data_c(:,1)-data_c(1,1);        % Substract initial time
data_c(:,4)=data_c(:,4)-data_c(1,4);        % Substract initial force
data_force(:,1)=data_c(:,4);
end
```

Algorithm D.2 Algorithm for finding peak locations and magnitudes

```
function [maxval, maxloc]=findpeakmax
global x3
[peakmax,peakloc]=findpeaks(x3(:,4));  % Find peaks and their locations
from the raw data
for j=1:length(peakmax);
if max(peakmax)==peakmax(j,1);
maxloc=peakloc(j,1);                    % Location of global maximum
maxval=max(peakmax);                    % Magnitude of global maximum
end
end
```

Algorithm D.3Algorithm for contraction timing

```
function [start_time_pt,max_time_pt]=findtiming  % inputs: magnitude
and location of global maximum in raw data, outputs: contraction start
time & global maximum time
global x3                                          % Raw data
tantheta_0=0;
[evfd_1, evfd_2]=findpeakmax;                      % Magnitude and
location of global maximum in raw data
for ivfd_1=1:evfd_2;
tantheta(ivfd_1,1)=(evfd_1-x3(ivfd_1,4))/(evfd_2-ivfd_1); %Slope of line
betwen the data point and global maximum
if tantheta_0<tantheta(ivfd_1,1);                  % Maximum of
the slope
tantheta_0=tantheta(ivfd_1,1);
ivfd_4=ivfd_1;
end
end
for ivfd_3=1:ivfd_4;
if (tantheta(ivfd_3,1))>(tantheta_0)*0.85;   % The data point for which the
slope exceedes 85 % of maximum slope is the moment of contraction start
ivfd_2=ivfd_3;
break
end
end
start_time_pt=ivfd_2;                          % Contraction start time
max_time_pt=evfd_2;                            % Time of global maximum
end
end
```

Algorithm D.4 is the objective function for genetic algorithm which finds the fiber transition rates acording to the model explained in Section 5.2. MATLAB optimization toolbox (optimization with genetic algorithm) is used to predict the model coefficients (fiber transition rates) for which the error between real and model is minimum.The parameters of genetic algorithm are given in Table D.1.

Table D.1 Genetic algorithm preferences

Population size	200
Creation function	Constraint dependent
Scaling function	Rank
Seclection function	Tournament
Mutation function	Adaptive feasible
Crossover function	Scattered
Migration	Forward and backward

Algorithm D.4 Objective function for genetic algorithm

```
function [meanerrnew]=psearchgach(inp) %inputs: Transition rate
variables, output: RMS error
global data_c
Ac=inp(1);  %Activation rate
Rc=inp(2);  % Recovery rate
Fc=inp(3);  % Fatigue rate
coef=1650; % (gr) Assumption for the maximum contraction force for the
muscle which is not fatigued
nn=length(data_c);
ratefunc=40000;
for jk=1:100:(nn)
t=(jk-1)/ratefunc;
Nactive=((exp(-Ac*t)*(Ac-Rc))/(Rc-Ac+Fc))-(((exp((-
(Fc+Rc))*t))*Fc*Ac)/((Fc^2)+(Rc^2)+(2*Rc*Fc)-(Fc*Ac)-
(Rc*Ac)))+(Rc/(Fc+Rc)); %Number of active fibers
err(jk,1)=((Nactive*coef)-data_c(jk,4))^(2);
end
meanerrnew=(sum(err(:,1)))/length(err); %RMS error between
experimental data and model output
end
```